**University of Alberta**

# An Empirical Analysis of Ozone Decay Kinetics in Natural Waters

by

Nicholas James Oke

A thesis submitted to the Faculty of Graduate Studies and Research in partial fulfillment of the requirements for the degree of Master of Science

in

Environmental Science

Department of Civil and Environmental Engineering

Edmonton, Alberta

Fall 1996

National Library
of Canada

Acquisitions and
Bibliographic Services Branch

395 Wellington Street
Ottawa, Ontario
K1A 0N4

Bibliothèque nationale
du Canada

Direction des acquisitions et
des services bibliographiques

395, rue Wellington
Ottawa (Ontario)
K1A 0N4

*Your file* *Votre référence*

*Our file* *Notre référence*

**The author has granted an irrevocable non-exclusive licence allowing the National Library of Canada to reproduce, loan, distribute or sell copies of his/her thesis by any means and in any form or format, making this thesis available to interested persons.**

**L'auteur a accordé une licence irrévocable et non exclusive permettant à la Bibliothèque nationale du Canada de reproduire, prêter, distribuer ou vendre des copies de sa thèse de quelque manière et sous quelque forme que ce soit pour mettre des exemplaires de cette thèse à la disposition des personnes intéressées.**

**The author retains ownership of the copyright in his/her thesis. Neither the thesis nor substantial extracts from it may be printed or otherwise reproduced without his/her permission.**

**L'auteur conserve la propriété du droit d'auteur qui protège sa thèse. Ni la thèse ni des extraits substantiels de celle-ci ne doivent être imprimés ou autrement reproduits sans son autorisation.**

ISBN 0-612-18308-4

Canada

**University of Alberta**

**Library Release Form**

**Name of Author:** Nicholas James Oke

**Title of Thesis:** An Empirical Analysis of Ozone Decay Kinetics in Natural Waters

**Degree:** Master of Science

**Year this Degree Granted:** 1996

Permission is hereby granted to the University of Alberta Library to reproduce single copies of this thesis and to lend or sell such copies for private, scholarly, or scientific research purposes only.

The author reserves all other publication and other rights in association with the copyright in the thesis, and except as hereinbefore provided, neither the thesis nor any substantial portion thereof may be printed or otherwise reproduced in any material form whatever without the author's prior written permission.

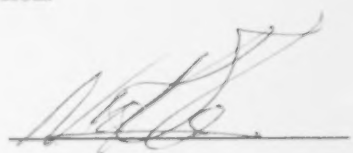

#304 10145 - 84th Avenue,
Edmonton, Alberta
T6E 2G8

Dated: OCTOBER 4, 1996

**University of Alberta**

**Faculty of Graduate Studies and Research**

The undersigned certify that they have read, and recommend to the Faculty of Graduate Studies and Research for acceptance, a thesis entitled An Empirical Analysis of Ozone Decay Kinetics in Natural Waters by Nicholas James Oke in partial fulfillment of the requirements for the degree of Master of Science in Environmental Science.

Dr. Daniel W. Smith

Dr. Stephen J. Stanley

Dr. John Feddes

2 October 1996

For my wife,
Deborah,
for her support and understanding,
and my parents,
Margaret and Timothy,
for their love and guidance.

**Abstract**

The use of a declining utilization rate "constant" was investigated for the decay of ozone concentrations in natural waters. An exponentially decreasing function, based on three kinetic parameters, was found to provide better estimates of the ozone decay curves than the commonly-used first order kinetic function. Through the use of batch testing and the measurement of physical water quality parameters in different dilutions of eight natural water samples, an empirically-based relationship between water quality and these kinetic parameters was determined. The predictive ability of this method was then examined through its application to bubble column profile generation using the back flow cell model for both cocurrent and countercurrent flow configurations. Countercurrent profiles were observed to fit the experimental data reasonably well, while cocurrent results were less definitive.

**Acknowledgements**

The author wishes to thank Dr. Daniel W. Smith for his advice, support and patience during the preparation, experimental and writing phases of this thesis.

Dr. Hongde Zhou deserves a great deal of gratitude, for his many hours of patient work and help in the understanding of numerous procedures and concepts.

The assistance of many people was very much appreciated. Experimental work was made so much easier thanks to the efforts of Nick Chernuka, Gary Solonynko, Maria Demeter, Kathy Black, and Sandra Kenefick.

The financial support of the Natural Sciences and Engineering Research Council of Canada through its research grant to Dr. D. W. Smith was greatly appreciated.

**Table of Contents**


INTRODUCTION ..... 1

LITERATURE REVIEW ..... 3
- Mass Transfer ..... 3
- Ozone Decomposition ..... 4
- Ozone Reactions with Organics ..... 8
- Modelling of Ozone Reactions ..... 15

METHODS ..... 23
- Collection of Samples ..... 23
- Preparation of Glassware ..... 24
- Determination of Ozone Concentration ..... 24
- Determination of Hardness ..... 25
- Determination of Alkalinity ..... 25
- Determination of Total Organic Carbon ..... 26
- Determination of Ultra-Violet Absorption ..... 26
- Determination of pH ..... 27
- Determination of Temperatures ..... 27
- Determination of Solids ..... 27
- Determination of Metals ..... 28
- Batch Testing ..... 28
- Reaction Kinetics ..... 29
- Column Testing ..... 30
- Back-Flow Cell Modelling ..... 31

RESULTS ..... 35
- Batch Testing ..... 35
- Pilot Testing ..... 37

DISCUSSION ..... 56

CONCLUSIONS AND RECOMMENDATIONS ..... 83

REFERENCES ..... 86

APPENDIX A: Batch Test Experimental Data ..... 89

APPENDIX B: Batch Test Log ($C/C_o$) vs. Time Plots ..... 96

APPENDIX C:Batch Test $K_w$ vs. $\Delta O_3$ Plots ..... 119

APPENDIX D: Pilot Scale Experimental Data ..... 139

APPENDIX E: FORTRAN Program Listing for Predicting Dissolved Ozone Profiles in Natural Waters ..... 146

APPENDIX F: Detailed Derivation of Back Flow Cell Model ..... 151

APPENDIX G: Final Back Flow Cell Model Data Input Files ..... 158

## List of Tables


| Table # | Description | Page |
|---|---|---|
| 1 | Compounds and their Functions in Ozone Decomposition | 6 |
| 2 | Hatta Numbers | 12 |
| 3 | Selected First Order Rate Constants | 13 |
| 4 | Alkalinity Species Calculations | 26 |
| 5 | Dimensionless Parameters Incorporated into the BFCM | 32 |
| 6 | Raw Water Quality Summary | 35 |

## List of Figures


| Figure # | Description | Page |
|---|---|---|
| 1 | Oxidation Scheme for Phenol | 11 |
| 2 | Diagrammatic Representation of Kinetic Regimes | 12 |
| 3 | Generalized Model Output | 16 |
| 4 | Batch testing Apparatus | 33 |
| 5 | Pilot Apparatus Schematic | 34 |
| 6 | First Order Plot for the Decay of Ozone in Milli-Q Water | 39 |
| 7 | Predicted Log b vs Observed Log b for Batch Test Ozone Decay | 40 |
| 8 | Predicted Log c/b vs Observed Log c/b for Batch Test Ozone Decay | 41 |
| 9 | Typical First Order Plot for the Decay of Ozone in Natural Waters | 42 |
| 10 | Typical Second Order Plot for the Decay of Ozone in Natural Waters | 43 |
| 11 | Rossdale Counter Current Ozone Concentration Profiles: Observations vs. BFCM-Generated | 44 |
| 12 | Red Deer Counter Current Ozone Concentration Profiles: Observations vs. BFCM-Generated | 45 |
| 13 | Hasse Lake Counter Current Ozone Concentration Profiles: Observations vs. BFCM-Generated | 46 |
| 14 | Wabamun Lake Counter Current Ozone Concentration Profiles: Observed vs. BFCM-Generated | 47 |
| 15 | Driedmeat Lake Counter Current Ozone Concentration Profiles: Observed vs. BFCM-Generated | 48 |
| 16 | Rossdale Cocurrent Ozone Concentration Profiles: Observations vs. BFCM-Generated | 49 |
| 17 | Red Deer Cocurrent Ozone Concentration Profiles: Observations vs. BFCM-Generated | 50 |
| 18 | Slave Lake Cocurrent Ozone Concentration Profiles: Observed vs. BFCM-Generated | 51 |
| 19 | Hasse Lake Cocurrent Ozone Concentration Profiles: Observed vs. BFCM-Generated | 52 |
| 20 | Wabamun Lake Cocurrent Ozone Concentration Profiles: Observed vs. BFCM-Generated | 53 |
| 21 | Pigeon Lake Cocurrent Ozone Concentration Profiles: Observed vs. BFCM-Generated | 54 |
| 22 | Driedmeat Lake Cocurrent Ozone Concentration Profiles: Observed vs. BFCM-Generated | 55 |

## List of Figures (Cont'd)


| Figure # | Description | Page |
|---|---|---|
| 23 | Effect of the Kinetic Parameter "a" on Batch Test Decay..... | 74 |
| 24 | Effect of the Kinetic Parameter "b" on Batch Test Decay..... | 75 |
| 25 | Effect of the Kinetic Parameter "c" on Batch Test Decay..... | 76 |
| 26 | Effect of the Kinetic Parameter "a" on Countercurrent Ozone Concentration Profiles Generated by the Back Flow Cell Model..... | 77 |
| 27 | Effect of the Kinetic Parameter "b" on Countercurrent Ozone Concentration Profiles Generated by the Back Flow Cell Model..... | 78 |
| 28 | Effect of the Kinetic Parameter "c" on Countercurrent Ozone Concentration Profiles Generated by the Back Flow Cell Model..... | 79 |
| 29 | Effect of the Kinetic Parameter "a" on Cocurrent Ozone Concentration Profiles generated by the Back Flow Cell Model..... | 80 |
| 30 | Effect of the Kinetic Parameter "b" on Cocurrent Ozone Concentration Profiles Generated by the Back Flow Cell Model..... | 81 |
| 31 | Effect of the Kinetic Parameter "c" on Cocurrent Ozone Concentration Profiles Generated by the Back Flow Cell Model..... | 82 |
| B1 - B22 | Log ($C/C_o$) vs Time..... | 97 - 118 |
| C1 - C19 | Fitted $K_w$ Curves for all Samples..... | 120 - 138 |

## List of Symbols

| Symbol | | Description |
|---|---|---|
| $\rho$ | - | water gravity, $kg/m^3$ |
| $\varepsilon$ | - | holdup, $m^3/m^3$ |
| a | - | specific interfacial area ($m^2/m^3$) |
| | - | kinetic parameter |
| A | - | absorbance |
| a | - | parameter defined in Table 5 |
| b | - | pathlength |
| | - | kinetic parameter |
| C | - | bulk liquid ozone concentration (mol/L) |
| c | - | kinetic parameter |
| $C^*$ | - | equilibrium ozone concentration (mol/L) |
| $D_a$ | - | Damkohler number |
| $D_{O_3}$ | - | diffusivity of ozone in water |
| $E_i$ | - | instantaneous reaction factor |
| f | - | proportionality constant |
| g | - | gravitational acceleration, $m/sec^2$) |
| H | - | Henry's Law constant |
| $H_a$ | - | Hatta number |
| $k_d$ | - | direct rate constant for reactions involving molecular ozone |
| $k_L$ | - | local liquid mass transfer coefficient (m/s) |
| $k_La$ | - | overall mass transfer coefficient ($s^{-1}$) |
| $k_w$ | - | specific ozone utilization rate |
| n | - | reaction order |
| N | - | total number of CSTRs in series |
| P | - | partial pressure of ozone in gas phase |
| | - | pressure, kPa |
| $Pe_L$ | - | Peclet number |
| r | - | ratio of backflow to convective flow |
| $St_G$ | - | Stanton number, gas phase |
| $St_L$ | - | Stanton number, liquid phase |
| t | - | time (sec) |
| u | - | superficial velocity, m/s |
| V | - | volume |
| X | - | dimensionless liquid phase concentration |
| Y | - | dimensionless gas phase concentration |
| z | - | stoichiometric ratio |
| | - | dimensionless column height |

**Introduction**

An improved understanding of chemical degradation by ozonation will enable improved design of ozone reaction vessels for full-scale water treatment. The back-flow cell model (BFCM) has been demonstrated by Zhou (1995) to predict ozone concentration profiles very accurately through the entire height of a bubble column when ozone demand-free water is used. By incorporating the kinetics of ozone degradation caused by material in natural waters into the BFCM, it may be possible to accurately predict the behaviour of natural waters in various treatment scenarios.

In theory, it is necessary to know the concentrations and reaction kinetics of all constituents of a water sample to calculate how that water will respond to ozonation. However, by performing various physical tests which may serve as indications of relevant water properties, it may be possible to form guidelines to predict how a given water sample will respond to oxidative treatment. For instance, it is known that ozone, generally, will react quickly with double bonds by a dipolar addition mechanism. Double bonds are also largely responsible for light absorption. Hence, running a UV spectrograph at a given wavelength may serve as one indication of the reactivity of the sample towards ozone. The effectiveness of ozone as an oxidant stems in part from its ability to decompose, forming highly reactive radical products, such as hydroxyl radicals, which then react non-selectively with dissolved substances. These radicals can be scavenged by certain inhibitory species, most notably carbonate and bicarbonate ions. Therefore, the alkalinity of the water may be used as an inverse measure of the effectiveness of oxidation. As many dissociating organic compounds will react much faster in their deprotonated forms, the pH of the solution will likely also be important. Other factors which may serve as useful indicators of kinetic properties include temperature, total organic carbon content, and the concentrations of certain metals which, among other effects, may serve to tie up scavenger species.

The determination of ozonation kinetics for natural waters is a much-discussed issue in the literature. While most authorities agree that simple first or second-order schemes do not adequately describe the process, there are few other descriptions offered. Some have suggested a two stage, first order process, the first stage representing the apparent initial demand, the second representing the remaining reaction. However, examination of decay curves shows the rate "constant" to be continually changing over the course of the reaction. Therefore, this research will investigate the possibility of a specific utilization rate, $k_W$, that changes exponentially with the amount of ozone consumed.

Using bench-scale batch tests to determine the kinetics of individual water samples, the resulting kinetic parameters will be regressed on the measured physical properties of the samples to determine if a relatively simple linear relationship exists. If so, the predicted kinetic parameters of several water samples will be used to mathematically model the ozone concentration profiles in a pilot-scale bubble column using the BFCM, and the results compared to the experimentally observed profiles for those samples.

## Literature Review

Ozone oxidation of organic contaminants in drinking water treatment is a complex process involving many different pathways, mechanisms and chemicals. This review of the literature on the subject divides the process into three components: mass-transfer, ozone decomposition, and reactions. Finally, various attempts to model the combined processes will be investigated.

### Mass-Transfer

Ozonation is a gas-liquid process that involves simultaneous mass transfer and chemical reactions (Beltran et al 1992; Gurol and Singer 1983). Therefore kinetic equations used for process design and specification must take both reactions and mass transfer into account (Singer and Gurol 1983; Beltran et al 1992, 1993; Zhou 1995). This requires knowledge and understanding of the relationship between the partial pressure of gaseous ozone, its solubility in water and the rate of mass transfer from gas to water (Gurol and Singer 1983).

The most widely accepted model for predicting the air-to-water mass transfer of ozone is the two-film model (Glaze 1987; AWWARF 1991; Zhou et al 1994).

$$dC/dt = \alpha k_L a(\beta C^* - C) = \alpha k_L a(\beta(P/H) - C) \quad (1)$$

where: $k_L$ = local liquid mass transfer coefficient (m/s)

a = specific interfacial area = interfacial area ($m^2$) / liquid volume ($m^3$)

($k_L a$ = overall mass transfer coefficient ($s^{-1}$))

$C^*$ = $[O_3]$ in equilibrium at the interface (mol/L)

C = $[O_3]$ in the bulk liquid (mol/L)

P = partial pressure of ozone in gas phase (atm)

H = Henry's Law constant = 0.082 atm $m^3$ g $mol^{-1}$

$\alpha$ = mixing intensity and tank geometry correction factor

$\beta$ = water characteristics correction factor

The difference in ozone concentration between the interface and the bulk liquid, ($C^*$ - C), sets up the concentration gradient that drives the dissolution. Therefore, rapidly

occurring reactions consuming ozone in the bulk liquid will increase the gradient, thus increasing the rate of ozone dissolution (Glaze 1987). In the extreme case of phenol, the rate of reaction between ozone and phenol is so fast as to be mass-transport-limited, causing the concentration of dissolved ozone to be close to zero until all of the phenol has reacted (Singer and Gurol 1983). In turn, the rate-limiting factor in the mass transfer process is the diffusivity of ozone in the liquid film, as diffusion in the gas phase is much more rapid (Zhou et al 1994).

The transfer efficiency is a measure of how much of the ozone in the feed gas is transferred to the liquid phase. It is a function of many factors, including the ozone feed concentration, gas flow rate, and hydrodynamic behaviour of the fluid (Roustan et al 1995). By increasing the concentration of ozone in the feed gas, Laplanche et al (1991) observed the transfer efficiency and the quantity of ozone dissolved to increase. Very little change in the transfer efficiency was observed when the pH was adjusted by 1 unit, or when the product of the reaction rate constant and the contaminant concentration was varied from 1 to 100. When the gas flow rate was increased, the transfer efficiency was observed to increase. This was due to an increase in the value of the overall mass transfer coefficient (the mass transfer in bubble columns is more closely related to the gas bubble velocity than the liquid phase velocity). The likely cause of the increase in $k_L a$ is an increase in interfacial area, a, not in $k_L$ which is mainly controlled by diffusion of ozone in the liquid film (Zhou 1995).

**Ozone Decomposition**

While gaseous ozone is relatively stable, solutions of ozone are generally unstable, undergoing autodecomposition to form highly reactive free radical products (Hoigne and Bader 1983a; Gurol 1985; Glaze 1987; Yurteri and Gurol 1988; AWWARF 1991; Zhou et al 1994; Zhou 1995). This decomposition is generally initiated by hydroxide ions (Yurteri and Gurol 1988; Yurteri and Gurol 1989; Beltran

et al 1993; Staehelin and Hoigne 1985) or other initiator species, such as formate ions (Glaze 1987; AWWARF 1991).

Ozone decomposition in natural waters is mechanistically complex (Guittonneau et al 1992). Many different mechanisms have been proposed for the decomposition process, hypothesizing various intermediate- and end-products, although they all portray the mechanism as being a radical chain reaction, with some of the reaction products or intermediates acting as promoters or initiators themselves (Hoigne and Bader 1983a). The Hoigne, Staehelin and Bader mechanism is one proposed set of decomposition reactions (AWWARF 1991):

| | |
|---|---|
| $1) O_3 + OH^- \xrightarrow{k_1} HO_2 + O_2^-$ | $k_1 = 7.0x10^1\ M^{-1}s^{-1}$ |
| $1') HO_2 \xleftrightarrow{k_i} O_2^- + H^+$ | $k_i = \text{ionization const.} = 10^{-4.8}$ |
| $2) O_3 + O_2^- \xrightarrow{k_2} O_3^- + O_2$ | $k_2 = 1.6x10^9\ M^{-1}s^{-1}$ |
| $3) O_3^- + H^+ \xleftrightarrow{k_3 k_{-3}} HO_3$ | $k_3 = 5.2x10^{10}\ M^{-1}s^{-1}$ |
| | $k_{-3} = 2.3x10^2\ s^{-1}$ |
| $4) HO_3 \xrightarrow{k_4} OH + O_2$ | $k_4 = 1.1x10^5\ s^{-1}$ |
| $5) OH + O_3 \xrightarrow{k_5} HO_4$ | $k_5 = 2.0x10^9\ M^{-1}s^{-1}$ |
| $6) HO_4 \xrightarrow{k_6} HO_2 + O_2$ | $k_6 = 2.8x10^4\ s^{-1}$ |
| $7) HO_4 + HO_4 \rightarrow H_2O_2 + 2O_3$ | |
| $8) HO_4 + HO_3 \rightarrow H_2O_2 + O_3 + O_2$ | |

In this mechanism, steps 1 and 1' constitute initiation, steps 2 through 6 are the propagation phase, while 7 and 8 are the chain breakdown stages. Another proposed mechanism is that of Gordon, Tomiyasu and Fukutomi (AWWARF 1991):

| | |
|---|---|
| $1) O_3 + OH^- \xrightarrow{k_1} HO_2^- + O_2$ | $k_1 = (40 \pm 2) M^{-1}s^{-1}$ |
| $2) HO_2^- + O_3 \xrightarrow{k_2} O_3^- + HO_2$ | $k_2 = 2.2x10^6\ M^{-1}s^{-1}$ |
| $3) HO_2 + OH^- \leftrightarrow O_2^- + H_2O$ | $k_a = 10^{-4.8}$ |
| $4) O_2^- + O_3 \xrightarrow{k_3} O_3^- + O_2$ | $k_3 = 1.6x10^9\ M^{-1}s^{-1}$ |
| $5) O_3^- + H_2O \xrightarrow{k_4} HO + O_2 + OH^-$ | $k_4 = 20 - 30 M^{-1}s^{-1}$ |
| $6) O_3 + HO \xrightarrow{k_5} O_2^- + HO_2$ | $k_5 = 6x10^9\ M^{-1}s^{-1}$ |
| $7) O_3^- + HO \xrightarrow{k_6} O_3 + OH^-$ | $k_6 = 2.5x10^9\ M^{-1}s^{-1}$ |
| $8) HO + O_3 \xrightarrow{k_7} HO_2 + O_2$ | $k_7 = 3x10^9\ M^{-1}s^{-1}$ |

$$9) HO + CO_3^{2-} \xrightarrow{k_9} OH^- + CO_3^- \qquad k_8 = 4.2x10^8\ M^{-1}s^{-1}$$
$$10) CO_3^- + O_3 \rightarrow products\ (CO_2 + O_2^- + O_2)$$

In addition to initiators and promoters that can start or accelerate the auto-decomposition of ozone, compounds known as scavengers or inhibitors can slow it down and break the cycle of the chain reaction by reacting with hydroxyl radicals without producing more radicals (Hoigne and Bader 1979; Staehelin and Hoigne 1985; Yurteri and Gurol 1988). This causes a lower concentration of hydroxyl radicals, and hence a lower rate of decomposition, which in turn will lead to a greater concentration of molecular ozone (Glaze 1987; AWWARF 1991; Le Sauze et al 1993). The most common scavengers are the bicarbonate and carbonate ions (Glaze 1987). Staehelin and Hoigne (1985) provide a table of typical compounds that can act as initiators, promoters and inhibitors.

Table 1: Compounds and Their Functions in Ozone Decomposition.

| Initiators | Promoters | Inhibitors |
|---|---|---|
| $OH^-$ | $R_2CHOH$ | $CH_3COO^-$ |
| $H_2O_2 / HO_2^-$ | aryl-R | alkyl-R |
| $Fe^{2+}$ | formate | $HCO_3^- / CO_3^{2-}$ |
| formate | (humics) | (humics) |
| humics | $O_3$ | (TOC) |
| (TOC) | | |

Compounds which appear in more than one column can act in different capacities under different conditions.

There has been a large volume of work published on the decomposition kinetics of ozone, although finding a consensus is difficult (Staehelin and Hoigne 1985). The simplest kinetic equations governing the process are of the form:

$$dC/dt = -k_d C^n \qquad (2)$$

where C is the ozone residual concentration at time t, $k_d$ is the apparent decomposition rate constant, and n is the order of the reaction (Marinas et al 1993). However, in studies that fit their data to this form, there is very little agreement on the value of n. Most studies apparently find the order of the decomposition to be adequately approximated by first order kinetics with respect to ozone concentration (Roth and Sullivan 1983; Marinas et al 1993; Zhou et al 1994; Zhou 1995), although Marinas et al (1993) cite studies which found second order kinetics to more accurately describe the process. Zhou et al (1994) and Zhou (1995) use a similar kinetic equation for clean water, although the $k_W$ is actually the "specific ozone utilization rate", which changes during ozonation due to variation in water character:

$$-dC_L/dt = k_w C_L \tag{3}$$

Other studies have found the rate of decomposition to be first order with respect to both ozone and hydroxide concentrations (AWWARF 1991),

$$-d[O_3]/dt = k[O_3][OH^-] \tag{4}$$

although this can be expressed as a pseudo-first order expression for a given pH.

$$-(d[O_3]/dt)_{pH} = k'[O_3] \tag{5}$$

$$k[OH^-] = k' \tag{6}$$

There are more detailed kinetic equations that have been proposed, such as those of Yurteri and Gurol (1988):

$$-d[O3]/dt = \sum(k_{d,i} + k_{b,i})[S_i][O_3] + k_1[OH^-][O_3] + k_2[O_2^-][O_3] + k_3[OH][O_3] \tag{7}$$

and Guittonneau et al (1992):

$$-d[O_3]/dt = [\sum K_D[D] + \sum k_I[I](1 + (\sum k_P[P]/\sum k_S[S]))][O_3] \tag{8}$$

where: $\Sigma K_D[D]$ = direct reaction with $O_3$

$\Sigma k_I[I]$ = initiation of $O_3$ decomposition to HO radicals

$\Sigma k_P[P]$ = reaction of $O_3$ with promoters to form more HO radicals
$\Sigma k_S[S]$ = scavenging of HO by generic scavengers

Guittonneau et al (1992) and Zhou (1995) both state that ozone decomposition in natural waters appears to take place in two stages. The first stage is a rapid process, followed by a set of much slower, first order decomposition reactions.

Due to the initiation of the decomposition reaction by hydroxide ions, the pH of a water sample will play a large role in the rate of ozone decomposition. As the concentration of hydroxide ions increases (increasing pH), so will the rate of decomposition (Hoigne and Bader 1979; Roth and Sullivan 1983; Staehelin and Hoigne 1985; Le Sauze et al 1993; Marinas et al 1993; Zhou et al 1994). Gurol and Singer (1983) found that ozone decomposition was negligible at pH's of less than 4, and Yurteri and Gurol (1988) state that ozone is relatively stable in solutions with low pH. It follows, therefore, that for waters with higher pH, higher ozone doses are required to achieve the same dissolved ozone concentration in the effluent (Le Sauze et al 1993).

Other factors which influence the rate of ozone decomposition are the temperature, the intensity of UV light, the organic and inorganic contents of the water, and the presence or absence of organic and inorganic inhibitors, initiators and promoters (AWWARF 1991; Zhou et al 1994). Marinas et al (1993) state that the rate constant decreases with increasing concentrations of radical scavenger species, while Zhou et al (1994) found that the more polluted a water is, the greater the ozone decay rate, and hence the greater the ozone dose necessary to obtain a desired residual.

**Ozone Reactions with Organics**

One major benefit of the oxidation of organic pollutants with ozone is the destruction of the compounds, unlike with other treatment processes such as reverse osmosis or activated carbon adsorption, in which the pollutant is merely concentrated in a phase other than the water which then still needs to be disposed of (Gurol 1985;

Glaze 1987). The oxidation can take place at different rates, yielding different intermediate and end products, or by different mechanisms and pathways depending on the compounds present and the conditions of the system (eg. treatment rate, temperature, pH, presence or absence of certain organic and inorganic compounds, etc.).

There are two major pathways which act in the ozonation of organic materials: direct oxidation by molecular ozone, and indirect oxidation by ozone decomposition products (Hoigne and Bader 1979, 1983a; Yurteri and Gurol 1988, 1989; AWWARF 1991; Guittonneau et al 1992; Beltran et al 1993; Blum et al 1993; Zhou et al 1994; Zhou 1995). Both of these pathways may be operating at the same time, or one may be dominant, depending on the conditions and the chemicals being oxidized. The two pathways will also lead to different selectivities with respect to which compounds are oxidized and hence what products are formed. Molecular ozone is very selective, while the free radical species formed as a result of ozone decomposition are far less selective. Only compounds that have bonds with special reactivity towards ozone will react with molecular ozone. Examples of these bonds are those often found in living cells, and in compounds that impart an odour, taste or colour to water (Hoigne and Bader 1979). Therefore, in the treatment of drinking water, most of the oxidation of trace organics occurs via the free radical pathway (Hoigne and Bader 1979; Yurteri and Gurol 1989; Guittonneau et al 1992), although certain conditions can decrease the rate of radical reactions, increasing the contribution from molecular ozone oxidation. The presence of high concentrations of carbonate or bicarbonate, which absorb hydroxyl radicals, will stabilize the molecular ozone, resulting in less decomposition, and hence lower contributions from the radical pathway (AWWARF 1991; Guittonneau et al 1992). Also, at low pH, the hydroxide ion concentration is lower, hence lowering the rate of initiation of decomposition, leading to a lower rate of oxidation by radical species (Hoigne and Bader 1983a; Beltran et al 1993).

Thermodynamically, molecular ozone has a very high free energy of oxidation, as seen in the following half-reaction:

$$O_3 + 2H^+ + 2e^- \rightarrow H_2O + O_2 \qquad (\Delta G^\circ = -400 kJ/mol) \tag{9}$$

However, this thermodynamic potential is limited by reaction kinetics. These kinetics are best when the ozone is able to act as an electron transfer acceptor for the oxidation of metals, an electrophile for the oxidation of phenol and other activated aromatics, or a dipole addition reagent when involved in the addition across carbon-carbon double bonds. Electron withdrawing groups on the oxidized compound will generally severely depress the rates of oxidation, as in the case of chloroform (Hoigne and Bader 1979, 1983a; Glaze 1987; Beltran et al 1993) due to the high electronegativity of chlorine. This effect is most apparent when highly electronegative groups, such as -COOH and $-NO_2$, are substituted around a double bond (the most common site of ozone attack) (AWWARF 1991). On the other hand, electron donating groups, such as -OH and $-NH_2$, can increase the reactivity of double bonds or aromatic structures (Hoigne and Bader 1983a; AWWARF 1991).

It is also possible for many consecutive, parallel reactions to be in progress, each using the same reactants, but proceeding via different mechanisms to produce different intermediate and end products. For example, the following oxidation scheme has been proposed for phenol (Singer and Gurol 1983):

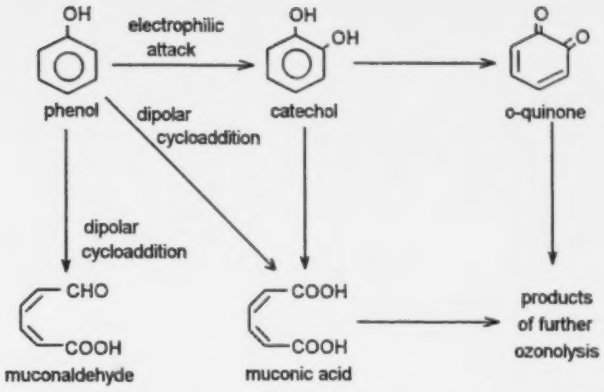


Figure 1. Oxidation scheme for phenol. (Singer and Gurol 1983)

When dealing with dissociating organic compounds, the general tendency is for the rate of reaction to increase with increasing deprotonation (Hoigne and Bader 1983b; Beltran et al 1993). Often the rate will change by a factor of 10 per unit pH difference. This is likely due to an enhancement of the nucleophilicity of the reaction site by an inductive or mesomeric effect (Hoigne and Bader 1983b).

When determining whether a reaction is proceeding via the direct or indirect pathway, the Hatta number will help to determine which of four kinetic regimes the reaction adheres to. The Hatta number, Ha, relates the rate of reaction to the rate of mass transfer across the gas-liquid film into the bulk solution, and is calculated as (Beltran et al 1992, 1993):

$$Ha = (\sqrt{k_d C_B D_{O3}})/k_L \qquad (10)$$

where: $k_d$ = direct rate constant for reaction between ozone and B (l $mol^{-1}$ $s^{-1}$ or $s^{-1}$)

$C_B$ = concentration of B (mol $l^{-1}$)

$D_{O3}$ = diffusivity of $O_3$ in water ($m^2$ $s^{-1}$)

$k_L$ = liquid phase mass transfer coefficient (m $s^{-1}$)

The kinetic regimes describe the rate and location of reactions. They range from the very slow regime, in which the reaction will occur almost entirely in the bulk solution, to the instantaneous regime in which the reaction occurs entirely in the liquid film.

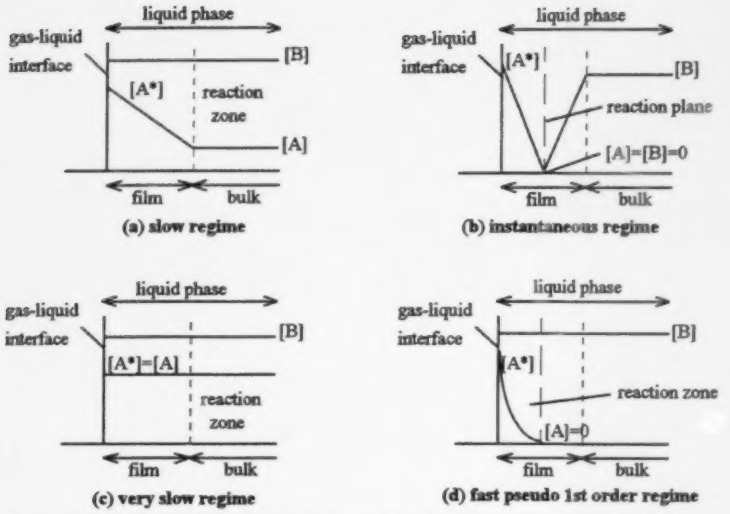


Figure 2. Diagramatic representation of the kinetic regimes. (Beltran et al 1992)

A* = concentration of dissolved gas A at the gas-liquid interface

The following table shows the values of the Hatta number that correlate to each kinetic regime:

Table 2. Hatta numbers (Beltran et al 1992).

| Kinetic Regime | Hatta Range |
|---|---|
| instantaneous | $Ha >> nE_i$ |
| fast pseudo first order | $3 < Ha < E_i/2$ |
| slow | $0.02 < Ha < 0.3$ |
| very slow | $Ha < 0.02$ |

$E_i = 1 + (zD_B[B]/D_A[A^*])$ = instantaneous reaction factor

z = stoichiometric ratio, moles of ozone consumed per mole contaminant oxidized

Beltran et al (1992) determined that Ha for the self decomposition of ozone is less than $2x10^{-3}$ at a pH value of less than 7, and 0.13 at pH 12. Therefore the self decomposition process is slow or very slow and occurs in the bulk liquid. Hence, for indirect reactions to be able to compete with direct reactions, the direct reactions must also fall into the slow or very slow regimes. In general, the direct reactions are

considerably slower than radical reactions, leading to the conclusion again that most ozone reactions in drinking water treatment will occur via the radical pathway (Yurteri and Gurol 1988).

Hoigne and Bader (1983a) determined the direct reaction rate constants for the reactions of ozone with different compounds, some of which are shown here:

Table 3. Selected 1st order rate constants. (Hoigne & Bader 1983a)

| Compound | 1st Order Rate Constant |
|---|---|
| nitrobenzene | 0.09 ± 0.02 |
| chlorobenzene | 0.75 ± 0.2 |
| benzene | 2 ± 0.4 |
| toluene | 14 ± 3 |
| phenol | 1300 ± 300 |
| tetrachloroethylene | < 0.1 |
| trichloroethylene | 17 ± 4 |
| methanol | ~ 0.024 |
| ethanol | 0.37 ± 0.04 |
| 1-propanol | 0.37 ± 0.04 |
| formaldehyde | 0.1 ± 0.03 |
| acetaldehyde | 1.5 ± 0.2 |
| carbon tetrachloride | < 0.005 |
| chloroform | < 0.1 |
| bromoform | < 0.02 |
| acetone | 0.032 ± 0.006 |
| dioxane | 0.32 ± 0.03 |
| glucose | 0.45 ± 0.05 |

It was observed that all of the reaction rates increased with increasing temperature. Hoigne and Bader determined that the reaction kinetics were first order, with respect to both the ozone and solute concentrations, for all solutes tested. This agrees with the results found by the same researchers in 1979. Other researchers have found the kinetic equation for combined direct and indirect reactions to be of the form (Yurteri and Gurol 1989; Beltran et al 1993):

$$-d[S]/dt = k_{direct}[O_3][S]+k_{indirect}[OH^{\bullet}][S] \qquad (11)$$

Yurteri and Gurol (1989) continued on to state that the concentration of hydroxyl radicals is a constant function of the ozone concentration,

$$[HO^{\bullet}] = \Psi[O_3] \tag{12}$$

where $\Psi$ is a function of all solutes and the rate constants of all initiators and inhibitors present, and therefore:

$$-d[S]/dt = k_T[O_3][S] \tag{13}$$

where:

$$k_T = k_{direct} + \Psi k_{indirect} \tag{14}$$

Beltran et al (1993) state that this is only valid for slow or very slow reactions where the reaction takes place in the bulk solution (ie. the reaction rate is not mass-transfer-limited). On the other hand, Guittonneau et al (1992), found that as the majority of oxidation proceeds via the radical pathway, the kinetics follow:

$$-d[S]/dt = k[OH^{\bullet}][S] \tag{15}$$

although there may be some very fast reactions occuring in the first 5 seconds. Zhou (1995) found that the kinetics do not follow a simple first order model, and refers to an immediate ozone demand, followed by changing reactivity as ozonation proceeds.

Blum et al (1993) investigated different methods for the prediction of rate constants for the reaction of organics with hydroxyl radicals. They found a good correlation between the values of the rate constants for reactions involving hydroxyl radicals in air and water, but then by including solvation effects (polarity and molecular volume) much better correlations were obtained for compounds reacting via hydrogen abstraction mechanisms.

$$\log(k_{OH})_{water} = 0.70\log(k_{OH})_{air} - 0.88(\Pi^*) + 0.66(v_i/100) \quad (R^2 = 0.93) \tag{16}$$

$\Pi^*$ is a parameter representing polarity
$v_i$ is the Van der Waals molar volume ($cm^3/mol$)

In general, an increase in polarity of a compound will lead to a decrease in the ratio of $k_{water}/k_{air}$, while a decrease in the molecular volume will lead to a decrease in the same ratio. The advantage to using such a correlation is that the large volume of work published on atmospheric ozone reactions contains rate constants for compounds which have very little work published on them in an aqueous environment. Also, they determined that a fragment constant equation can be of use where other information is not available. This is an equation that will provide an estimate of the rate constant from the structural formula of the compound.

$$k_{OH} = \sum k(CH_3(X)) + \sum k(CH_2(X)(Y)) + \sum k(CH(X)(Y)(Z)) \qquad (17)$$

where X, Y, and Z are functional groups that each have factors assigned to them.

**Modelling of Ozone Reactions**

Chang and Chian (1981) modelled the ozonation of methanol in an ozone-sparged column. They assumed the liquid phase to be well-mixed, and the gas to approximate plug-flow. Their model did not take stripping of the methanol into account. Their results were found to adequately predict the TOC of the effluent and the individual concentrations of methanol, formaldehyde and formic acid. It was observed that the TOC removal efficiency could be increased by raising the partial pressure of ozone in the feed gas, the superficial gas velocity, or the residence time. The reasons for these improvements were postulated to be different in all three cases though. For the ozone partial pressure, the improvement was believed to be due to an increase in the driving force behind the mass transfer of ozone into the bulk liquid. The increase in superficial gas velocity was believed to cause an increase in $k_La$, while the increase in residence time simply gave the compounds more time to react. When they

investigated the scale-up practice of maintaining a constant superficial gas velocity, they found that TOC removals dropped in larger columns because the volume increases faster than the cross-sectional area for vessels of the same relative dimensions.

Gurol and Singer (1983) state that formulating a model requires knowledge and understanding of the relationship between the partial pressure of ozone and its solubility in water and rate of mass transfer from gas to water, the kinetics of self-decomposition, and the kinetics of oxidation of solutes and their oxidation products. They proposed the following generalized mass-balance formula as a starting point:

$$\underset{\text{total}}{d[O_3]/dt} = \underset{\text{absorption}}{d[O_3]/dt} - \underset{\text{decomposition}}{d[O_3]/dt} - \underset{\text{oxidation reactions}}{\sum d[O_3]/dt} \qquad (18)$$

In formulating a model for the batch oxidation of water contaminated with phenol, they determined mass balance equations for phenol, ozone and the reaction intermediates: catechol, hydroquinone and muconic acid. When the equations were solved simultaneously as a function of time, the calculated concentrations were found to adhere to the following generalized output:

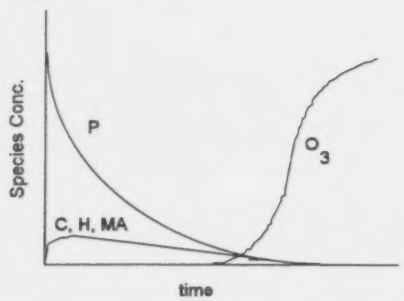


Figure 3. Generalized model output (Gurol and Singer 1983).

The results were found to be very sensitive to changes in $k_L a$ and the saturation concentration of ozone, and when compared to empirical data, the model output was found to adequately predict the observed results.

Yurteri and Gurol (1988, 1989) have modelled the rate of ozone consumption in natural waters. They have used a parameter, "w", known as the specific ozone utilization rate, which is determined by the pH and the raw water chemical matrix. The utilization rate differs from a rate constant in that it can take into account the changing nature of the raw water. Using synthetic water samples and regression analysis, they determined a formula for the prediction of "w":

$$\log w = -3.98 + 0.66\,pH + 0.61\log(TOC) - 0.42\log(alkalinity/10) \qquad (19)$$

where the units of "w" are $hr^{-1}$. They found that TOC was able to be used as a measure of promoters, while the alkalinity could serve as a measure of inhibitors. They tested the formula over ranges of parameters commonly found in natural waters:

$1 < TOC < 5$ mg/L

$10 <$ alkalinity $< 500$ mg/L as $CaCO_3$

$7 < pH < 9$

The model was then tested against several natural water samples, for which the predictions appear to adequately predict the ozone utilization rate. They caution against the use of the model with samples heavily contaminated with synthetic organic carbons (SOC), however, as some SOC's can change "w" more than is predicted by the equation, possibly due to the promotion of the radical cycle. Roustan et al (1995) performed a similar study and proposed a similar equation for the prediction of the overall kinetic constant, $k_C$:

$$\log(k_C) = -4.0 + 0.29(pH) + 1.19\log(TOC) + 0.41\log(total\,alkalinity) \qquad (20)$$

The investigators do caution, however, that the validity of the equation is limited to the tap water used in their experiments.

Laplanche et al (1991) simulated the transfer of ozone in water, and compared the model to a pilot unit. They used two assumptions in their modelling. The first was that the air and water circulated in plug flow and perfect counter-current mode, and

the second was that for a small increment in height, dh, the ozone in the water and air are constant. They determined the ozone balance between heights h and h+dh to be:

$$C_{L(h+dh)} = C_{L(h)} + k_L aE[C_{(h)} - C_{L(h)}]dV - C_{L(h)}\{1 - \exp[-k_1[OH^-]dt\} - C_{L(h)}\{1 - \exp[-k_2[P]dt\} \quad (21)$$

ozone transferred from gas to liquid — self-decomposed ozone — ozone consumed by oxidation

The model does not take into account the oxidizability of oxidation products, but does predict the ozone concentration profiles fairly well. They point out that their sampling method for the pilot unit probably entrained ozone bubbles in the sample, rather than just extracting liquid. By manipulating model parameters, they found the transfer efficiency to be relatively insensitive to small changes in pH or in the reaction rate constant, and that increasing the value of $k_L a$ raised the transfer efficiency and the effluent ozone concentration significantly.

Guittonneau et al (1992) propose a kinetic model that uses first order kinetics:

$$-d[O_3]/dt = [\sum K_D[D] + \sum k_I[I](1 + \frac{\sum k_P[P]}{\sum k_S[S]})][O_3] \quad (22)$$

where: $\Sigma K_D[D]$ = direct reaction with $O_3$ ( $s^{-1}$)

$\Sigma k_I[I]$ = initiation of $O_3$ decomposition (to HO radicals) ($s^{-1}$)

$\Sigma k_P[P]$ = reaction of $O_3$ with promoters to form more HO radicals ($s^{-1}$)

$\Sigma k_S[S]$ = scavenging of HO by generic scavengers, S ($s^{-1}$)

From their experimental work, the researchers claim that the reactions do indeed follow first order kinetics, although there may be some very fast reaction occurring within the first five seconds, indicating that ozone decay consists of a rapid process followed by much slower decomposition that is kinetically first order.

Marinas et al (1993) assumed that mixing can be modelled mathematically if the dispersion can be represented by diffusion laws, the concentration profile is uniform in a radial direction, and the axial dispersion is uniform. In addition, to calculate the ozone transfer, they assumed that steady state flow conditions existed, dispersion occurred only in the liquid, the two-film model was valid, the apparent ozone decomposition rate followed $dC/dt=-k_dC^n$, and ozone was stable in the gas

phase. Their model used closed-vessel axial dispersion. From their experimental work, they found that n=1 best represented the data. Applying the model to experimental conditions, they observed that ozone residuals in the contactor effluent decreased as the feed gas flowrate increased or the ozone concentration decreased. Under common operating conditions, the mixing environment varied from highly mixed to nearly plug-flow. The dispersion was observed to increase with increasing gas flowrate, and with decreasing water flowrate.

Le Sauze et al (1993) modelled the ozone transfer in a bubble column. They divided the column into three separate compartments for modelling purposes to simulate their assumption that the two ends are mixed due to water and gas input, while the middle can be represented as plug-flow. Other assumptions made were that the gas can be represented as plug-flow, the reactor was at steady state, the temperature was constant and homogeneous within a small volume element, dV, the ozone transfer can be described by the two-film model, the transfer coefficient, $k_L a$, is constant along the reactor, and there is no radial ozone gradient. They chose to use the specific ozone utilization rate as proposed by Yurteri et al (1988) for the reaction rate constant. By manipulating the model parameters, the researchers observed the ozone concentrations in the reactor to decrease with increasing pH. The ozone consumption was greater with increasing TOC levels, and therefore a TOC increase will lead to lower ozone concentrations. The transfer efficiency and ozone concentration in the effluent were observed to increase if the ozone concentration in the feed gas was increased. With a small amount of mixing, the counter-current arrangement was observed to out-perform the co-current flow scheme, but with increasing mixing, both co-current and counter-current patterns gave similar results.

Kallas et al (1995) presented a set of model differential equations and boundary conditions that were derived to predict ozone concentrations in both co- and counter-current bubble columns. They attempt to take into account the volatilization of

organics and use backmixing coefficients for both the gas and liquid phases. However, the model was not shown to adequately predict experimental results.

Zhou et al (1994) examined the axial dispersion model (ADM) to determine its validity in determining ozone concentration profiles in bubble columns. Instead of assuming complete mixing or plug flow characteristics, the model assumes some degree of backmixing (redistribution due to slippage or eddies). The assumptions made were that the pressure varies linearly with the column height, the gas holdup and interfacial area were constant along the column height, the mass transfer resistance was confined to the liquid side and was not enhanced by ozone decay in the liquid, the ozone decay was kinetically first order in the liquid and negligible in the gas phase, and that Henry's Law applied. Applying the model to counter-current operation, the concentration of dissolved ozone was observed to be highest at the bottom of the column, where the water leaves the column. A concentration jump was predicted at the top of the column due to backmixing, and the profile curve was observed to have a gradually increasing slope, except at the bottom where the slope is set to zero as the boundary condition. Backmixing was characterized by the Peclet number, $Pe_L$, which has an inverse relationship to the amount of backmixing. Increases in $Pe_L$ (decreases in backmixing) caused steeper profiles and higher effluent ozone concentrations. More polluted waters were observed to give a greater ozone decay rate, while waters with higher pH also had increased rates of ozone decay, requiring higher ozone doses to obtain the desired residual concentration. When simulating co-current conditions, the absorption was observed to be inferior to the counter-current geometry. The ozone concentration was observed to be more uniform through the profile in the co-current than in the counter-current mode, and the profile maximum was located in the middle of the column, not in the effluent, due to competitive effects of mass transfer and ozone decay in co-current configurations.

Smith and Zhou (1994) and Zhou (1995) all examined the development of the back-flow cell model (BFCM). Smith and Zhou (1994) compares the BFCM to the ADM. While the ADM assumes plug-flow with axial dispersion, the BFCM uses back-flow and exchange flow to characterize the dispersion. Both models provide almost identical profile curves, but the BFCM was able to be solved more simply than the ADM, as it uses algebraic rather than differential equations. Zhou (1995) discussed much of the mathematics behind the BFCM calculations, and the use of the model with natural waters was investigated. Zhou noted that ozone decay does not follow simple first order kinetics, as there is a large immediate ozone demand, followed by the much slower decomposition reactions that appear to adhere to first order kinetics. Using these modified two-stage kinetics, the BFCM was able to predict column performance fairly well, while applying simple first order kinetics produced relatively poor predictions of dissolved ozone profiles.

Westerhoff et al (1995) investigated the effects of natural organic materials on ozonation byproducts, and the potential for prediction of kinetic constants using measured UV absorbances at 254 and 280 nm. Their results demonstrated that chemical structure (aromaticity, acidity and functionality) significantly influence ozone decomposition. For instance, they illustrated that ozone reacts selectively with electron-rich organics, such as those containing double bonds. Similar to other works, Westerhoff et al (1995) found that ozone decay can be represented by a two-stage process, with two distinct rate constant values. They modelled the first, rapid reaction phase, by zero order kinetics, although the authors state that this is probably not accurate, but their experimental design allowed them only a limited ability to sample during the early stages of reaction. Following the zero order stage, they assigned a first order kinetic regime to account for the remainder of reaction. By regressing the UV absorbance readings on the measured values of both rate constants, the authors

managed to demonstrate an adequate relationship between a physical property of a natural water sample and its rate of reaction with ozone.

## Methods

In order to determine the kinetics of ozone concentration decay in natural waters, batch testing was performed on all of the samples at various dilutions. Samples were ozonated, and the ozone concentrations then monitored for a period of 30 minutes. Various tests were performed on the samples to determine their physical properties, the results of which were used in a linear regression procedure to develop a set of equations that are able to be used in the prediction of the kinetics of ozone decay.

These equations were then used to predict the kinetics of samples taken from the same sources in the pilot testing portion of the experiment. Samples were run through a pilot column, and once steady state was acheived, a profile was generated of the ozone concentrations through the column. The BFCM was then used, along with the predicted kinetics, to generate predicted profiles, which were compared with those observed.

### *Collection of Samples*

Water samples were collected from various rivers and lakes in the Edmonton area. 180 L plastic rainwater barrels were loaded into the back of a truck, which was then backed up to the edge of a water body. A gasoline-powered electric generator was used to power a small submersible pump which was lowered from the back of the vehicle into the water, taking care not to collect the water from a depth too close to the bottom, so as to avoid sediment intake. The pump was started while water was discharged back into the water body in order to clean the collection system. A small volume was then added to the barrel which was then agitated and emptied. This step was repeated twice more to ensure the barrel was clean. These steps were performed,

although not necessary, because all analysis was performed on samples after collection, and there was no need for the water to actually be representative of the exact composition of each particular water source, only for each sample to be different. Following the cleaning steps, the barrel was filled with water, and sealed until analysis was initiated in the laboratory.

*Preparation of Glassware*

Any glassware that was to come into contact with ozonated water had to be ozone-demand-free. To prepare glassware, an ozone-saturated solution was prepared by bubbling ozone through Milli-Q water for approximately thirty minutes. This water was then poured into the glassware and left overnight so as to satisfy any ozone demand present. The items were then emptied, oven-dried, and sealed with aluminum foil until use.

*Determination of Ozone Concentration*

The concentrations of ozone in solution were determined according to the method of Bader and Hoigne (1982). The method is based on the stoichiometric decolourization of indigo trisulfonate by ozone. A standard indigo stock solution was made, from which two reagent solutions were made. The two reagent solutions contain different concentrations of indigo, and are used for measuring different anticipated ozone concentrations. Higher ozone concentrations require higher initial indigo concentrations, in order to avoid complete decolourization.

To determine the concentration of dissolved ozone in a sample, a 100 mL volumetric flask was prepared by adding 10 mL of the appropriate indigo reagent, and possibly a quantity of water in cases where the expected ozone concentration was greater than 0.3 mg/L. The sample was then drawn into the flask, making the volume

up to 100 mL, taking care to quickly mix the solution while not creating bubbles which can cause ozone degassing.

Absorbance measurements were then taken on a Milton Roy Spectronic 601 spectrophotometer at a wavelength of 600 ± 5 nm using 50 mm quartz cells, and compared to a blank indigo solution which had not been exposed to ozone. The difference in absorbance between the blank and sample solution is directly proportional to the sample ozone concentration, which can be calculated using the following equation:

$$[O_3]\,(mg/L) = \frac{\Delta A \bullet 100}{f \bullet b \bullet V} \qquad (23)$$

where: $\Delta A$ = (absorbance of blank) - (absorbance of sample)
b = cuvette path length (cm)
V = volume of sample added to 100 mL volumetric flask (mL)
f = 0.42 $cm^{-1}$ / mg/L

*Determination of Hardness*

The total hardness of samples was determined by titrating standard .01M EDTA into a 50 mL aliquot containing approximately 1 g of UniVer indicator until the solution changed from red to blue. The calcium hardness was determined by performing the same titration but using CalVer indicator. Magnesium hardness could then be calculated as the difference between the two, assuming that calcium and magnesium are the predominant hardness contributors.

*Determination of Alkalinity*

To determine the alkalinity, and hence the carbonate, bicarbonate and hydroxide concentrations, 50 mL aliquots of sample water were titrated with standardized 0.02 N sulfuric acid. After adding 5 drops of phenolphthalein indicator solution, acid was added until the red to colourless colour change took place. The titre ($V_p$) was recorded, and 5 drops of bromcresol green indicator were added. Acid was then added

again until the colour changed, and the titre ($V_{bg}$) once again recorded. Once the titrations were complete, the following table was used to approximate the concentrations of alkalinity-contributing species:

Table 4: Alkalinity Species Calculations

| Condition | Predominant Forms | Species Concentrations (M) |
|---|---|---|
| $V_p = V_{bg}$ | $CO_3^{2-}$ | $[CO_3^{2-}] = V_p \times N \times V^{-1}$ |
| $V_p = 0$ | $HCO_3^-$ | $[HCO_3^-] = V_{bg} \times N \times V^{-1}$ |
| $V_{bg} = 0$ | $OH^-$ | $[OH^-] = V_p \times N \times V^{-1}$ |
| $V_{bg} > V_p$ | $CO_3^{2-}$ & $HCO_3^-$ | $[CO_3^{2-}] = V_p \times N \times V^{-1}$<br>$[HCO_3^-] = (V_{bg} - V_p) \times N \times V^{-1}$ |
| $V_p > V_{bg}$ | $OH^-$ & $CO_3^{2-}$ | $[OH^-] = (V_p - V_{bg}) \times N \times V^{-1}$<br>$[CO_3^{2-}] = V_{mo} \times N \times V^{-1}$ |

*Determination of Total Organic Carbon*

A Dohrmann Carbon Analyzer was calibrated for total carbon using a 10 ppm solution of KHP (potassium hydrogen phthalate). Three replicates were performed on each sample to determine the total carbon concentration. The UV lamp was then turned off and the instrument calibrated for total inorganic carbon using a 10 ppm solution of sodium carbonate. Each sample was analyzed using three replicates, and the results subtracted from the total carbon measurements to yield the total organic carbon (TOC) concentrations.

*Determination of Ultra-Violet Absorption*

Before each set of samples was analyzed, a blank consisting of Milli-Q water was scanned and the resulting spectrum saved in memory. Samples were prepared for ultra-violet absorption scans by vacuum-filtering through Whatman EPM 2000 glass microfibre filters with a pore size of 0.3 μm. The 10 mm pathlength cell was rinsed twice with the sample before being filled and inserted into the Hewlett Packard diode

array spectrophotometer. Wavelengths from 190 to 820 nm were then scanned, and the results printed in hardcopy form and saved on disk.

*Determination of pH*

Before adding ozone to batch test samples, a Fisher 915 Accumet pH meter electrode was rinsed with a small amount of sample water before immersion in an appropriately diluted sample. After allowing time for the reading to stabilize (approximately 2 minutes), the digital reading was recorded. For post-ozonation pH measurement, the electrode was immersed directly in the reaction vessel after reaction completion and the measurement taken after readout stabilization. For column tests, the pH electrode was immersed directly in the sample barrel.

*Determination of Temperatures*

A mercury thermometer was used to measure the temperatures of all samples.

*Determination of Solids*

A full gravimetric analysis was performed on all samples to determine total solids (TS), total dissolved solids (TDS), total suspended solids (TSS), total volatile solids (TVS), volatile suspended solids (VSS) and volatile dissolved solids (VDS). TS was determined by evaporating all liquid from a nickel crucible containing sample on a steam bath, and then drying the crucible and its contents in a 103°C oven for 60 minutes. The difference between the initial, empty weight of the crucible and its final weight, divided by the volume of sample used is the TS content. By then igniting the crucible in a 550°C furnace for 30 minutes, volatiles were driven off, and the change in weight divided by the original sample volume is the TVS measurement.

TSS was determined by washing a glass fibre filter with Milli-Q water and drying it in an oven. The filter was transferred to a Gooch crucible which was then

weighed. Suction was applied to the crucible by a vacuum filter apparatus and 40 mL of sample was poured through and collected in a clean vacuum flask. The crucible was then dried for 60 minutes in a 103°C oven and reweighed. The change in weight divided by the sample volume yielded the TSS measurement. By then igniting the crucible for 30 minutes and reweighing the crucible, the VSS measurement was obtained.

By transferring 25 mL of the filtrate from the TSS filtration to a nickel crucible which was then subjected to the same treatment as in the TS and TVS determinations, the TDS and VDS were determined.

*Determination of Metals*

Metals analyses were performed by atomic emission spectroscopy at the University of Alberta Spectral Services Laboratory. Metals analyzed were: P, Tl, Mo, Zn, Cd, Pb, Ni, Co, Ba, B, Si, Mn, Fe, Cr, Mn, Al, V, Ca, Cu, Ag, Ti, Sr, Na, and K. For economic reasons, only one sample was submitted from each sample source, along with a sample of Milli-Q water. It was assumed that the metal concentrations in the diluted samples would be adequately represented by calculating the contributions from the appropriate proportions of sample water and Milli-Q water.

*Batch Testing*

Batch testing of eight natural waters was performed at different dilution factors, to determine kinetic parameters, in a floating lid zero-headspace reactor vessel (Figure 4). Depending on the dilution factor, appropriate volumes of raw test water and Milli-Q water were added to the batch reactor. Milli-Q water was ozonated for approximately one hour, at which time 240 mL was added to the batch reactor, making the total liquid volume up to 1200 mL. The 1200 mL volume was chosen because it allowed for an adequate number of samples to be withdrawn during the

course of the experimental run while still leaving enough water in the reactor so as not to allow headspace to develop when the floating lid contacted the baffles. The stopwatch was started immediately upon the addition of ozonated water to the reactor. At the same time, 3 mL of ozonated Milli-Q water was added to a volumetric flask containing 10 mL indigo reagent, 75 mL Milli-Q water, and appropriate volumes of raw test water and additional Milli-Q water to generate the initial (time = 0) ozone concentration. At pre-determined times, 15 mL samples of reactor water were drawn off directly into 100 mL volumetric flasks containing 10 mL indigo reagent and 75 mL Milli-Q water. The 100 mm extension on the sample port was found to significantly reduce the ozone lost due to volatilization during sampling, yielding more consistent results. Sample absorbances were then measured and compared to a blank solution consisting of 10 mL indigo reagent, 75 mL Milli-Q water and 15 mL of appropriately diluted test water. Ozone concentrations were then determined and plotted against time to determine reaction kinetics.

*Reaction Kinetics*

In order to determine the kinetic parameters "a", "b" and "c" in the hypothesized kinetic equation, a first order plot (log $C/C_o$ vs. time) was made of each set of pooled replicate data. A best-fit curve was plotted by hand through the points, and the slope measured at each sample time by drawing a straight line tangent to the curve. Sample times were used because of the certainty of the values of log $C/C_o$ at those times. The slope of the curve at each point is a measure of the specific ozone utilization rate, $k_w$. The specific utilization rate was then plotted as a function of the change in ozone concentration. A non-linear least squares regression was then performed on the data, varying the values of "a", "b", and "c" to minimize the sum of squares of the residuals.

To generate the empirical model equations for the prediction of the kinetic parameters, the average observed parameter values were regressed upon the average analytical variables measured for all of the water samples. Non-significant parameters were gradually removed from the regressions, until only significant parameters remained. To verify that the model could adequately predict the kinetic parameters, the model generated kinetic parameter values were plotted against the experimentally observed parameters. A straight line plot with slope equal to unity and an intercept of zero is indicative of an effective model.

*Column Testing*

Using the apparatus depicted in Figure 5, column tests were performed on samples to evaluate the applicability of the kinetic predictions made from batch testing data to pilot-scale continuous-flow column tests. By adjusting valve positions, the apparatus can be configured to perform co-current and counter-current tests. The 2 m tall cylindrical glass column has an inside diameter of 100 mm. Six sample taps are located on one side of the column, the upward-opening conical inlets of which were designed to minimize gas bubbles being trapped in liquid samples. A 25 mm diameter fused crystalline aluminum stone sphere was installed at the bottom of the column to diffuse the ozone-containing extra dry oxygen which was generated by a PCI ozone generator and quantified using a PCI Ozone Monitor unit.

Sample water was pumped from a barrel into the column at a location appropriate to the flow configuration being tested. A minimum of 8 reactor volumes were pumped through the column before sampling began in order to ensure that the system had come to a steady state.

A modified version of the ozone concentration determination procedure was employed. Samples from the six taps were taken directly into 100 mL volumetric flasks containing 10 mL indigo solution after purging the taps to ensure that the

samples were as fresh as possible. The volume was then made up to the 100 mL mark by adding a measured amount of Milli-Q water to each flask, the volume of which was taken into account during the calculation of the ozone concentration. This method was used in order to allow faster sampling than could be performed if the samples were taken to the mark.

Vertical profiles were then generated for each test which could then be compared with profiles generated by the backflow cell model using the kinetic parameters determined from the batch tests.

*Back-Flow Cell Modelling*

Calculations were performed to generate the required data for the BFCM data input file for each column test. A listing of the dimensionless parameters is included as Table 5. The model was modified so as to allow for the correct flow configuration (See Appendix E for a listing of the FORTRAN program.) Initial guesses and estimations were used for the first run of the model. The output data were then used to calculate the amount of ozone utilized, which was then used to calculate a better approximation of the ozone utilization rate for each cell in the column using the kinetic parameters determined from the batch testing. These values were then recycled back into the input file, and the model was run again, this time yielding better results. This iterative process was repeated until the output data converged and stabilized.

Table 5: Dimensionless parameters incorporated into the BFCM.
(Source: Zhou 1995)

| Parameter | Definition | Parameter | Definition |
|---|---|---|---|
| z | $(j - 0.5) / N$ | $Pe_L$ | $(u_L L) / (D_L \varepsilon_L)$ |
| X | $C_L / C_o^*$ | $D_a$ | $(k_w \varepsilon_L L) / (N u_L)$ |
| Y | $y / y_o$ | $St_G$ | $(k_L a L / N u_{Go}) (R T / H)$ |
| $q_G$ | $Q_G / Q_{G,o}$ | $St_L$ | $(k_L a L) / (N u_L)$ |
| $\alpha$ | $-(\rho g \varepsilon_L L) / (N P_o)$ | r | $(N / Pe_L) - 0.5$ |

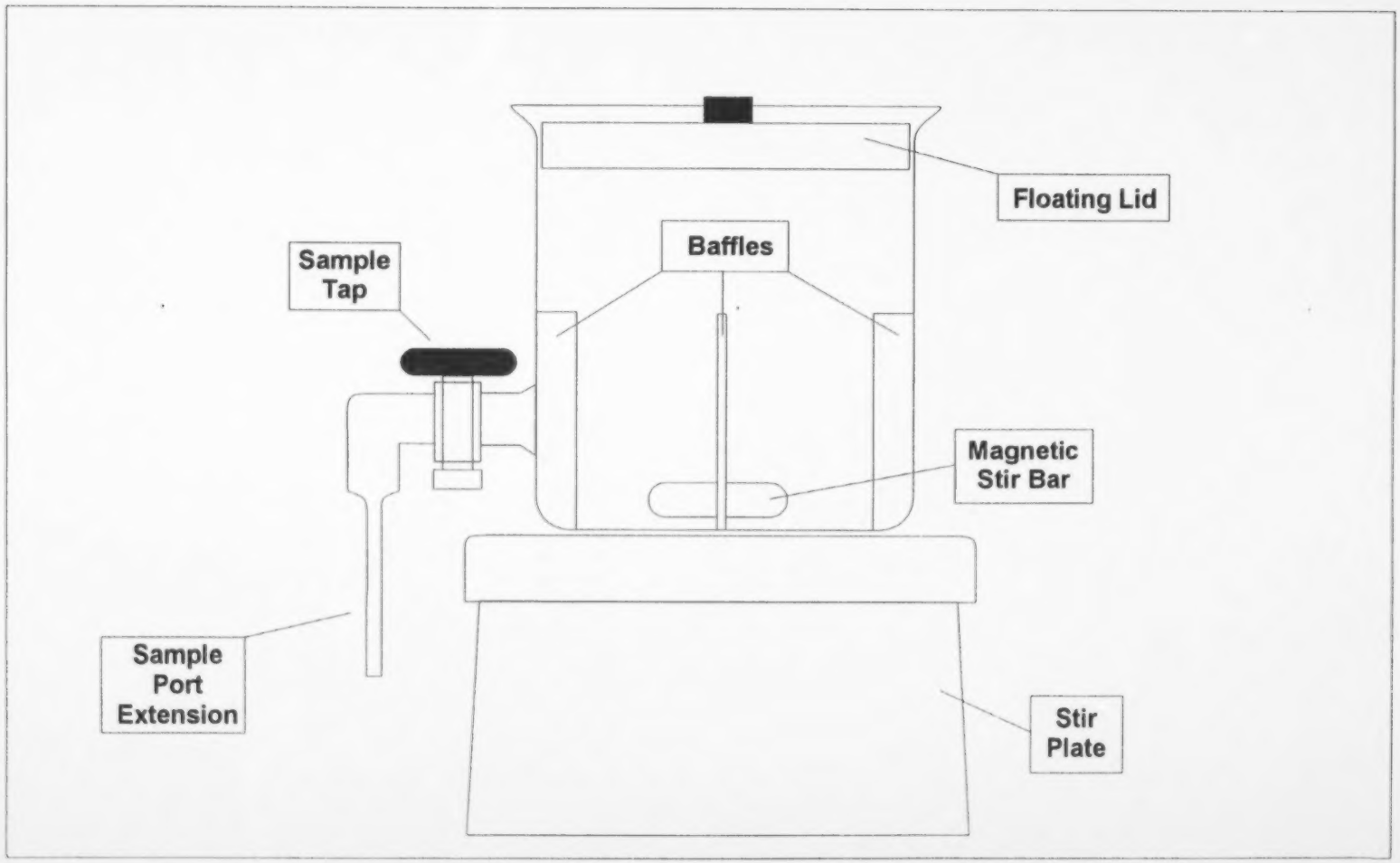


Figure 4: Batch Testing Apparatus

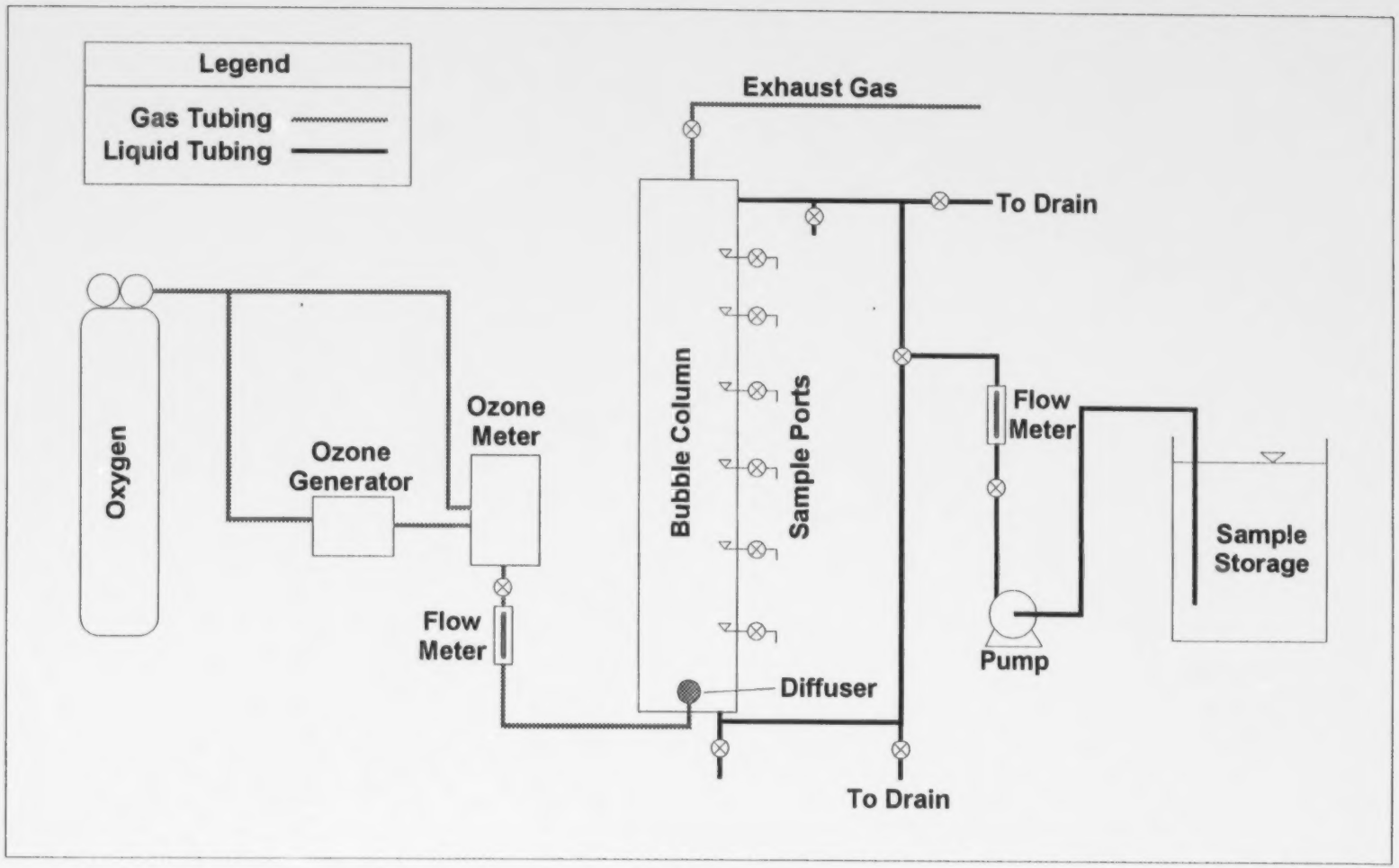


Figure 5: Pilot Apparatus Schematic

## Results

*Batch Testing*

To test the experimental protocols, batch testing was first performed on Milli-Q water. From Figure 6, a typical first order plot, it can be seen that a straight line can be fitted to the data, indicating that first order kinetics are adequate to describe the decomposition of ozone in clean water. It was noted that the addition of the sample port extension on the batch testing apparatus (Figure 4) contributed to significantly straighter first order plots, indicating that the feature greatly decreased the amount of mass transfer that occured during sampling due to turbulence.

For runs involving natural waters, the experimentally observed values for all measured parameters are included in Appendix A. A table summarizing major water quality parameters is provided below.

Table 6. Raw Water Quality Summary

| Source | $[Ca^{2+}]$ | $[Mg^{2+}]$ | $[CO_3^{2-}]$ | $[HCO_3^-]$ | TOC | $UV_{254}$ | $UV_{280}$ | pH | T** | TS |
|---|---|---|---|---|---|---|---|---|---|---|
| | mg/L $CaCO_3$ | mg/L $CaCO_3$ | eq/L | eq/L | ppm | | | | °C | mg/L |
| Rossdale WTP* | 96.5 | 31.5 | .00016 | .00168 | 12.83 | 0.12 | 0.10 | 7.9 | 20.6 | 196 |
| Pigeon L. | 59.8 | 25.3 | .00020 | .00198 | 15.19 | 0.08 | 0.06 | 8.3 | 20.0 | 66.7 |
| Wabamun L. | 43.0 | 47.0 | .00031 | .00259 | 24.86 | 0.14 | 0.10 | 8.1 | 19.2 | 258 |
| Slave L. | 47.7 | 18.6 | .00008 | .00120 | 12.78 | 0.15 | 0.10 | 7.6 | 20.3 | 116 |
| Driedmeat L. | 87.6 | 40.7 | .00067 | .00237 | 28.70 | 0.29 | 0.20 | 9.1 | 19.4 | 302 |
| Miquelon L. | 82.1 | 626.0 | .00705 | .01248 | 76.85 | 0.59 | 0.27 | 9.5 | 20.3 | 5201 |
| Hasse L. | 85.1 | 100.0 | .00015 | .00178 | 21.60 | 0.13 | 0.08 | 8.2 | 19.9 | 177 |
| Red Deer R. | 99.5 | 22.1 | .00013 | .00189 | 14.28 | 0.18 | 0.14 | 7.9 | 20.9 | 153 |

* Rossdale sample is at 4/5 dilution. All others are 3/4.

** Temperatures are those at time of testing.

Examination of the log $C/C_o$ vs time plots (Figures B-1 through B-22 in Appendix B) shows just how poorly a first order decay, or a two-stage first order decay model could fit the decomposition of ozone in natural waters. Most plots show a gradually decreasing rate constant, resulting in a concave up orientation. In order for first order kinetics to apply, the plots would have to show predominantly straight line forms. Due to reasons that will be covered in the discussion section, this changing rate constant is expected and can be accounted for. Plots of $k_w$ vs

$\Delta O_3$ and the non-linear regression curves are presented as Figures C-1 through C-19 in Appendix C.

It should be noted that the log $C/C_o$ vs time plots for Driedmeat Lake and Miquelon Lake presented difficulties. The initial ozone demand for all six source/dilution combinations was satisfied before the second ozone concentration sample (30 seconds) could be taken. Without a known concentration in this portion of the graph, it was not possible to determine a reasonable estimate for the slopes at the first two sample points. Therefore, samples from Driedmeat Lake and Miquelon Lake were discarded before non-linear regressions were performed to determine kinetic parameters. Experimental protocols that would allow one to take more closely spaced samples would allow waters such as these to be included in future work.

The linear regressions of the calculated kinetic parameters were performed by the linear regression feature of Microsoft Excel. It was found that log b yielded far more significant regressions than "b". For the determination of "c", regressing the values of log(c/b) was found to yield the most significant results, helping to take into account the rising, then falling values of "c" with increasing dilution factor. The resulting regression equations for all three parameters are presented as equations 24, 25 and 26. The values of the parameters predicted by the equations generated were then plotted against their respective observed values. Straight line plots with slope equal to 1 and passing through the origin are indicative of good predictive powers of the equations. These Predicted vs Observed plots are presented as Figures 7 and 8, with their regression equations and $R^2$ values. Both the log b and log(c/b) plots show slopes of greater than 0.9, intercepts very close to the origin, and $R^2$ values very close to 1. In both the log b and log(c/b) plots, it is apparent that there is a good distribution of points throughout the range covered. For the kinetic parameter "a", many of the non-linear regressions

generated a value of zero, while the others yielded values between 0.000242 (Rossdale 1/5 dilution) and 0.00473 (Rossdale 3/5 dilution). Because of the difficulties involved in performing a regression with so many zero values, all values of "a" were assumed to be zero for the purposes of kinetic predictions.

$$a = 0 \tag{24}$$

$$\log b = -6.892 + 3.443(UV254) + 0.0330(TOC) + 1252([CO_3^{2-}]) + 0.134(T) + .00137(TS) + 0.170(pH) \tag{25}$$

$$\log(c/b) = 6.005 - 0.157(TOC) - 0.0104(Ca\ Hardness) + 911.6([HCO_3^-]) + 0.0109(Mg\ Hardness) - 0.388(pH) \tag{26}$$

The units of all parameters are as follows:

| Parameter | Units |
|---|---|
| T | °C |
| pH | log units |
| TOC | ppm |
| $[CO_3^{2-}]$ | eq/L |
| $[HCO_3^-]$ | eq/L |
| $UV_{254}$ | absorbance |
| $UV_{280}$ | absorbance |
| Ca Hardness | mg/L $CaCO_3$ |
| Mg Hardness | mg/L $CaCO_3$ |
| TS | mg/L |

These terms are listed in order of decreasing statistical significance in each equation.

*Pilot Testing*

Pilot testing results are summarized in Appendix D. Concentration profiles are illustrated in Figures 11 to 22. The error bars used in these figures represent the stated uncertainty of the indigo method, and do not represent errors observed in replicate runs as each column test was performed only once.

Model profiles were not able to be performed on samples from Miquelon Lake. The Miquelon Lake sample physical properties were well outside those measured for other samples, and therefore the calculated kinetic parameters were several orders of magnitude different from the others, and cannot be considered accurate, as the regression results cannot reliably be extrapolated to this extreme.

Also missing are the BFCM generated profiles for the Slave Lake and Pigeon Lake counter-current configurations. Errors were made during the determination of ozone concentrations in some samples, and as the samples were all used, repeats of the runs could not be performed.

The final data input files for the back flow cell model calculations are provided in Appendix G.

## Figure 6: First Order Plot for the Decay of Ozone in Milli-Q Water

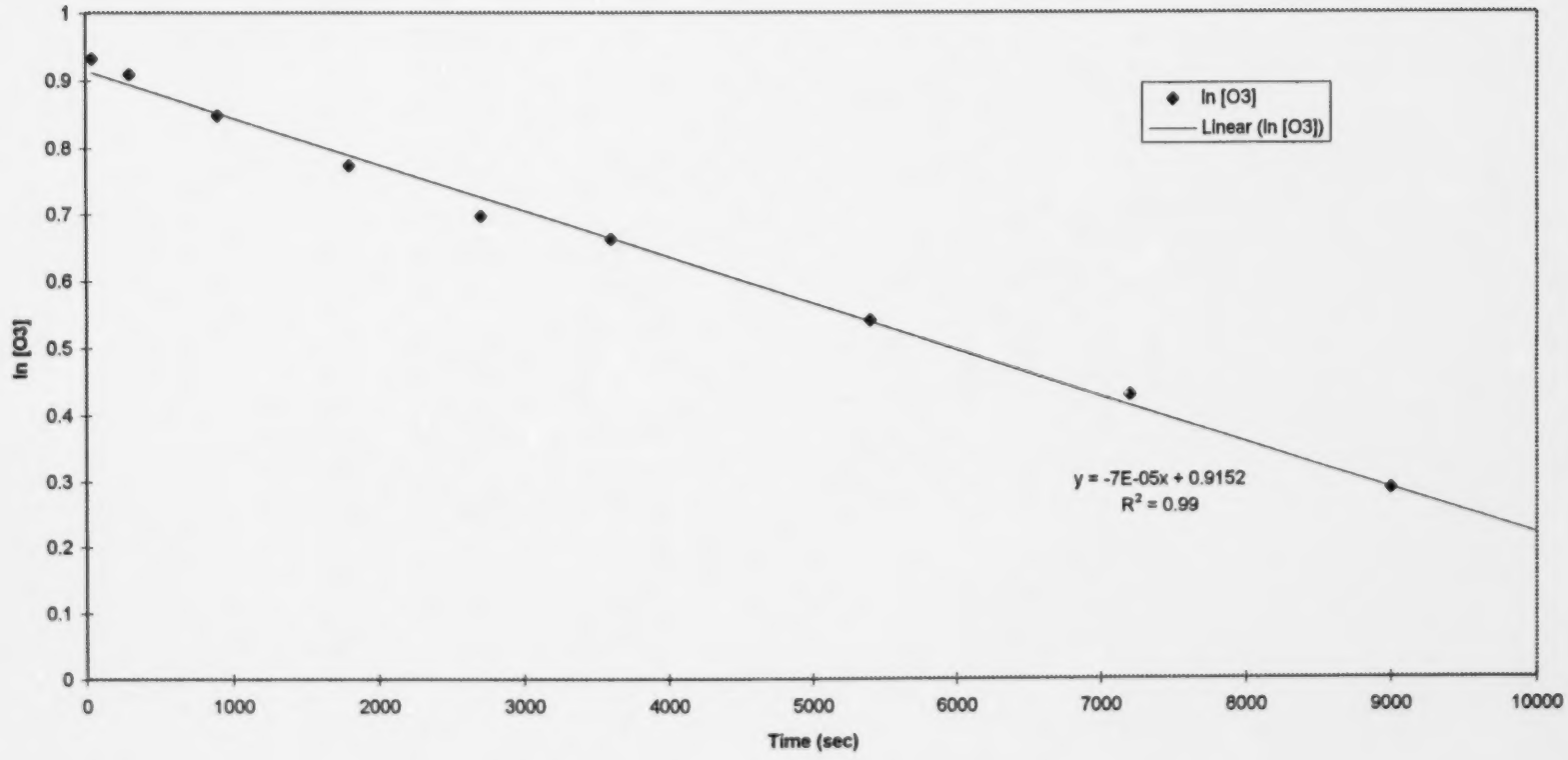

**Figure 7: Predicted log b vs Observed log b for Batch Test Ozone Decay**

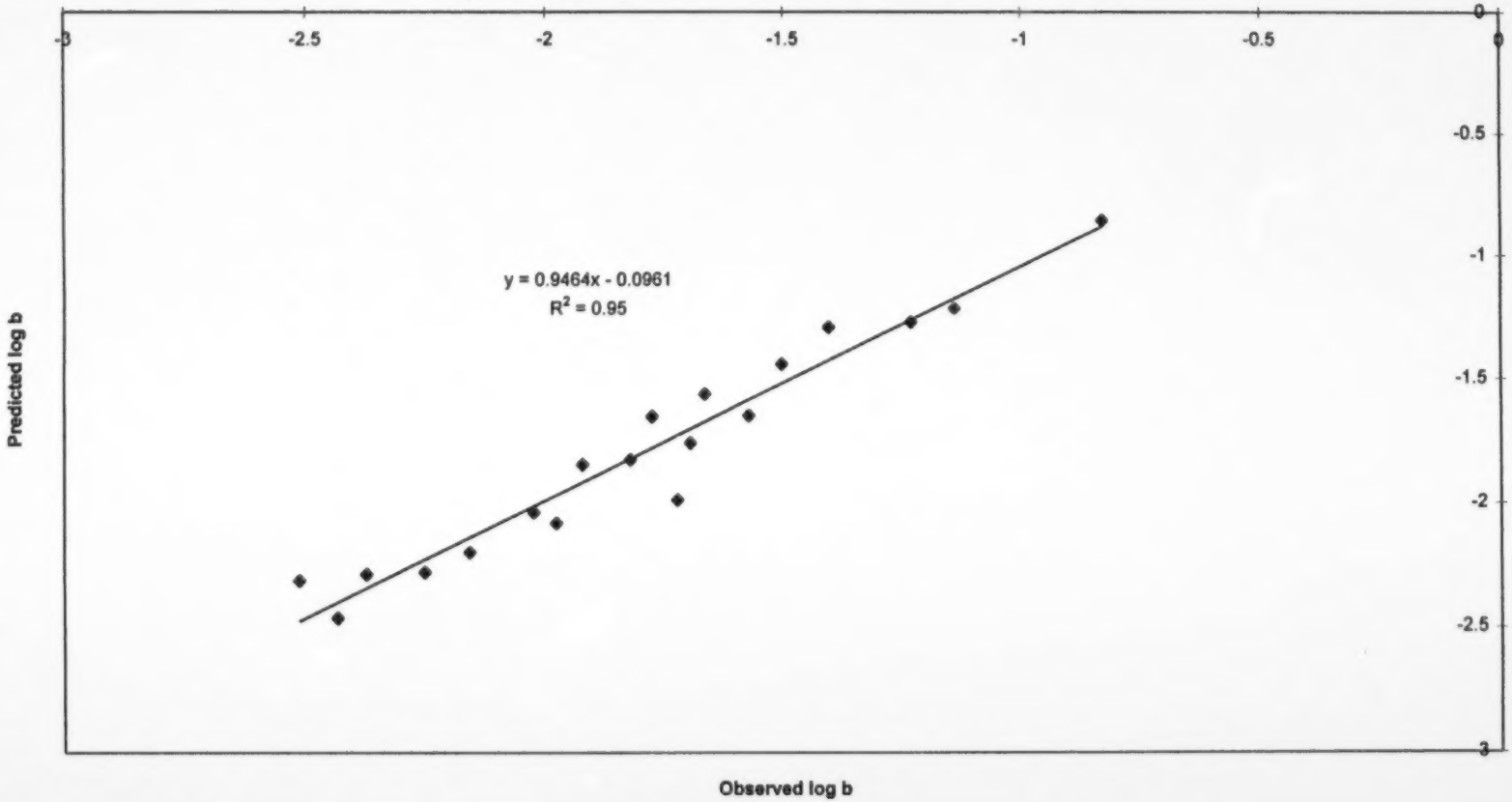

**Figure 8: Predicted log c/b vs Observed log c/b for Batch Test Ozone Decay**

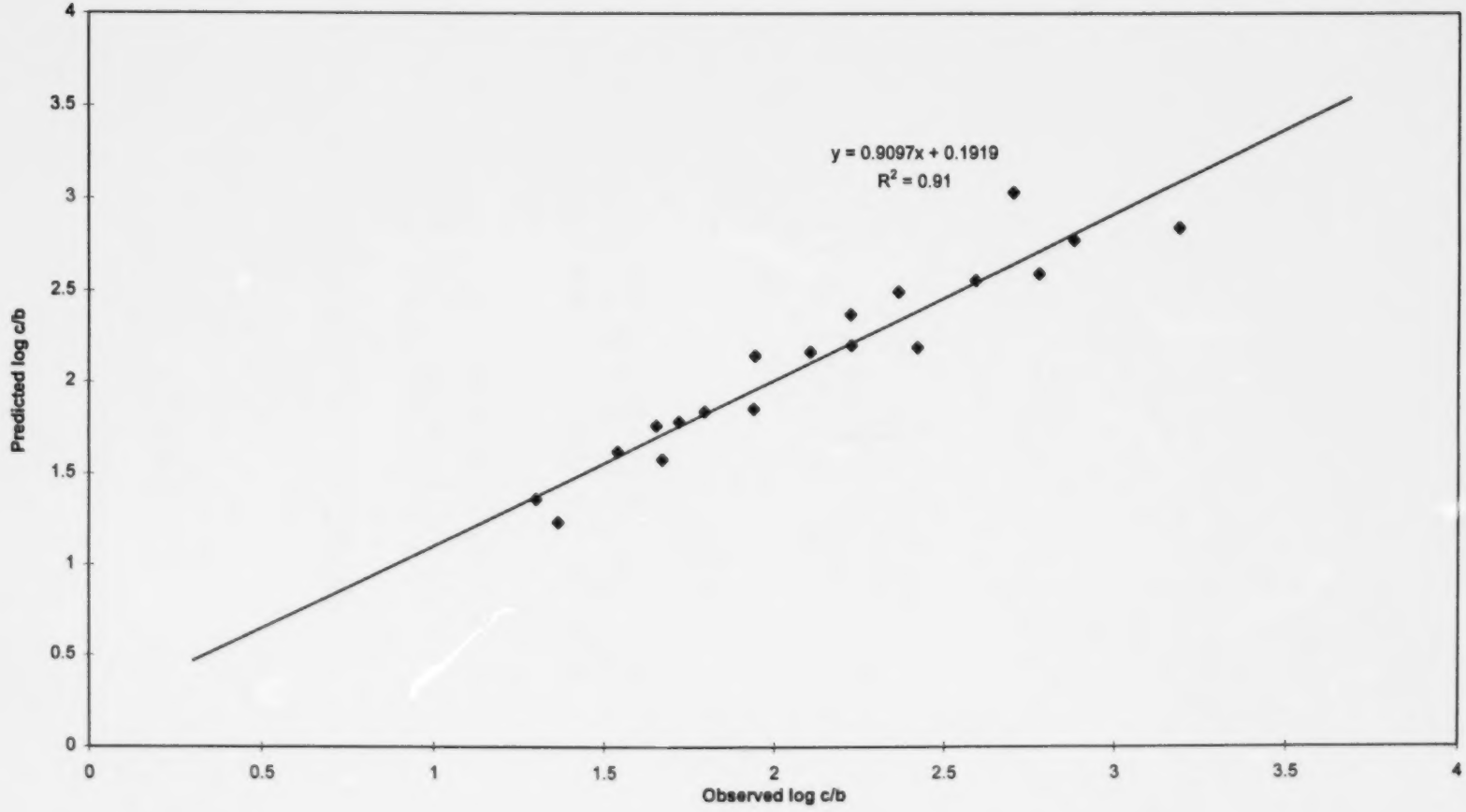

**Figure 9: Typical First Order Plot for the Decay of Ozone in Natural Waters**

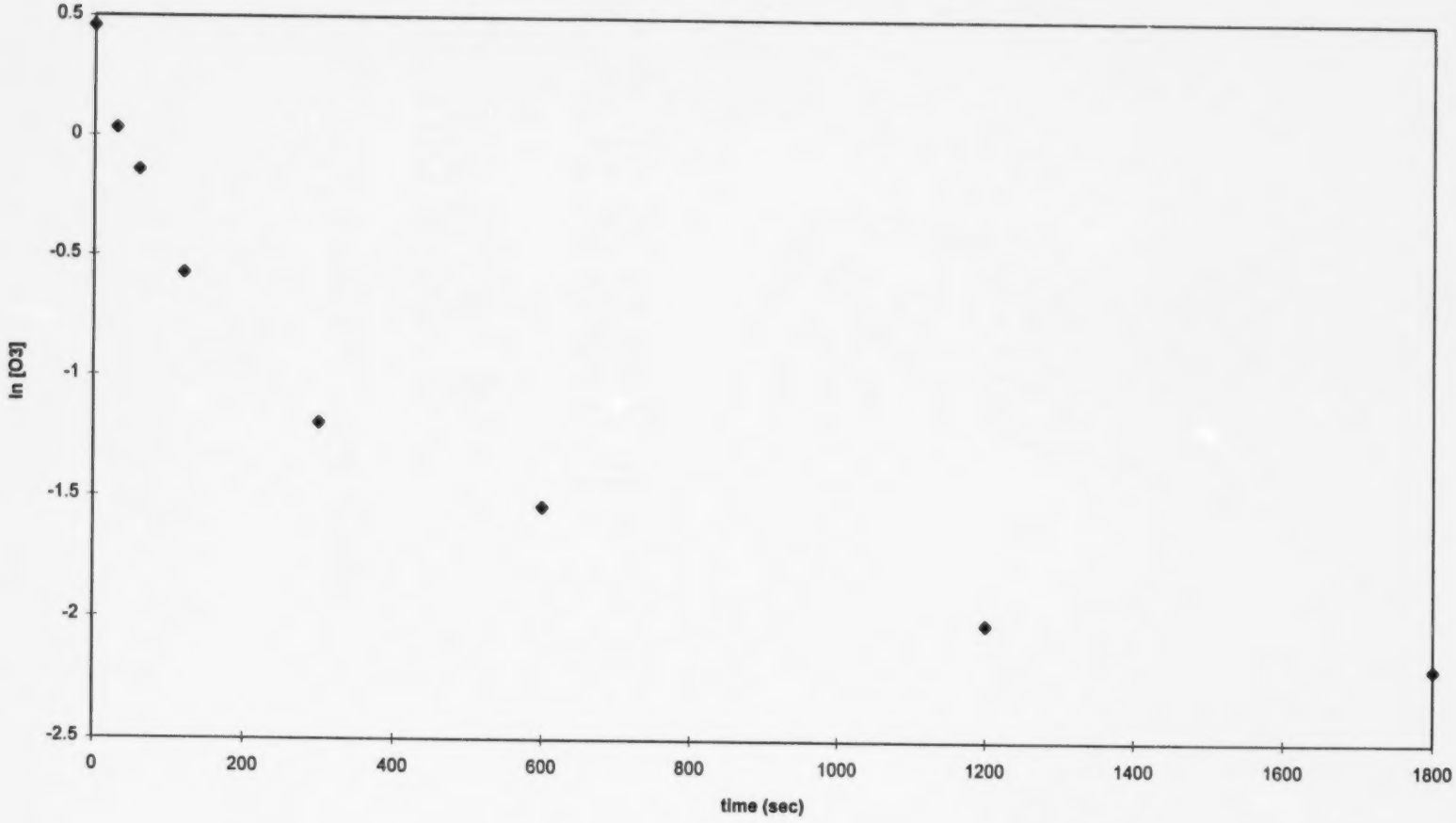

**Figure 10: Typical Second Order Plot for the Decay of Ozone in Natural Waters**

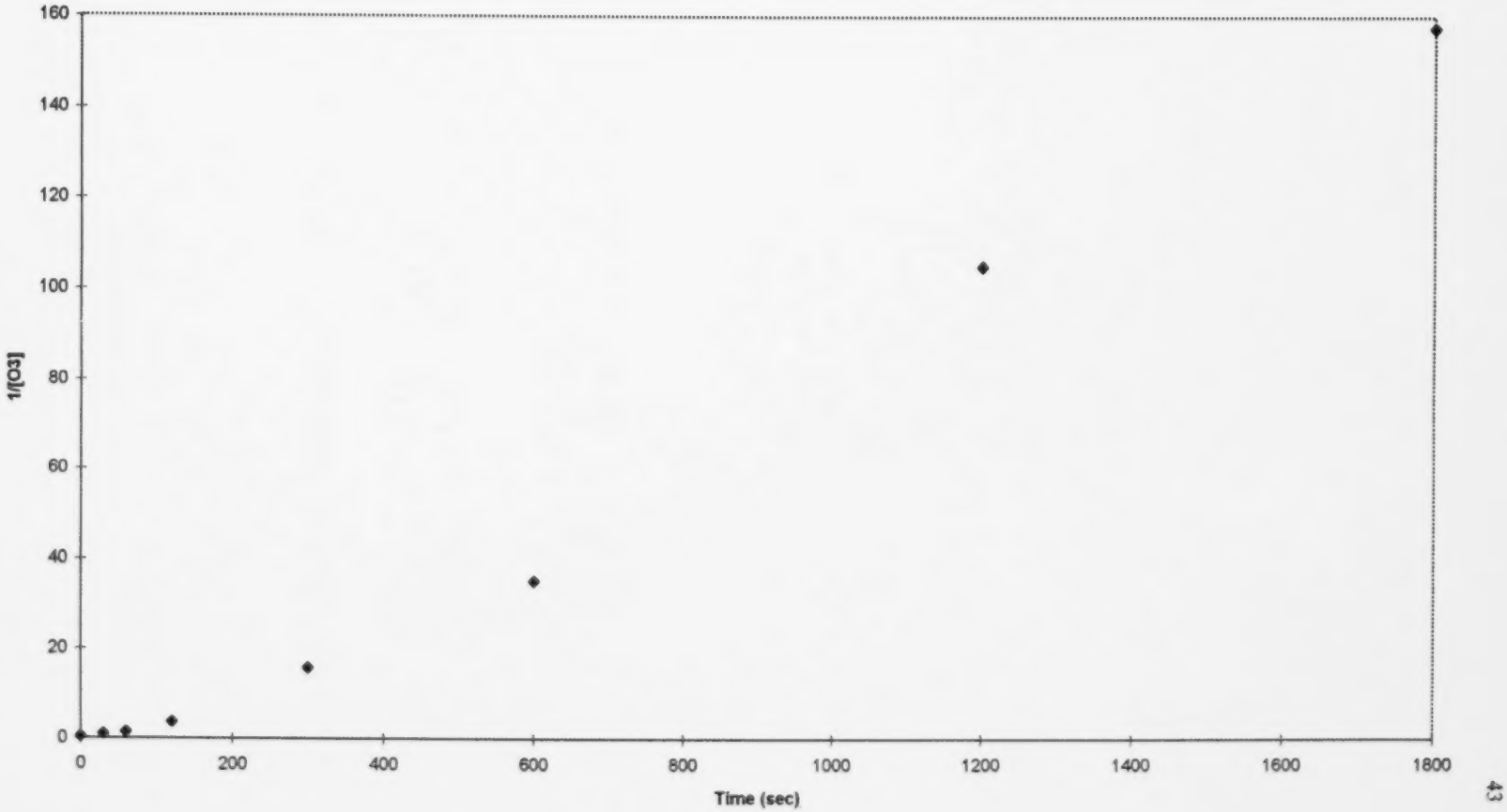

**Figure 11: Rossdale Counter Current Ozone Concentration Profiles: Observations vs. BFCM-Generated**

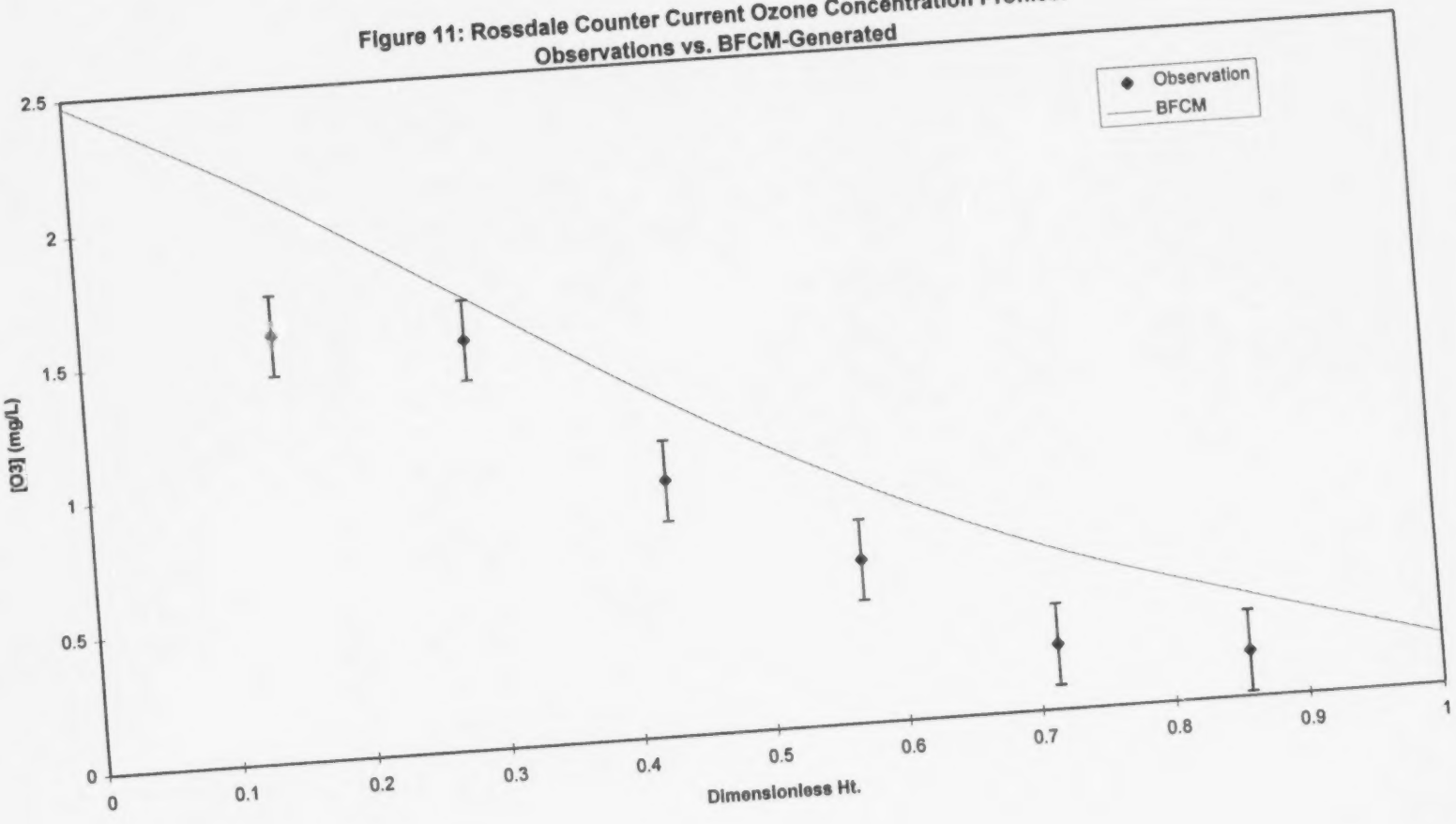

**Figure 12: Red Deer Counter Current Ozone Concentration Profiles: Observations vs. BFCM-Generated**

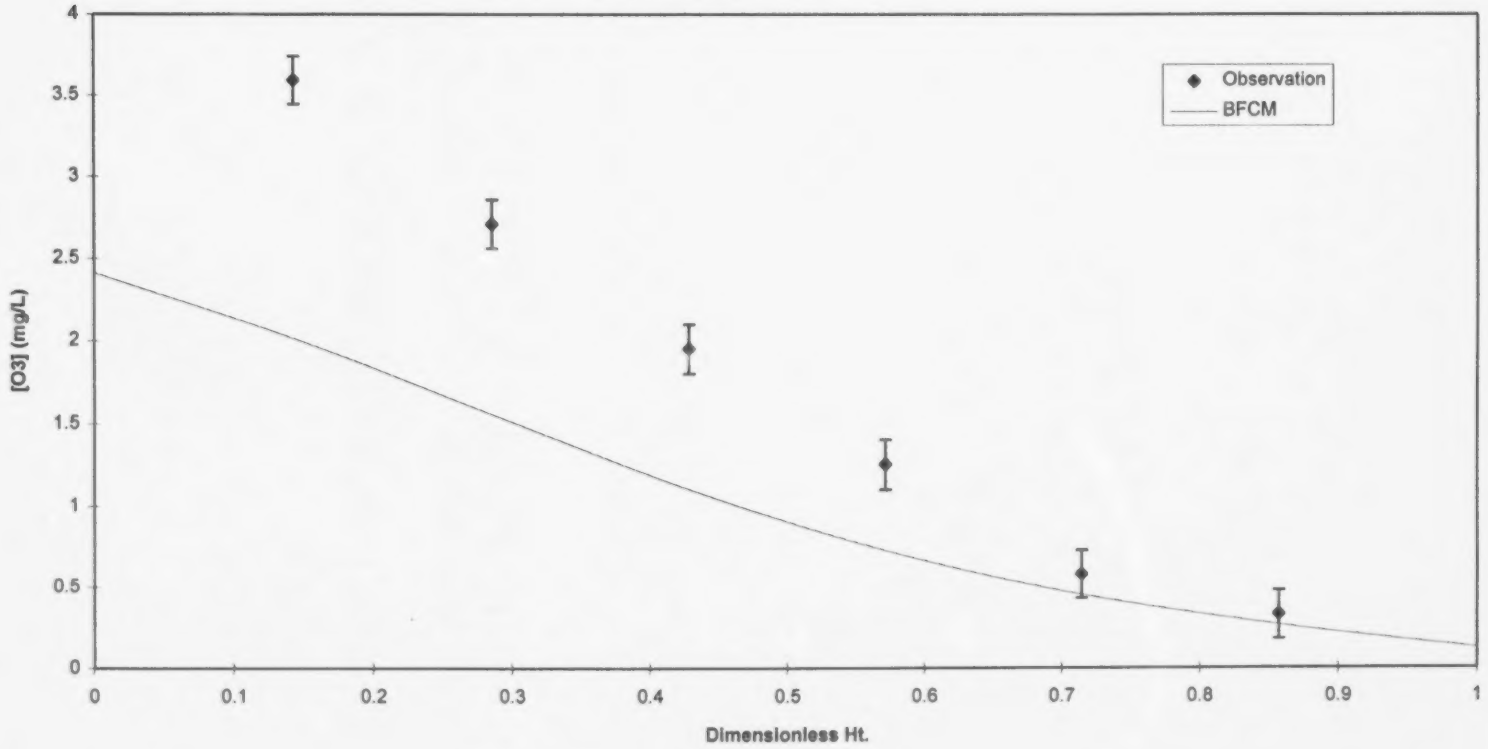

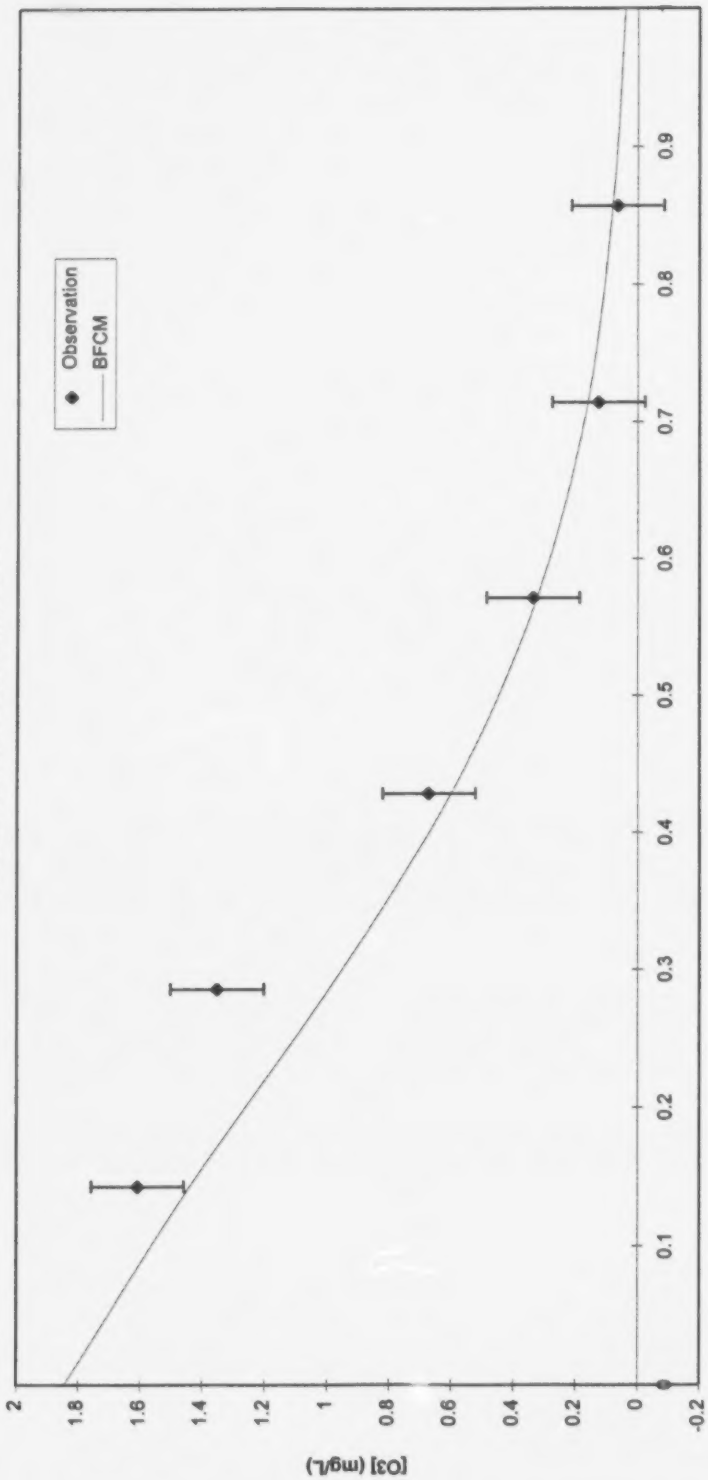


**Figure 13: Hasse Lake Counter Current Ozone Concentration Profiles: Observed vs. BFCM-Generated**

**Figure 14: Wabamun Lake Counter Current Ozone Concentration Profiles: Observed vs. BFCM-Generated**

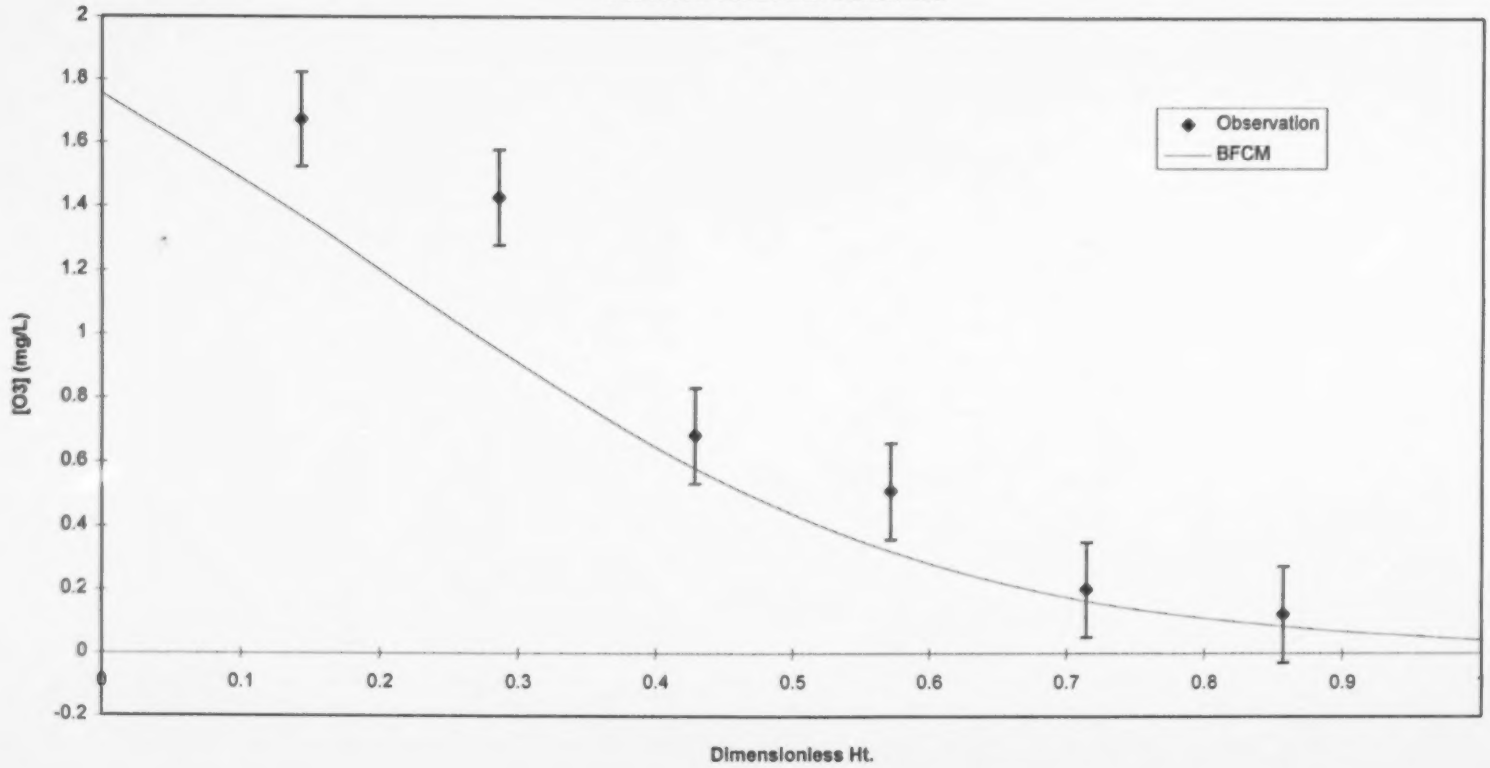

**Figure 15: Driedmeat Lake Counter Current Ozone Concentration Profiles: Observed vs. BFCM-Generated**

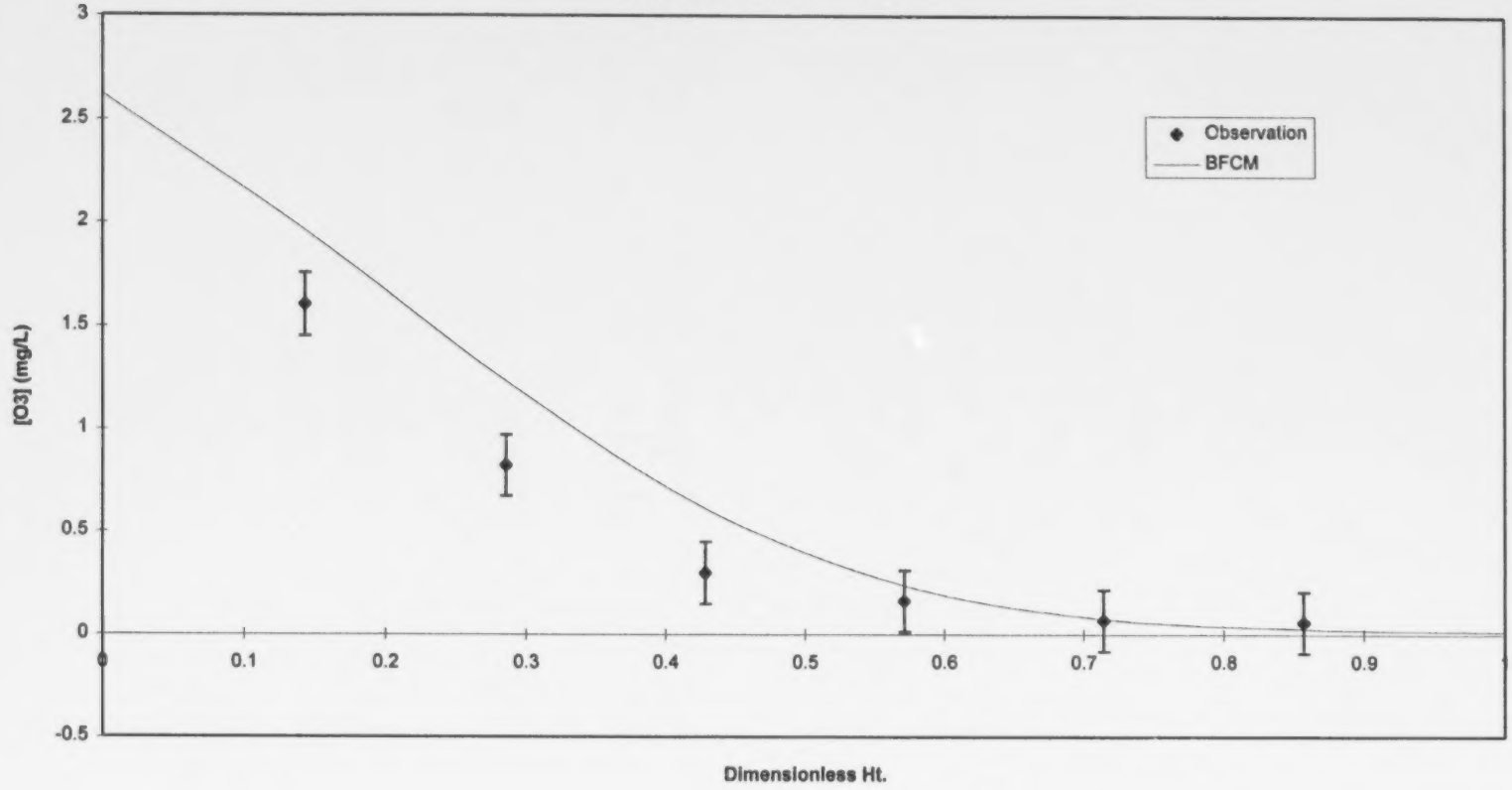

**Figure 16: Rossdale Cocurrent Ozone Concentration Profiles: Observations vs. BFCM-Generated**

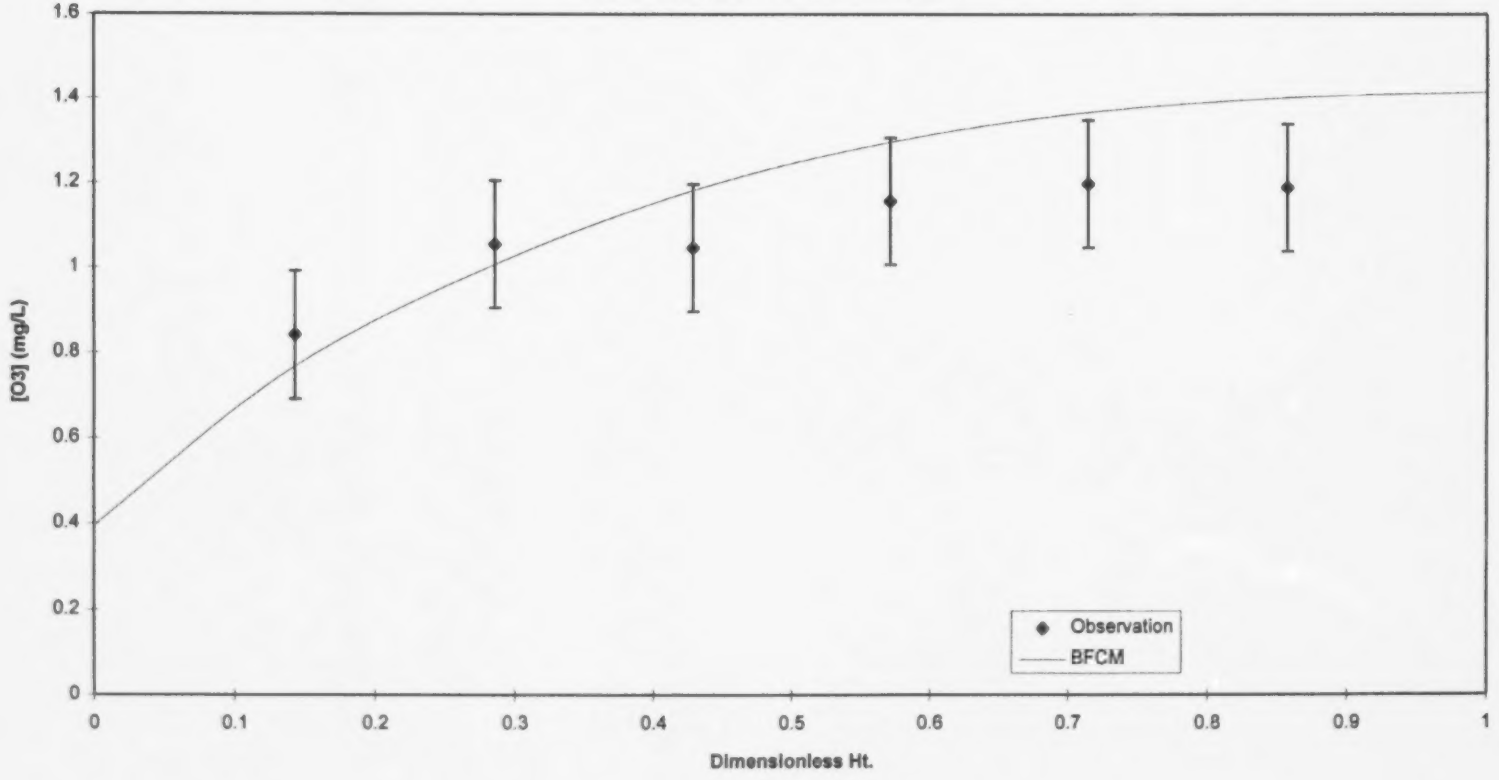

**Figure 17: Red Deer Cocurrent Ozone Concentration Profiles: Observations vs. BFCM Generated**

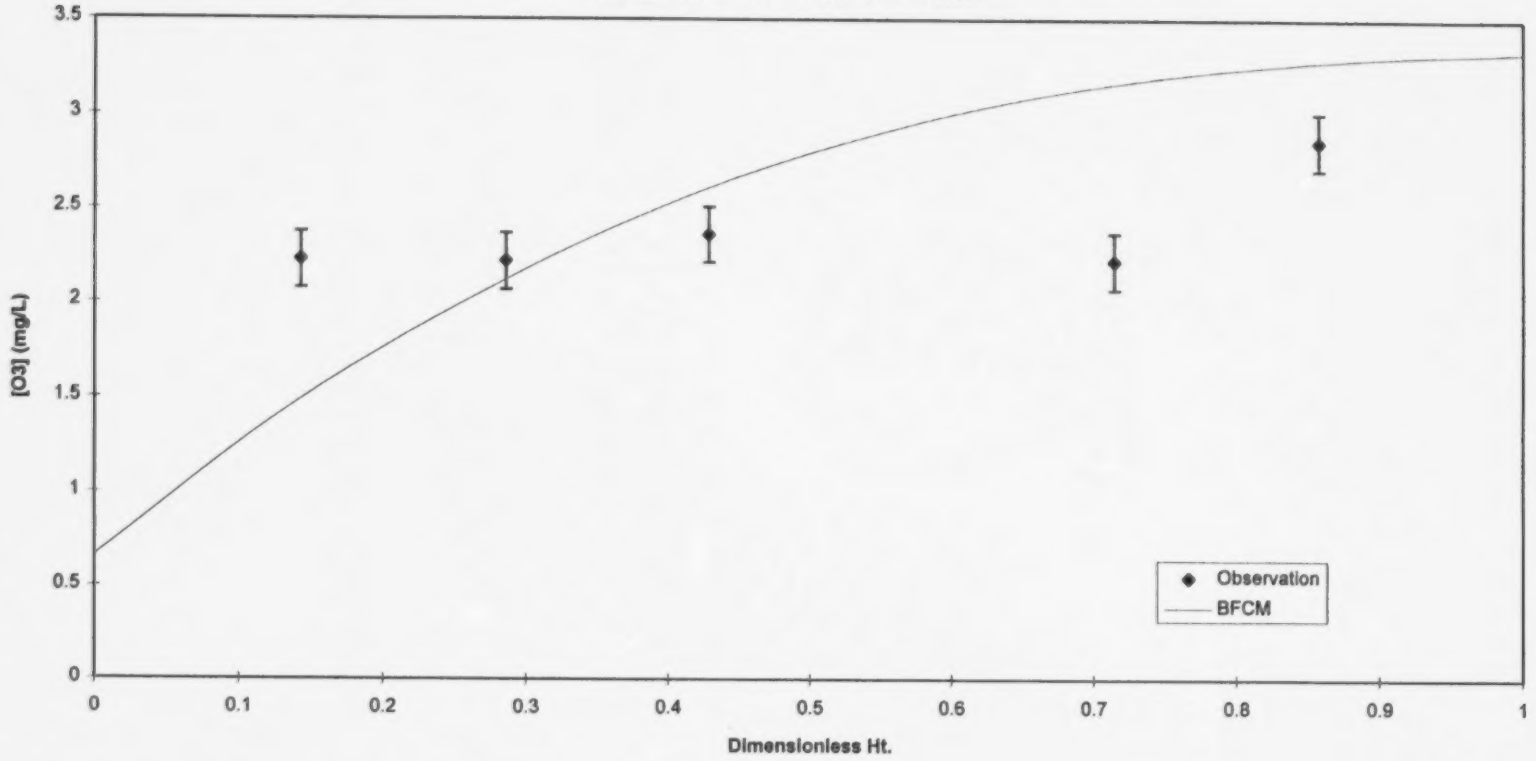

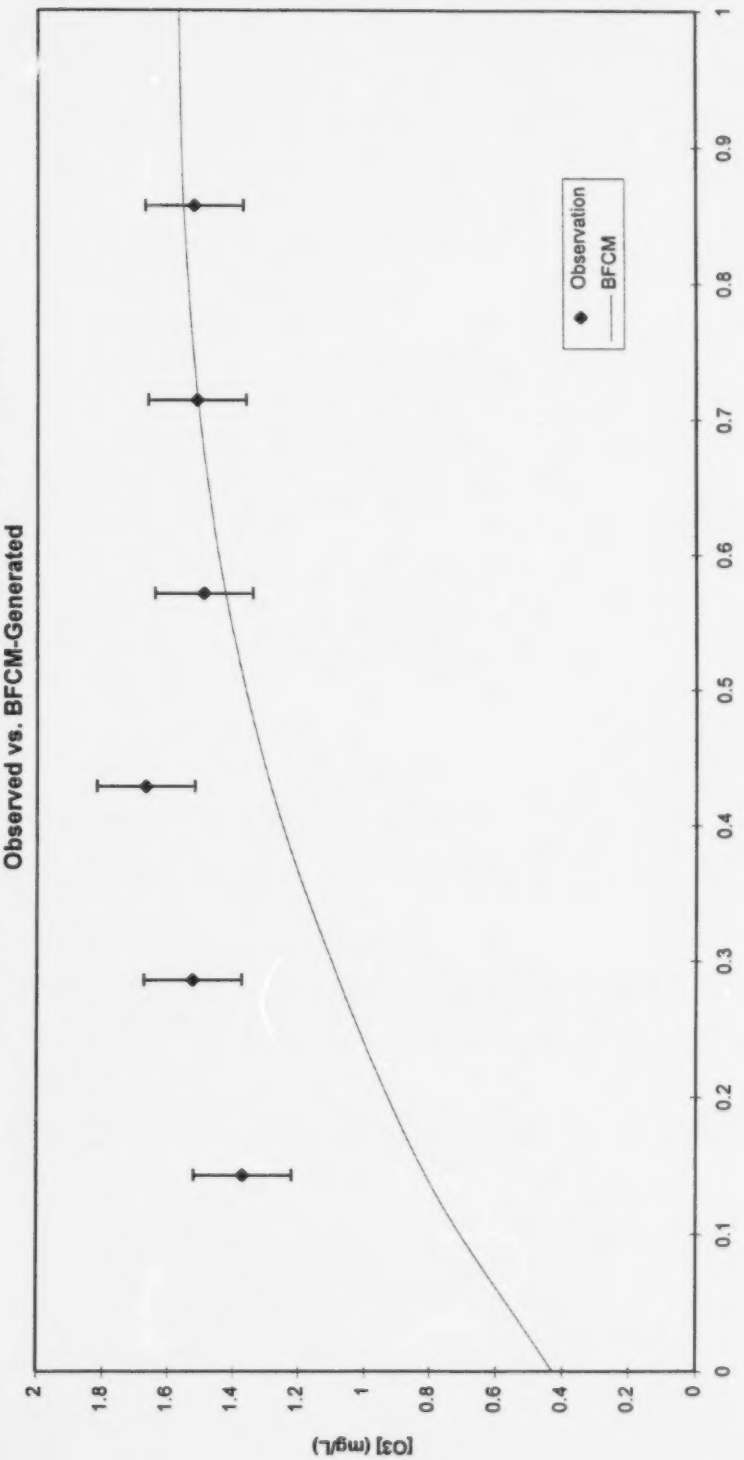


Figure 18: Slave Lake Cocurrent Ozone Concentration Profiles:
Observed vs. BFCM-Generated

**Figure 19: Hasse Lake Cocurrent Ozone Concentration Profiles: Observed vs. BFCM Generated**

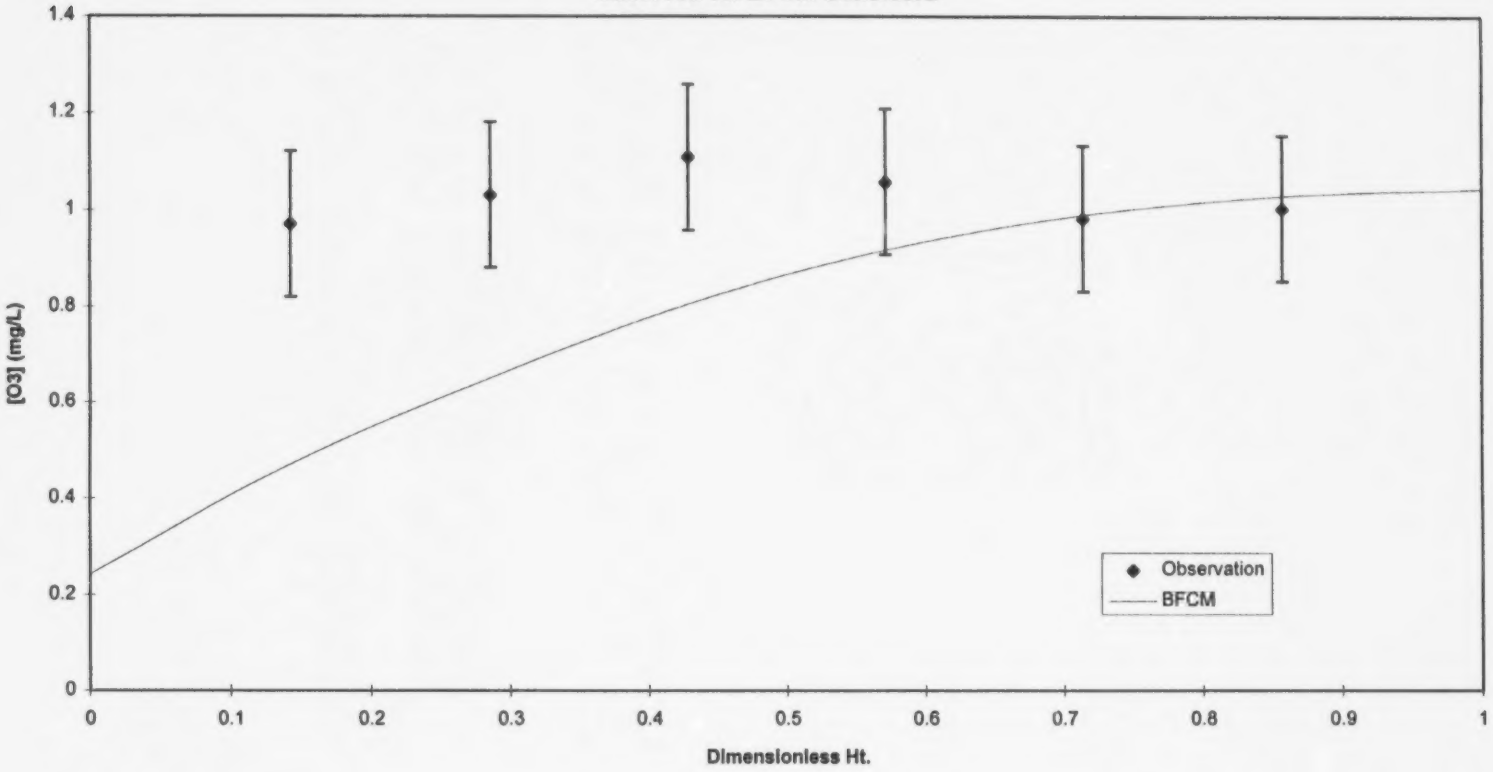

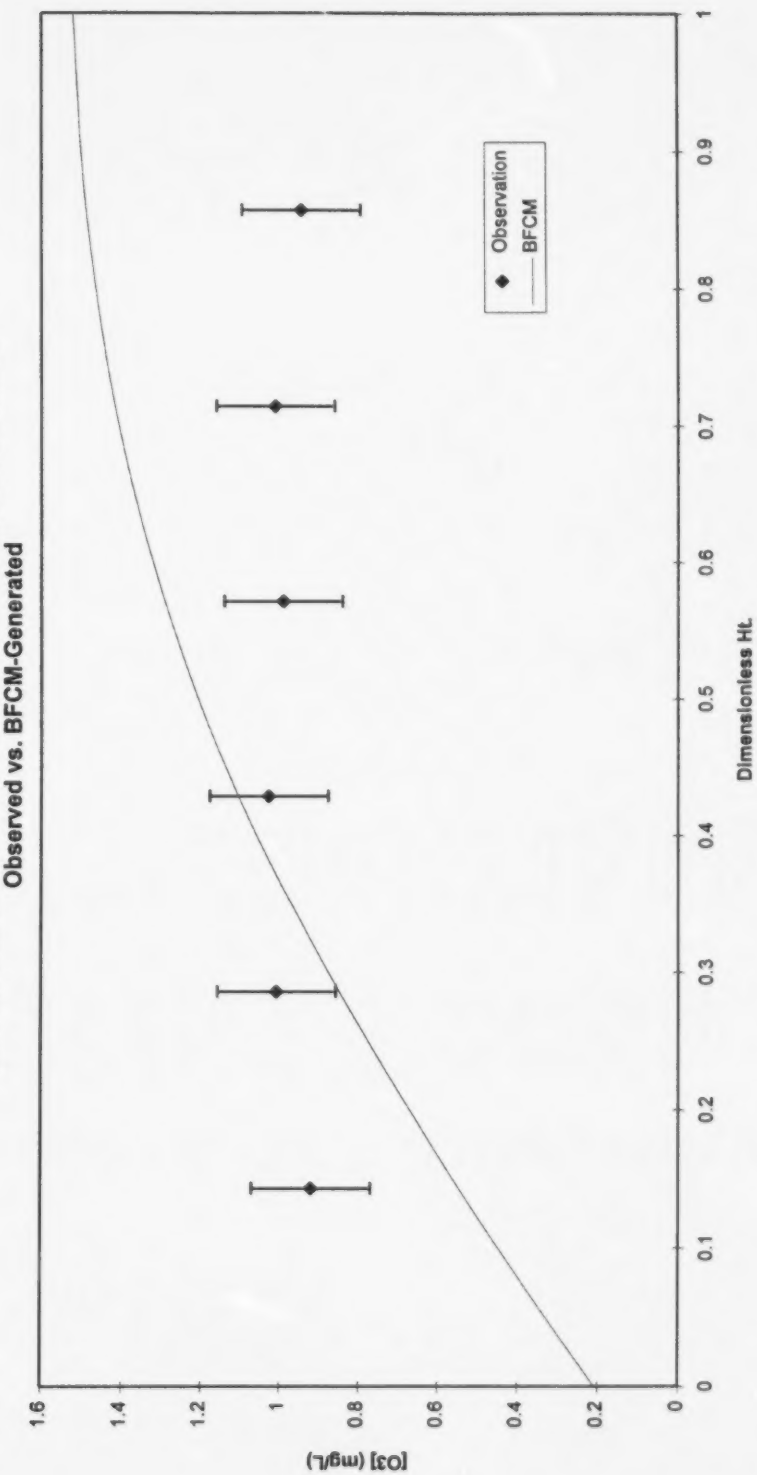


**Figure 20: Wabamun Lake Cocurrent Ozone Concentration Profiles: Observed vs. BFCM-Generated**

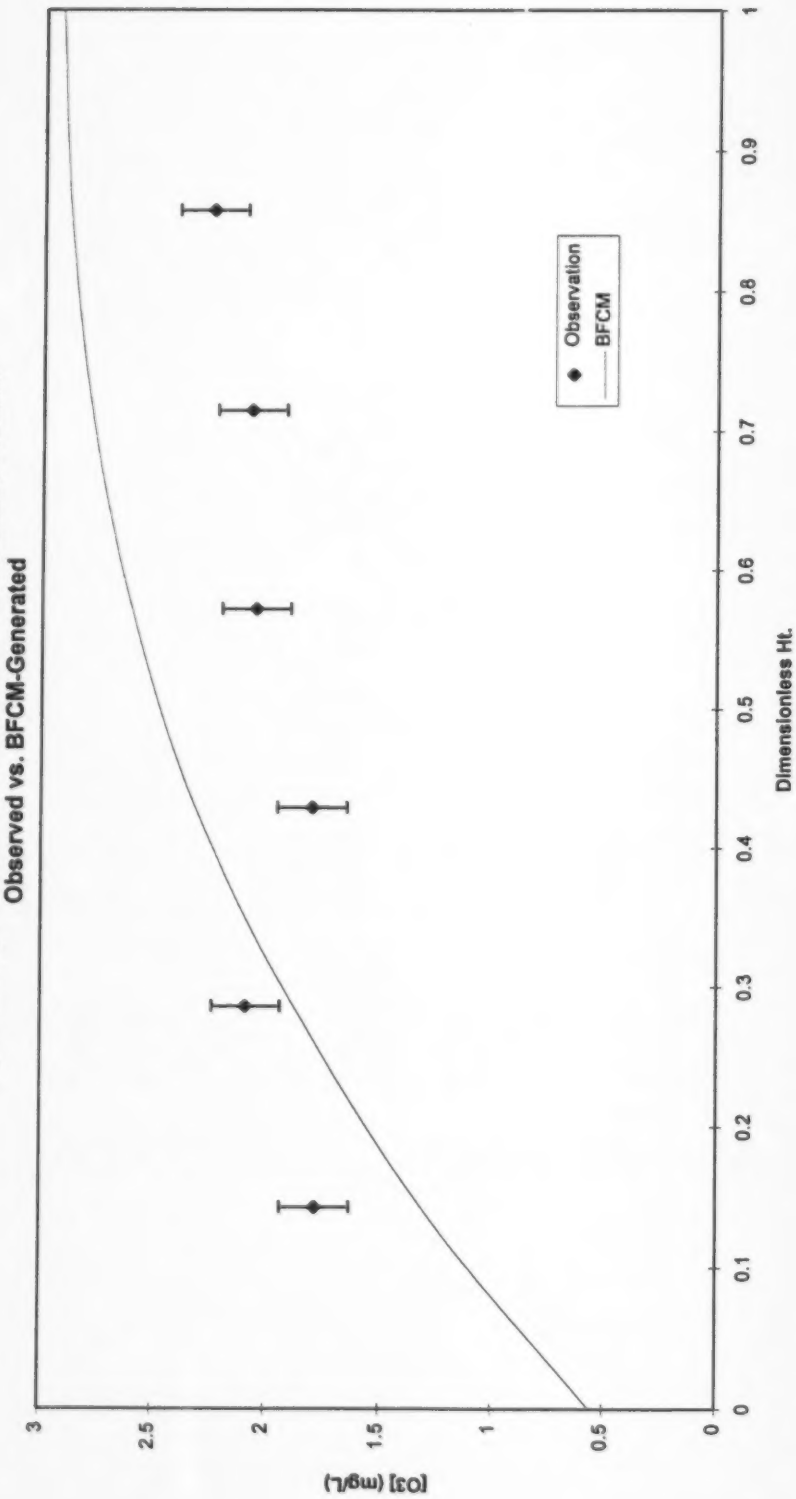


**Figure 21: Pigeon Lake Cocurrent Ozone Concentration Profiles: Observed vs. BFCM-Generated**

**Figure 22: Driedmeat Lake Cocurrent Ozone Concentration Profiles: Observed vs. BFCM-Generated**

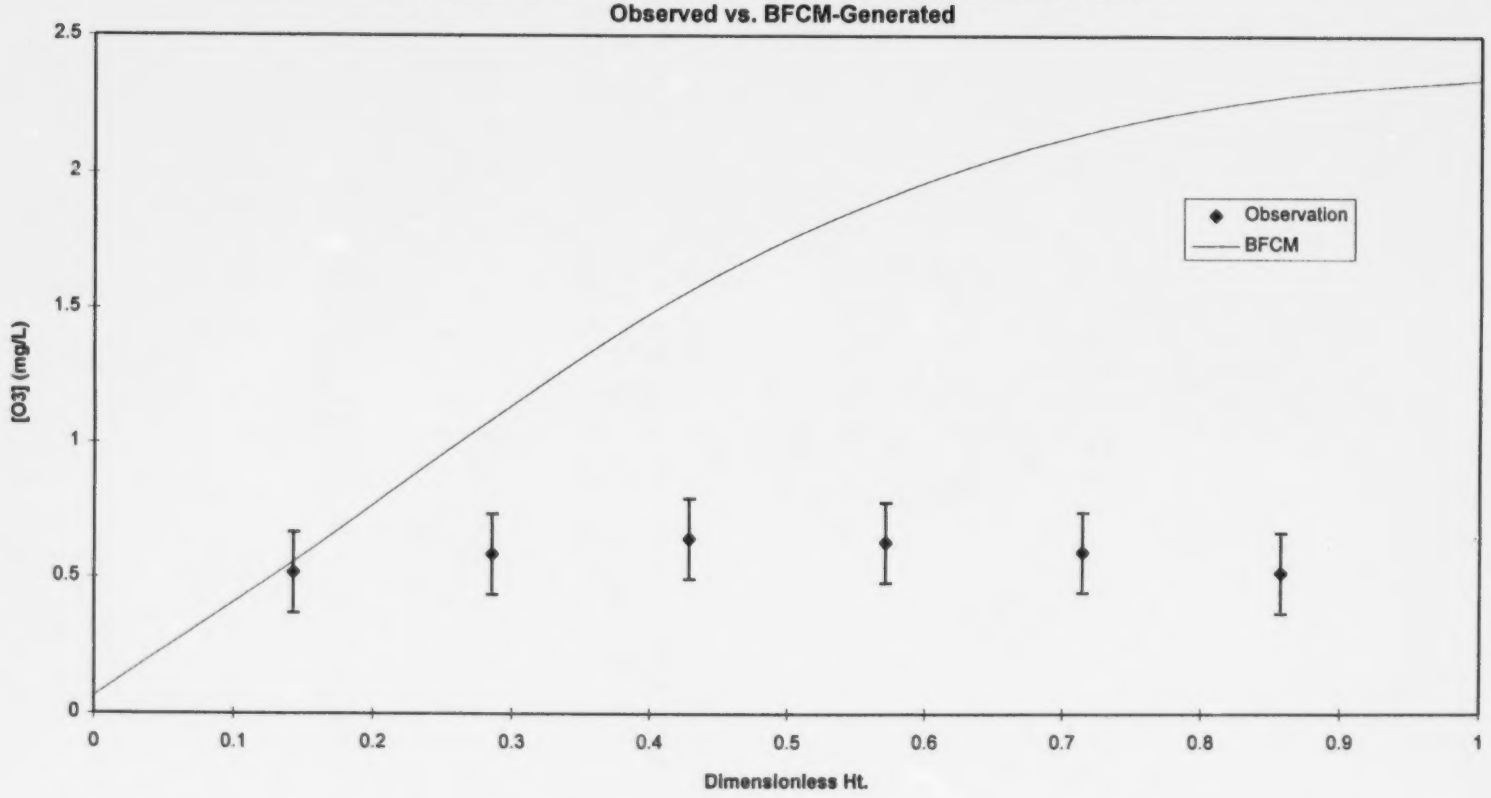

## Discussion

*Bench Kinetics*

As observed in the results from the batch tests involving the ozonation of Milli-Q water, first order kinetics are adequate to describe the decay of ozone in pure water. The straight line yielded by the ln C vs time graph demonstrates this. However, as experience has shown, such simple kinetics are not generally applicable to natural waters containing a multitude of compounds, including highly complex humic and fulvic substances.

Initially, data from the bench-scale tests involving natural water samples were plotted as log $C/C_o$ vs time to test the validity of first order kinetics. Figure 9 demonstrates a typical first order plot. The resultant plots do not support the application of such simple kinetics to the entire decomposition process, although following the initial ozone demand, decay may be approximated as first order. However, as a great percentage of the applied ozone dose is utilized during the initial, rapid decay, using first order kinetics to represent the process in a treatment situation cannot be justified. Second order plots of 1/C vs. t did not yield results any more convincing than first order, as demonstrated by Figure 10.

A function which accounts for the initial, rapid decay but then levels out to approximate first order kinetics is therefore required. The exponential decay equation described by Zhou (1995) allows for a changing specific ozone utilization rate, $k_w$.

$$d(C/C_o)/dt = -k_w(C/C_o) \quad (27)$$

$$k_w = a + be^{-c\Delta O_3} \quad (28)$$

Values of $k_w$ were calculated, for the times at which the samples were taken, by multiplying the slopes of the log $C/C_o$ vs time plots by 2.303 (to account for the plot being log $C/C_o$, rather than ln $C/C_o$). $k_w$ was then plotted against the change in ozone concentration, $\Delta O_3$. Non-linear regression was used to calculate values for "a", "b" and "c" which yielded a best-fit line. $k_w$ vs $\Delta O_3$ plots are included as Figures C-1

through C-19 in Appendix C. The fit is generally good, with the exception of the calculated values of "a".

Inspection of the log $C/C_o$ vs time plots shows a smooth decrease in the magnitude of the value of the specific ozone utilization rate, rapidly dropping initially, but slowing down with greater ozone usage. In natural waters, which contain numerous different compounds all in different concentrations, this trend is logical. On the addition of ozone to the water, individual compounds which react rapidly with ozone will dominate the apparent rate constant, resulting in a rapid decrease in ozone concentration. However, as these fast-reacting compounds are oxidized, compounds which react more slowly with ozone remain, and begin to dominate the overall reaction. The more dominant these slower reacting compounds become, the smaller the magnitude of the rate constant becomes, until eventually, in theory, the utilization rate should approach that of the pure water trials once all organic compounds have been oxidized (assuming other physical characteristics of the water to be similar - pH, temperature, etc.).

*Calculated Values of "a"*

In eight of the 19 batch test sets, the non-linear regressions found the best value of "a" to be zero. It should be noted that a restriction was placed on the regression that the value of "a" must not be less than zero, as this would imply the production of ozone. This was not an expected result. Theoretically, it would be expected that the value of "a" would tend towards the first order rate constant for the decay of ozone in pure water, as that would be similar to the case once all natural organic matter had been oxidized (although some contribution from the inorganic reaction products would be expected). The answer to this may lie in the fact that the hypothesized equation for the change in specific ozone utilization rate is not perfectly fitted to the actual kinetics taking place. Another possibility is the influence of points

of low ozone concentration on the regression. Due to limitations of the indigo method, ozone concentrations below 0.01 mg/L are not considerred reliable. Observing the $k_w$ vs $\Delta O_3$ plots (Figures C-1 through C-19), it is noted that, in cases where there exists a high concentration of oxidizable material in the batch sample (most of the 0.75 and 0.50 dilution samples), the $k_w$ values take a sharp concave down curve at high $\Delta O_3$ values, generally at a point before a consistent $k_w$ value has been reached. This implies that it was the organic compounds present in the waters which were in excess, and not the applied ozone dose, which would have allowed a more reliable estimate of the kinetic parameter to be determined. It may be pointed out that by diluting samples to the point where this will cease to pose a problem, one would be reducing organic material concentrations below what would normally be found in water treatment scenarios, and thus the applicability of such a study is diminished. However, in order to gain a better understanding of the kinetics involved in any situation, it may be necessary to start with a scenario that can be adequately monitored before moving to a more realistic set of conditions. In this case, data from the more concentrated samples were truncated at a point before the downward curve began, and the non-linear regressions performed on what remained.

*General Effects of Kinetic Parameters*

Figures 23 through 25 depict the effects of changing the parameters "a", "b" and "c" on the ozone utilization rate as it changes with the amount of ozone utilized. Figure 23 shows the effects of changing the value of "a". In the examples shown, the values of "b" and "c" are held constant at 1.0 and 3.0 respectively, while the value of "a" is decreased from 0.20 to 0.00 in steps of 0.05. One can see that for every increase in the value of "a", the entire curve is shifted up by that value, resulting in higher utilization rate constants at all points. Theoretically, with a high enough ozone dose that all organic matter is oxidized before the ozone is depleted, the value of "a"

represents the final rate constant associated with the auto-decomposition of ozone without the presence of natural organic material, as in the case of the Milli-Q water.

The effects of changing the value of "b" are demonstrated in Figure 24. The values of "a" and "c" are held constant at 0.0 and 3.0 respectively, while "b" is assigned values of 3.0, 2.0, 1.0, 0.5, and 0.05. The effect of increasing the value of "b" is to increase all points on the curve by a factor equal to the ratio of the successive values of "b". For example, by changing the value of "b" from 1.0 to 2.0, all points on the curve would be increased by a factor of 2 (=2.0/1.0) (taking into account that if "a" is greater than 0, the entire plot will be shifted up). The lower the value of "b", therefore, the less the magnitude of the change in $k_w$ with increasing amounts of utilized ozone, and the flatter the curve. The initial value of "b", when added to "a", will yield the initial value of $k_w$ (ie. the value of $k_w$ before any ozone has been used). Higher values of "b" will be associated with water samples containing compounds which react very fast with ozone.

Changing the value of "c" while holding "a" and "b" constant (0.0 and 1.0 respectively) yields the set of curves presented in Figure 25. By increasing "c", the value of $k_w$ decreases towards its eventual asymptotic minimum ("a") at a much faster rate initially, yielding a steeper curve which bottoms out sooner than a curve with a lower value of "c". A higher value of "c" for a natural water would correspond to a low concentration of high oxidation rate compounds, which therefore are destroyed much faster leading to the rapid decrease in reaction rate associated with the steep initial slope.

*Solids Data*

Inspection of the gravimetric analysis data obtained for all of the water samples indicates that significant errors were present. Negative values were encountered for some measurements in all categories except for total solids (TS). The most likely

origin of the errors was the drying process. It is possible that either drying was incomplete or that atmospheric moisture contaminated the filters following drying, although filters were stored in a dessicator prior to weighing. Another potential error source was the vacuum filtering process. While the filters were each washed and oven-dried prior to use, glass fibres may have become detached from the filters and washed into the filtrate, thus decreasing the apparent suspended solids load, and increasing the apparent dissolved solids. If, in fact, the problem did lie in the filtration step, then the only measurements that can be considered reliable are the total solids and total volatile solids, as these are the only two measured parameters that do not involve filtration in their determination methods. Therefore, for the purposes of linear regression, only the TS and TVS were considered as possible influencing parameters in the determination of ozone decay kinetics.

*High $d[O_3]/dt$*

Due to physical experimental limitations, the earliest that a second sample could be taken during batch testing was after 30 seconds. In some cases, by this time the ozone concentration had already reached very low levels at which the rate of its decomposition was relatively slow and slow to change (the nearly horizontal portion of the decay curve). In these situations, it becomes impossible to accurately interpolate the decay curve between sample points for times less than thirty seconds. As a result, slopes cannot be determined for the first two sample times. It could not be considered reliable to base the non-linear least squares curve-fitting procedure on the decay rates at the remaining sample points due to the minimal differences between different waters in this portion of the curve. For this reason, all of the results from Miquelon Lake and Driedmeat Lake were discarded for the purposes of the linear regression analysis.

*Regression Fit*

In performing the linear regressions to generate the parameter estimation equations, a stepwise reduction of variables approach was used. Regressions were performed starting with all available variables being used. After each regression, the least significant variable was removed, and another regression performed, until all variables remaining were judged to be significant. By removing each variable, a very small reduction in the $R^2$ value was observed, but at the same time, a greater simplicity in the resulting equation was achieved. The final parameter estimation equations are judged to be a good tradeoff between the accurate prediction of the parameters in question, and simplicity in terms of the number of variables included. The final equations for both log b and log c/b yield $R^2$ values of greater than 0.90, indicating that a good fit has been obtained.

*Effects of Water Quality Parameters on Ozone Decay Kinetics*

Examining equations 25 and 26 on page 37, the effects of the various physical properties of a water sample on the ozone decay kinetics can be inferred. It is observed that the value of "b" increases with increases in temperature, pH, TOC, carbonate ion concentration, UV absorbance at 254 nm, and total solids concentration. As increases in "b" lead to increases in the ozone utilization rate, the only one of these relationships which comes as a surprise is the carbonate ion concentration dependence. All of the available literature points to carbonate ion as being an inhibitor of ozone decay, acting as a radical chain terminator, and therefore one expects to see increases in its concentration having a negative effect on ozone decay rates. However, it is possible that the carbonate ion may be interacting with another parameter to cause the increase. Inspecting the equation regarding the value of "c", it is observed that "c" is increased by increases in bicarbonate ion concentration and the magnesium hardness, while it is decreased with increases in the pH, total organic carbon and calcium hardness. As increases in "c" lead to faster decay of the ozone utilization rate,

parameters that increase the value of "c" will, in effect, decrease the rate of ozone consumption. Hence, we see the expected inhibitory effect of bicarbonate ions, and the promotion of ozone decay by higher pH values and TOC levels, all of which are expected.

It should be noted that the overall effect of the pH to increase the rate of ozone concentration decay is due to the combined effects of increasing the number of hydroxyl radicals available to initiate the free radical chain reaction, and the increase in deprotonation of organic compounds, leading to an enhanced nucleophilicity of their reaction sites, and hence faster reactions.

*Pilot Testing*

*General Effects of Kinetic Parameters on Generated Profiles*

To demonstrate the effects of changing the kinetic parameters "a", "b" and "c" on both countercurrent and cocurrent back flow cell model output, model runs were performed using the same test values as were used for the batch test demonstration. For these model tests, other parameters (backflow ratio, flow rates, etc.) were set to those used in the Rossdale pilot tests. By understanding what effects changing these parameters has on the model output, this knowledge can be used to help analyze the actual model output for the pilot tests conducted, and to compare the model output to the empirically observed data.

Figure 26 depicts the effect of changing the value of "a" on the model-generated countercurrent profile. Increasing the value of "a" from 0.00 to 0.20 in steps of 0.05, the greatest effect is observed in the dissolved ozone concentration at the column outlet (z=0).Very little effect is observed near the inlet (z=1), but near the column midpoint, the profiles are observed to diverge sharply. Near the inlet "a" is observed to have very little effect, as the magnitude of its contribution to the specific utilization rate is very small. However, as the utilization rate decreases with increasing

utilized ozone, the value of "a" becomes much more significant. Near the column outlet, profile #1 ("a" = 0.00) shows a large ozone concentration, as $k_w$ has dropped to almost zero. However, in profile #5 ("a" = 0.20) the larger $k_w$ value leads to a much lower ozone concentration.

In Figure 27, the effect of different "b" values on countercurrent concentration profiles is investigated. With "a" and "c" set at 0.0 and 3.0, respectively, the value of "b" was set at 0.05, 0.5, 1.0, 2.0 and 3.0. With increasing "b", the profile is observed to shift to lower concentrations of dissolved ozone, as would be expected with the higher rate of ozone decay associated with "b". There is a difference in the inlet concentration observed, associated with the large difference in initial decay rates. By approximately the 2/3 point in the water's travel through the column (z=0.4) we observe the profiles to be well separated, but running approximately parallel to each other. By this point, the rate of ozone dissolution far exceeds the rate of decay ($k_w \sim 0$), and therefore we are observing the concentrations increasing linearly due to the large concentration gradient (high gas concentration and relatively low liquid concentration). In a taller column, one would expect to observe these aqueous concentrations to level off again, as they approached the equilibrium concentration (based on the Henry's Law constant and the feed gas ozone concentration).

Figure 28 shows the effects of "c" on countercurrent profiles by maintaining "a" and "b" at constant values (0.0 and 1.0 respectively) while "c" is varied from 5.0 down to 1.0 in steps of 1.0. All five profiles start with very similar inlet concentrations, although there is a small difference due to the contribution of backmixing. The profiles are observed to diverge almost immediately, as profile #1 ("c" = 5.0) curves up rapidly, while profiles with successively smaller values of "c" bend less sharply and appear to do so further towards the bottom of the column. As was seen in Figure 25, "c" controls how rapidly the utilization rate decreases. Therefore, we can link the

lower profile concentrations with the higher utilization rates caused by low values of "c".

In Figure 29, the effect of "a" on cocurrent profiles is examined. Keeping "b" at 1.0 and "c" at 3.0, a is assigned values of 0.0, 0.05, 0.10, 0.15, and 0.20. The profiles show decreasing concentrations with increasing values of "a", as is expected with the higher decay rates associated with higher "a" values. However, whereas in profile #1 ("a" = 0.0) the dissolved ozone concentration is observed to continue increasing right to the column outlet, the other profiles show the concentration attaining a maximum before declining towards the top of the column. In cases where "a" imparts a significant decay rate, even after large quantities of ozone have been utilized, the decay rate may exceed the rate at which ozone transfers from the gas phase, leading to a net decrease in concentration. The decreased rate of ozone dissolution is due to the lower concentration gradient near the top of the column, where ozone content in the gas phase has been depleted near the column bottom. The larger the value of "a", the closer to the bottom of the column the net aqueous concentration is observed. This phenomenon is not observed in the countercurrent configuration due to the reversal of water flow direction, which brings gas with a high ozone concentration into contact with water near the end of its residence time in the column, thus keeping the concentration gradient between gas and liquid phases high.

The effects of different values of "b" on cocurrent profiles are shown in Figure 30, in which "b" is varied, while "a" and "c" are held constant at 0.0 and 3.0, respectively. With increasing values of "b", the concentration profile is observed to drop. The profile curvature is also observed to decrease, while the inlet concentration can be seen to drop dramatically. By increasing "b", the utilization rate is increased at all points, as observed in Figure 24, leading to the decrease in ozone concentration.

Figure 31 depicts the effects that changing the value of "c" has on cocurrent concentration profiles. By decreasing the value of "c", the concentrations are observed

to decrease throughout the column, very minimally at the inlet, while to a much greater extent at the outlet. By the time "c" is given a value of 1.0 (profile #5), the profile is observed to attain a maximum value before starting to decrease, similar to the situation in Figure 29, when the value of "a" was increased. The reasons are similar, in that with a low value of "c", the utilization rate remains higher for a longer period, reaching the point where utilization becomes greater than dissolution in column regions where the concentration gradient between gas and liquid phases is reduced due to prior removal of ozone from the gas phase through dissolution in the lower regions of the column. Very little difference is seen in the profile concentrations at the inlet, because very little ozone has been utilized by this point, and hence the effect of "c" has not yet been manifested.

*Instantaneous Concentration Jump at Column Inlet*

In all profiles, both cocurrent and countercurrent, a concentration jump is observed at the column inlet. This was discussed by Zhou (1995) who states that the jump is a function of the backmixing taking place in the column. In an ideal plug flow situation, there would be no such jump, as water, on immediately entering the column could have had no opportunity to contact ozone-containing gas. However, with the addition of backmixing to the scenario, a fraction of water from further up the column, where it has had an opportunity to contact ozone-containing gas, is recycled back down towards the inlet, carrying any dissolved ozone with it, and thus yielding a measurable ozone concentration at the inlet. By increasing the amount of mixing in the column, and therefore increasing the backflow ratio, the concentration jump will become larger. Other effects of increasing the backflow ratio include the flattening of profiles, until profiles become a horizontal line at the extreme of complete mixing in both cocurrent and countercurrent configurations. In cocurrent flows, while the inlet concentration increases with increasing mixing, the outlet concentration does not

change. For countercurrent configurations, the inlet concentration increases, while the outlet concentration is observed to decrease. It should be noted that Zhou (1995) obtained these results for situations assuming first order kinetics, but the fundamental principles should still apply.

*Analysis of Individual Profiles*

**Rossdale Countercurrent Profile (Figure 11):** The BFCM-generated profile for this sample yielded a relatively good fit with the experimentally observed data. However, it appears that the inlet concentration is slightly high, and that the concentration begins to rise too early. Both of these problems could be explained by a "b" value that is slightly low. The predicted outlet concentration does not take into account the well-pronounced concave-down curve that appears near the bottom of the column in the observed data. None of the figures depicting the effects of kinetic parameters can explain this feature. However, in some of Zhou's profiles (1995), this feature is evident. This may be due to the fact that Zhou's theoretical liquid height was 5.0 m, allowing the aqueous ozone concentration more time to approach its equilibrium concentration. This is not believed to be the case here, as the equilibrium concentration, given the feed gas concentration used for this sample, was 5.92 mg/L, almost a factor of 4 greater than the concentration involved.

**Red Deer Countercurrent Profile (Figure 12):** The Red Deer countercurrent profile appears to estimate the inlet concentration very well, but gets progressively worse, underestimating the concentration towards the column bottom. Comparing the plot to Figure 28, it appears that the main problem is an overestimation of "c". By decreasing the value of "c", the inlet concentration would remain virtually the same, but would increase the slope of the profile right through to the outlet.

**Hasse Lake Countercurrent Profile (Figure 13):** The calculated profile appears to predict, with very good accuracy, the actual profile generated by the experimentally observed concentrations. Between the dimensionless column heights of 0.45 and 0.0, there does seem to be a slight underestimation of the concentration, but the outlet concentration appears to be very close. Again, there appears to be a slight concave-down curvature of the observed profile near the bottom of the column that is not reflected in the model profile.

**Wabamun Lake Countercurrent Profile (Figure 14):** The computer generated profile for the Wabamun Lake countercurrent sample underestimates the dissolved ozone concentration throughout the entire height of the column. However, near the top of the column, the difference is minimal, and the outlet concentration appears to be a good approximation, based on visual extrapolation of the observed data points. However, in the lower half of the column, the model fails to account for a relatively rapid rise in concentration, which then appears to level out once again as it nears the outlet. In general, however, the model provides a good fit.

**Driedmeat Lake Countercurrent Profile (Figure 15):** Near the inlet, the model provides a very accurate representation of the concentration profile. Near the $z$=0.6 point, however, the model starts to overestimate the profile concentrations by an apparently constant difference through to the column outlet. The model profile appears to run parallel to the observed data points, indicating that the most likely problem is either an underestimated value of "b", or possibly a slightly overestimated value of "c" (see Figures 27 and 28).

**Rossdale Cocurrent Profile (Figure 16):** The BFCM-generated profile provides a relatively good fit with the observed data for this sample. The model does slightly underestimate the concentrations in the bottom third of the column, and then slightly overestimates concentrations in the top two-thirds. This could

indicate one of three scenarios. First, it is possible that the value of "b" is too high and the value of "a" is too low. Adjusting these, respectively, would shift the entire plot up, and flatten it, bringing the profile more into line with the observed data. Second, by increasing "b" and decreasing "c", the same effect could be achieved. Finally, if the "b" were decreased and the backflow ratio were increased the inlet concentration would increase, while the outlet concentration would decrease.

**Red Deer Cocurrent Profile (Figure 17):** The cocurrent profile for the Red Deer sample suffers from the same problem as did the Rossdale cocurrent profile, but to a slightly greater degree. There is more of a discrepancy at both the inlet and outlet ends of the column, with the transition between under- and over-estimation occurring at around the one-third height mark. Likely solutions to the problem are therefore the same as for Rossdale, but with larger adjustments to the parameters being necessary.

**Slave Lake Cocurrent Profile (Figure 18):** For the Slave Lake cocurrent sample, the generated profile appears to significantly underestimate the concentrations near the column bottom, while the top one-third is very accurate. The simplest explanation involves an underestimated backflow ratio. Increasing its value would increase the inlet concentration, flatten the curve, and leave the outlet concentration as is. Other possible explanations are a high "b" value combined with either a low "a" value or a high "c" value. Any of these could have the desired effect.

**Hasse Lake Cocurrent Profile (Figure 19):** The Hasse Lake cocurrent profiles, both computer-generated and observed, appear almost identical to their respective Slave Lake profiles, except that the Hasse Lake concentrations are slightly lower. The relative positioning, however, appears the same. Therefore, the

same possible problems and their associated solutions apply as in the Slave Lake case.

**W..bamun Lake Cocurrent Profile (Figure 20):** The Wabamun Lake cocurrent profiles appear to be of the same configurations as the Red Deer and Rossdale cocurrent profiles, implying that the same problems and corrective measures apply as did in that case. This would call for an increase in "b" coupled with either an increase in "a" or a decrease in "c", or a decrease in "b" coupled with an increase in the backflow ratio.

**Pigeon Lake Cocurrent Profile (Figure 21):** Pigeon Lake's cocurrent profiles fit the same pattern as do Rossdale's, Red Deer's and Wabamun Lake's. Hence, the same possible causes and solutions apply.

**Driedmeat Lake Cocurrent Profile (Figure 22):** The Driedmeat Lake cocurrent profile generated by the model is very poor. It appears to underestimate the inlet concentration (although this is based upon extrapolation based on the observed data points), but then overestimates the outlet concentration by nearly a factor of 5. There is no apparent explanation for the magnitude of the apparent errors. The backflow ratio used was similar to other plots, as were the operating conditions. The only conclusions are either a grossly underestimated value of "a", or an overestimated value for "c". It should be noted that because Driedmeat Lake batch tests were not able to be used in the linear regressions which generated the predictive equations for "b" and "c" due to their very steep decline in $k_w$ values, it is possible that the sample lies outside of the boundaries of applicability of the equations. While the equations generated "b" and "c" values within the ranges generated for other samples, there may be some other parameter(s) involved that was not investigated during the course of this research, was discarded during the linear regressions

as being non-significant in the samples which were useable, or a parameter value may be beyond the linear range of the equations.

In general, the countercurrent configuration yielded good profiles which matched the observed data without any significant trends. Of the five profiles, one profile demonstrated a low "b" value, one exhibited a high "c" value, and one could have been either or a combination of the two. In three of the profiles, it was observed that, while the observed concentrations seemed to begin to level out near the column bottom, the model did not account for this. While Zhou (1995) demonstrated this possibility in 5 m columns where the dissolved ozone concentration has an opportunity to near the Henry's Law equilibrium concentration, this was not the case in the column in question, as aqueous concentrations did not approach equilibrium.

The cocurrent profiles, generally, did not provide accurate approximations of observed data. All seven profiles underestimated the inlet concentrations, while five profiles overestimated the outlet concentrations. Inlet profile concentrations are only significantly affected by the values of "b" and the backflow ratio, while outlet concentrations can be affected by "a", "b", and "c". The assumption that "a" be equal to zero may help to account for the outlet concentrations, as increasing the value of "a" could serve to lower them. However, given that the countercurrent profiles are relatively accurate, which would appear to validate the kinetics, the poor fit of the cocurrent profiles remains unexplained. The remaining explanations involve physical, rather than kinetic, factors. Zhou (1995) found that the backflow ratios were not affected by the flow configuration, but the data obtained in this investigation might suggest otherwise. Increasing the backflow ratios serves to flatten the profile, eventually reducing it to a constant concentration once the column is acting as a single CFSTR. If backflow ratios for the cocurrent configuration are larger than for the counter-current, this may account for the flatter profiles being observed than are

predicted. Also, the assumption that backflow ratios are constant over the height of the column is possibly invalid. Inlet and outlet conditions may significantly affect the hydrodynamics at the boundaries. Mass transfer may also deviate from ideal, clean water conditions, based on the water quality in use. Variations in $\alpha$ and $\beta$ (Equation 1) from unity may cause changes in the concentration profile. Changes in $\alpha$ will essentially cause the same changes as changes in $k_L a$, which were studied by Zhou et al (1994). Changes in $\beta$ values would alter the effective concentration gradient that drives the mass transfer, probably decreasing it, and therefore reducing the rate of mass transfer between gas and liquid phases. The effect of this would be to lower all profile concentrations along the column height.

*Limitations of Kinetic Methods*

There exists one major limitation in the methods used for this investigation. With the method used, it was not possible to obtain valid concentration readings between 0 and 30 seconds in the batch testing phase of the experiment. This did not pose a major problem in cases where the dilution factor was great enough that a reliable curve could be interpolated between measured points. However, in more concentrated samples, the decline in ozone concentration was sometimes large enough to reduce the utilization rate constant to a near constant, low value, making it impossible to interpolate with any degree of certainty, which in turn, made it impossible to estimate curve slopes for the first two data points.

The same limitation also caused problems with some samples which exhibited the sudden, late decline in $k_w$ values. Because these points had to be discarded, this often left only 3 or 4 points with which to estimate the best-fit, non-linear regression curve in some cases. Given that the nature of scientific measurements yields a small amount of variation around a true value, even a small variation could cause relatively large variations in the regressed kinetic parameter values, due to the small number of

useable observations. This factor, could possibly have been the reason for the uncertainty in the calculated values of "a". By utilizing a method which could provide a greater resolution of observations, the chance of such errors occurring could be minimized, and the confidence in results obtained could be greater.

Another limitation, which could have affected the calculated values of "b" and "c", is the ability to accurately measure the slope of the $k_w$ vs. $\Delta O_3$ curve at $\Delta O_3 = 0$. Drawing an accurate tangent line to the endpoint of a curve proved a very difficult task. Without the curve continuing on both sides of the tangent point, judging the correct slope necessitated a judgment being made regarding the slope at that particular point. If a tangent is drawn in the middle of a curve, this judgment is made easier by observing the tangent line's position relative to the curve on both sides of the point of contact. Add to this, the fact that the curve is often very steep at this point, and what seems like a small difference in slopes could easily affect the value of "b" by a factor of two or three. The only way to approach this problem was to attempt to be consistent in the drawing of tangent lines for the first point.

A limitation existed regarding the time that a sample sat before certain parameters were measured or tests performed. Due to the large number of tests involved, and the large amount of time required to perform some of them (for instance, the solids analysis) some samples stood for up to ten or eleven days before all the required analyses were performed. Therefore, it is possible that changes in the composition occurred before certain tests were performed. For instance, some organic matter may have volatilized and escaped as gas, even though the sample barrels were kept sealed. Also, while every attempt was made during field sampling to sample from a point in the water column well above the bottom of the water body, some solid organic or mineral matter may have entered the raw water samples, as no filtering was performed. Such materials may have continued to degrade in the sample while stored in the lab prior to testing.

During the modelling phase of the investigation, it was noted that not all of the model runs achieved a perfect steady state. This occurred when both a cell's aqueous concentration and $k_w$ value were right on the verge of shifting to the next decimal value. For example, if a cell's aqueous ozone concentration implied a certain $k_w$ value on one run, inputting that $k_w$ value sometimes led to the model returning a slightly lower concentration. On the next iteration, when the new concentration was input into the cell, the model would sometimes return a lower $k_w$ value, which on the next iteration would yield a higher concentration due to the lower utilization rate, and so on. However, due to the very small magnitude of the differences encountered, it is not believed that this limitation affected any concentration by more than 1 or 2%, and therefore cannot be considerred a significant source of error.

Figure 23: Effect of the Kinetic Parameter "a" on Batch Test Decay
(b=1, c=3)

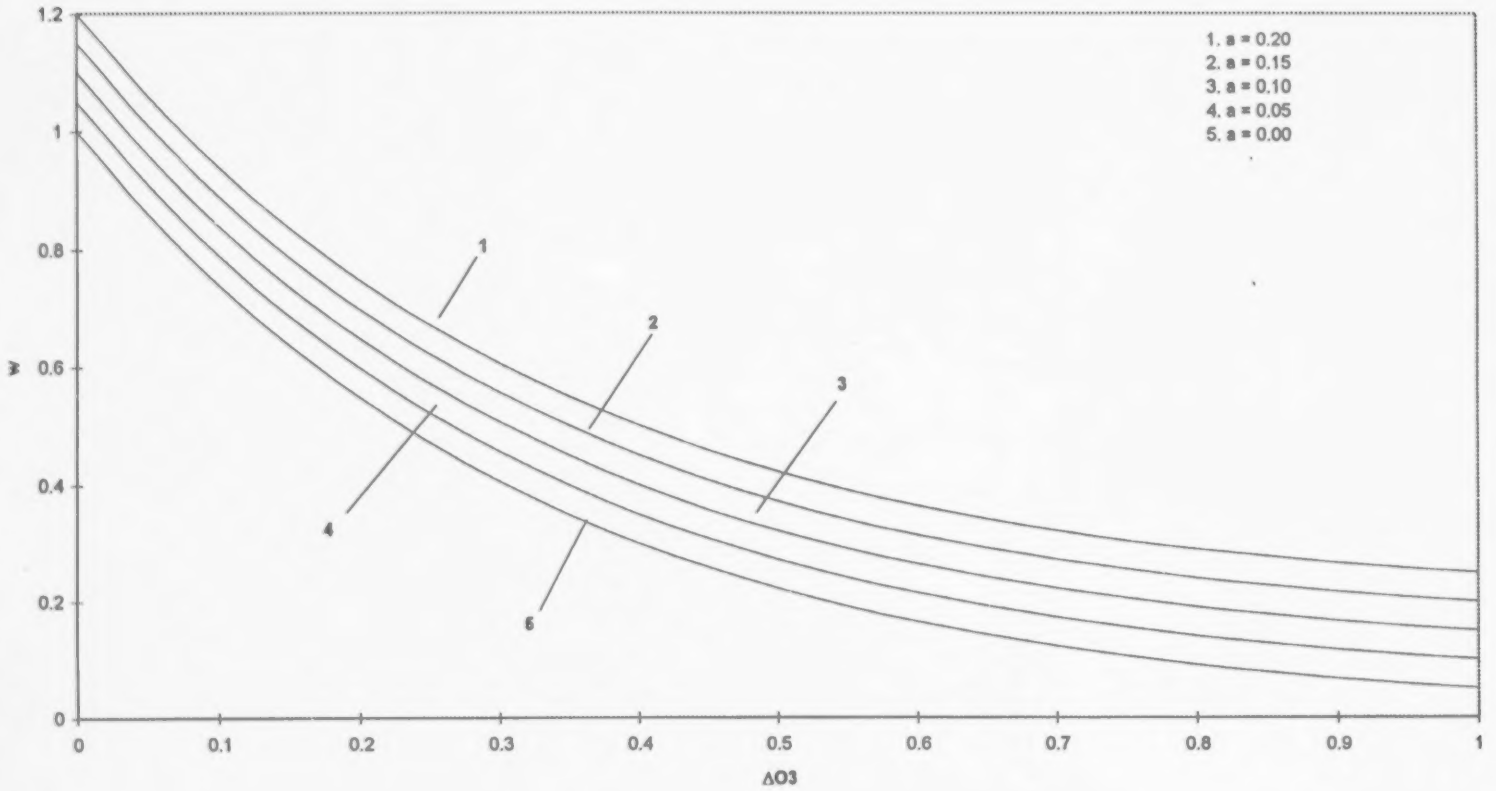

**Figure 24: Effect of the Kinetic Parameter "b" on Batch Test Decay**

a=0, c=3

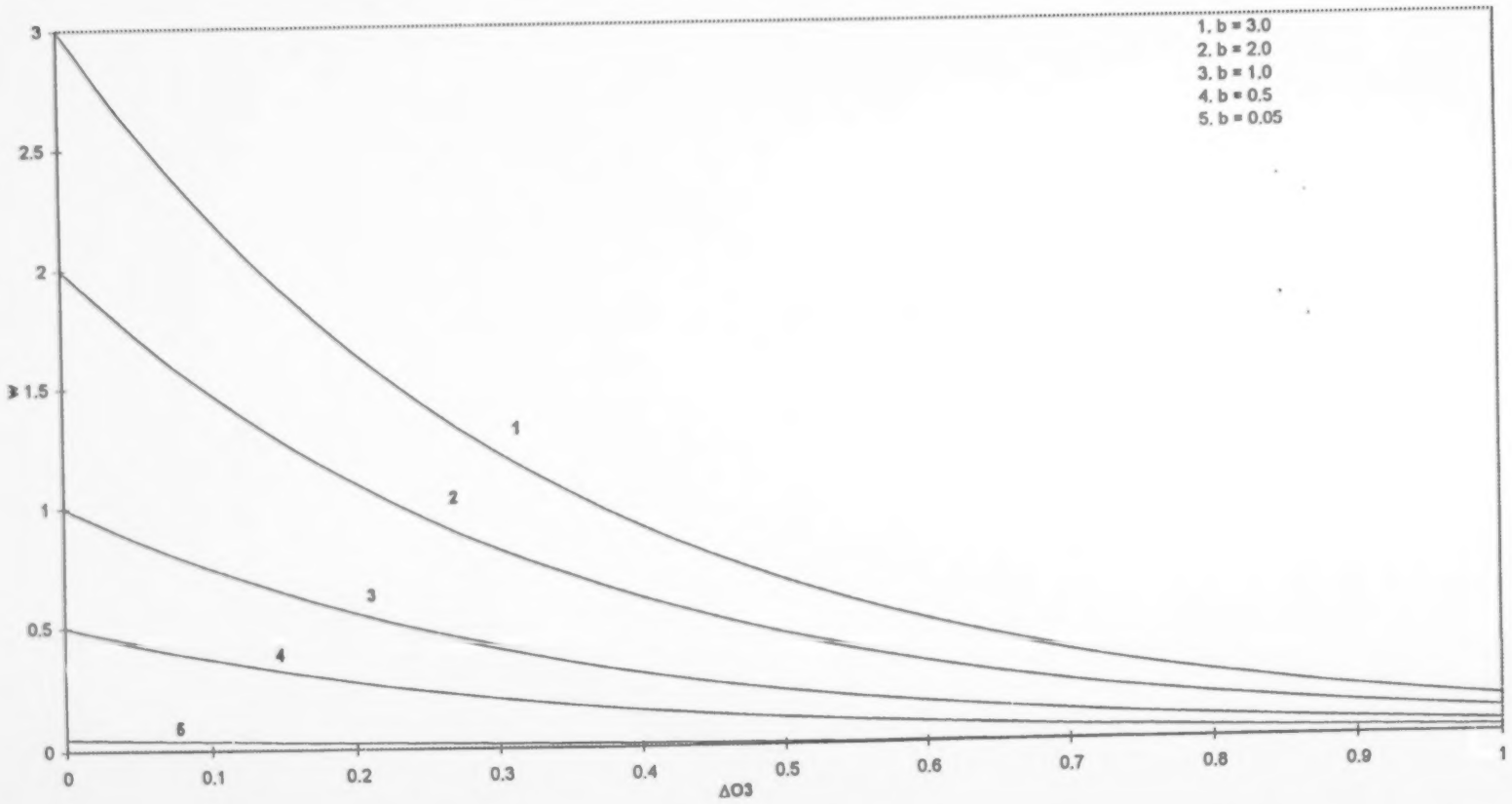

**Figure 25: Effect of the Kinetic Parameter "c" on Batch Test Decay**
a=0, b=1

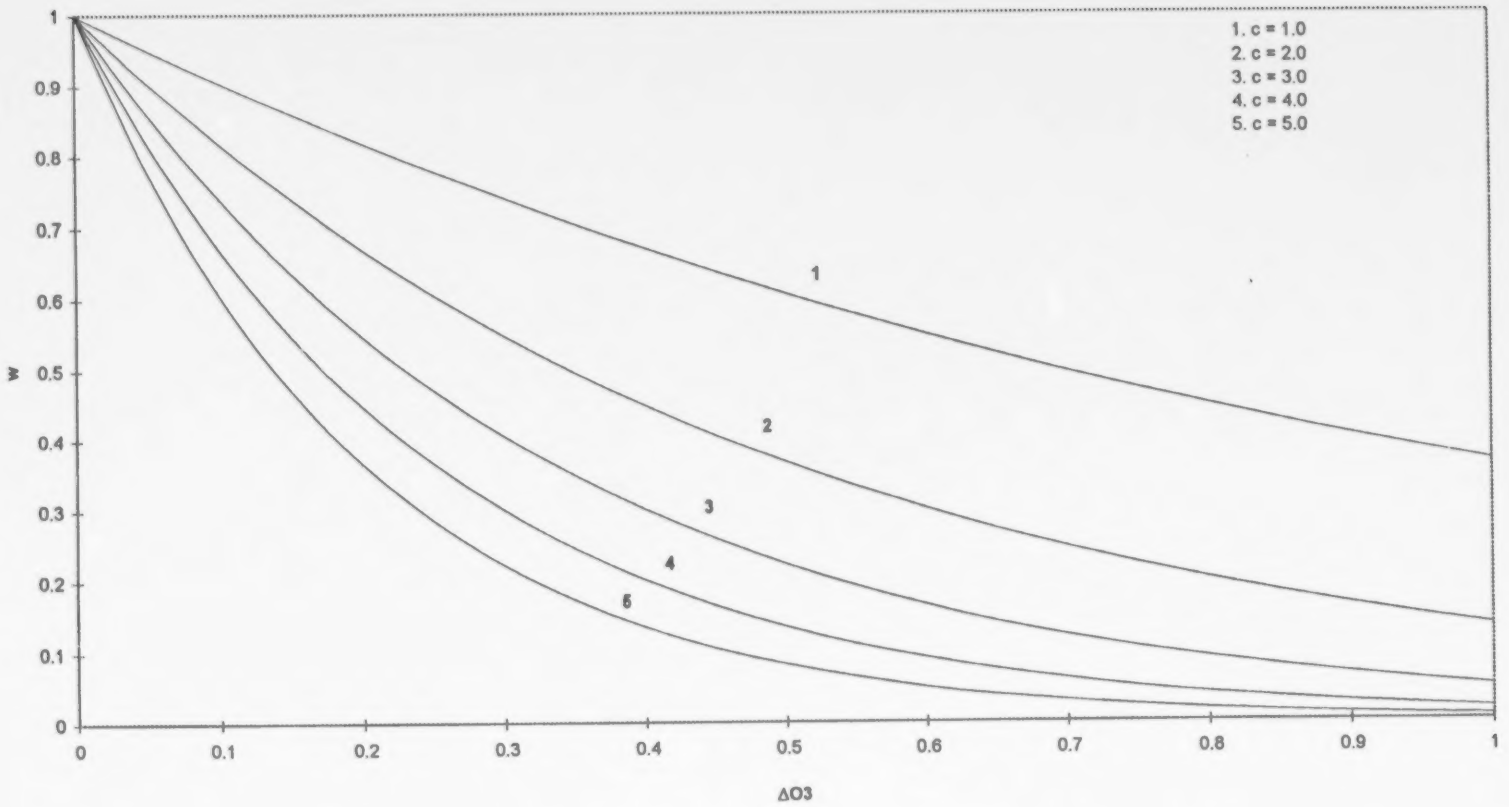

**Figure 26: Effect of the Kinetic Parameter "a" on Countercurrent Ozone Concentration Profiles Generated by the Back Flow Cell Model**

b = 1.0, c =3.0

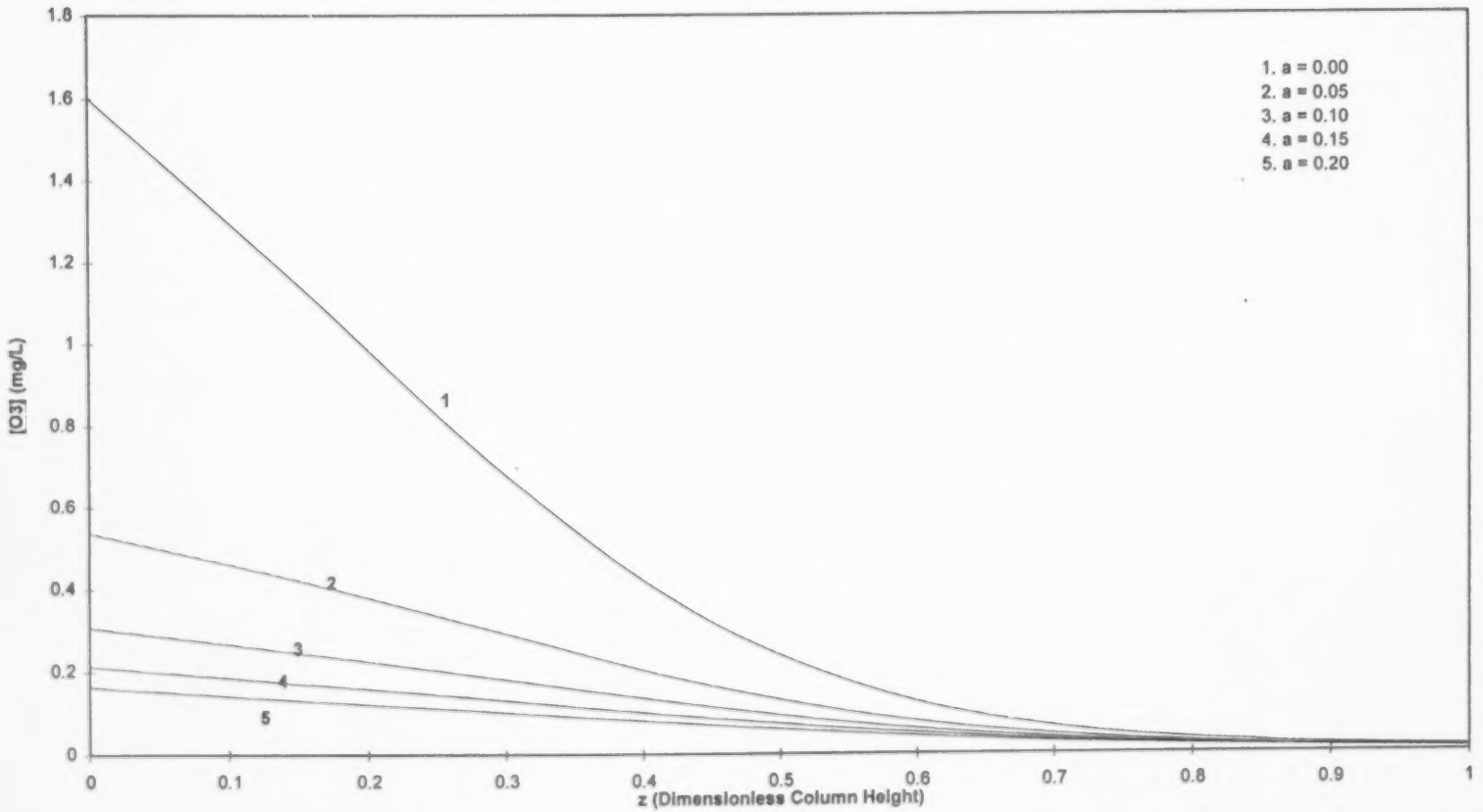

**Figure 27: Effect of the Kinetic Parameter "b" on Countercurrent Ozone Concentration Profiles Profiles Generated by the Back Flow Cell Model**

a = 0.0, c = 3.0

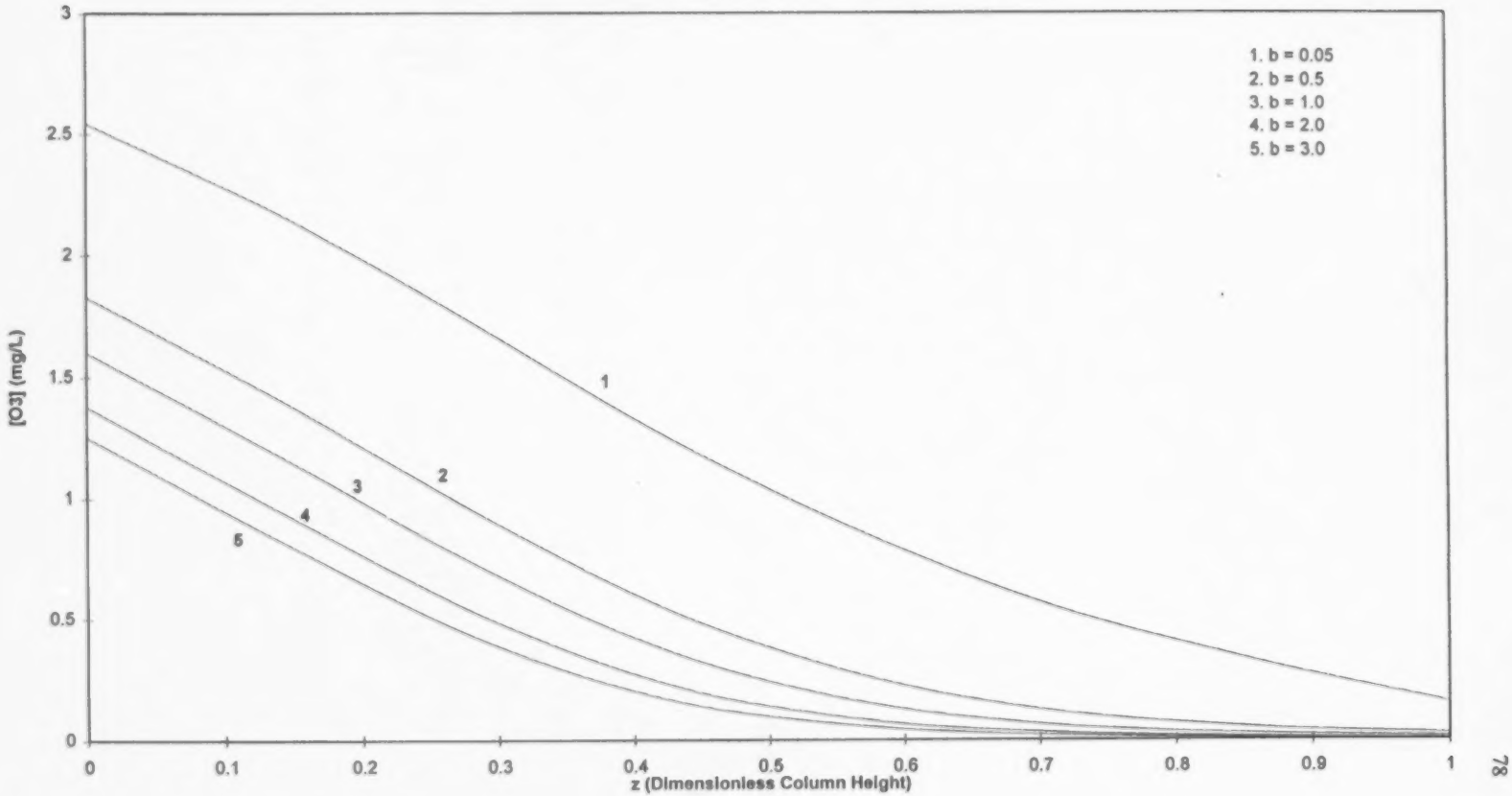

**Figure 28: Effect of the Kinetic Parameter "c" on Countercurrent Ozone Concentration Profiles Generated by the Back Flow Cell Model**

**a = 0.0, b = 1.0**

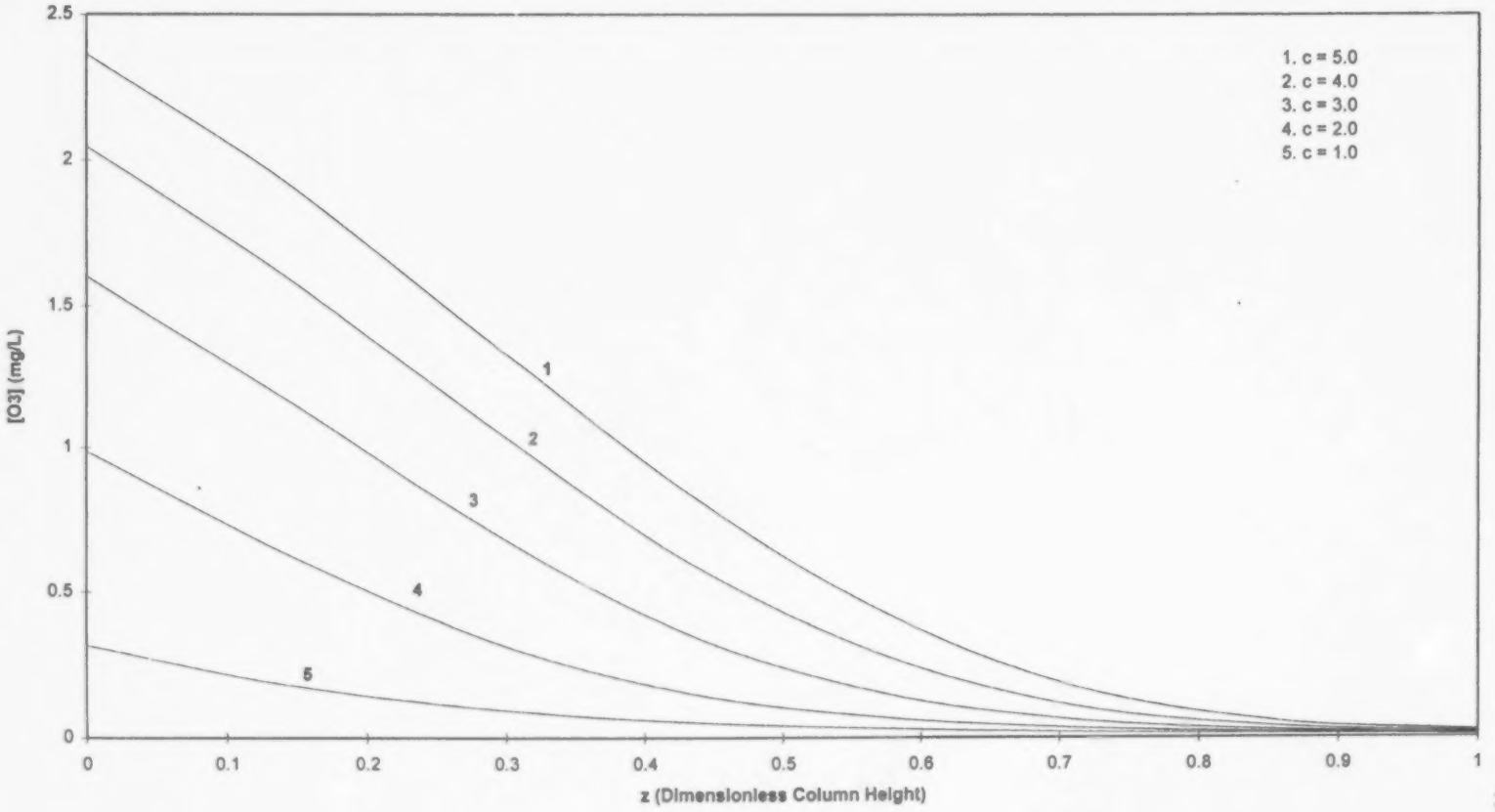

**Figure 29: Effect of the Kinetic Parameter "a" on Cocurrent Ozone Concentration Profiles Generated by the Back Flow Cell Model**

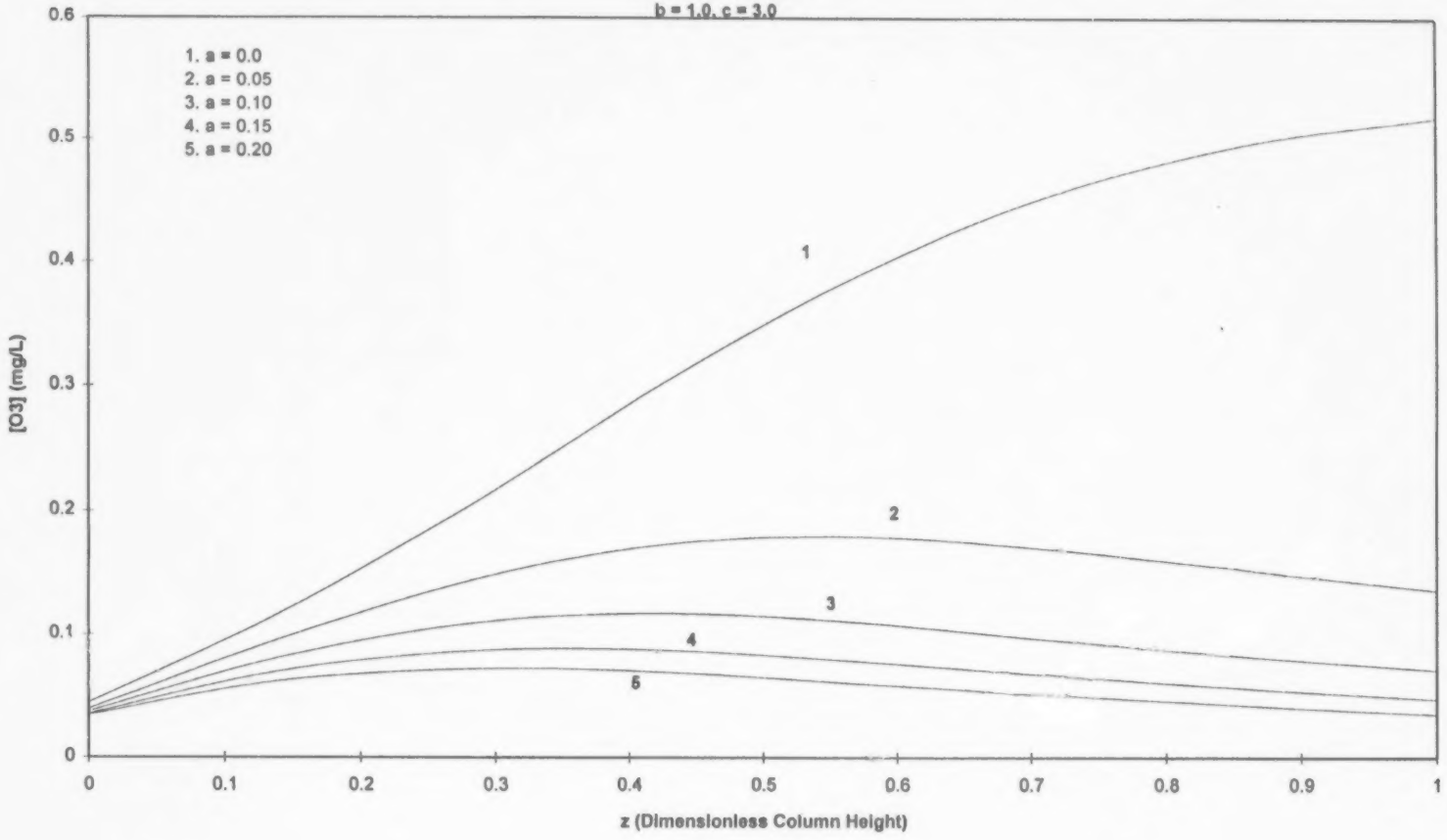

Figure 30: Effect of the Kinetic Parameter "b" on Cocurrent Ozone Concentration Profiles Generated by the Back Flow Cell Model

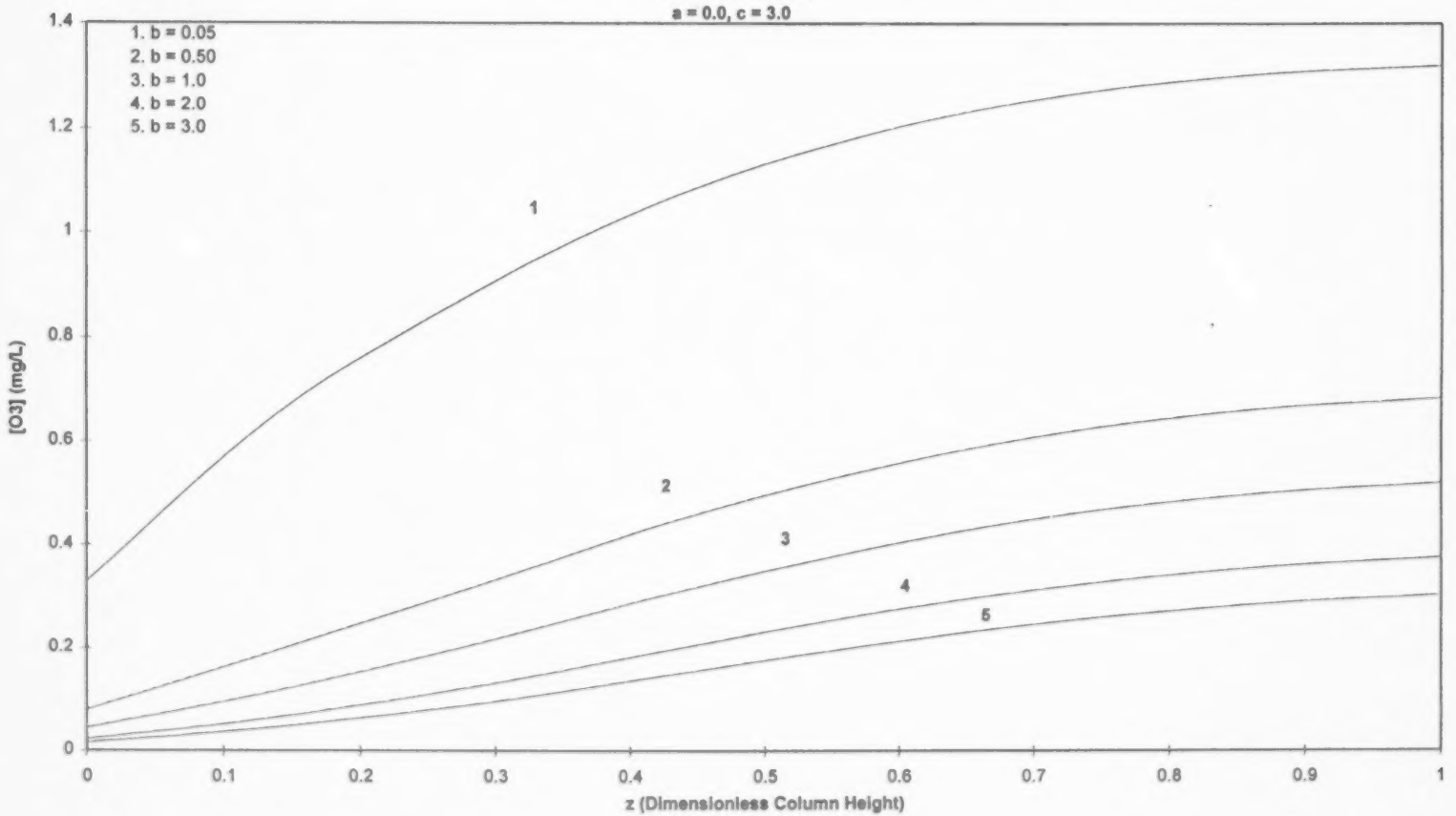

**Figure 31: Effect of the Kinetic Parameter "c" on Cocurrent Ozone Concentration Profiles Generated by the Back Flow Cell Model**

(a = 0.0, b = 1.0)

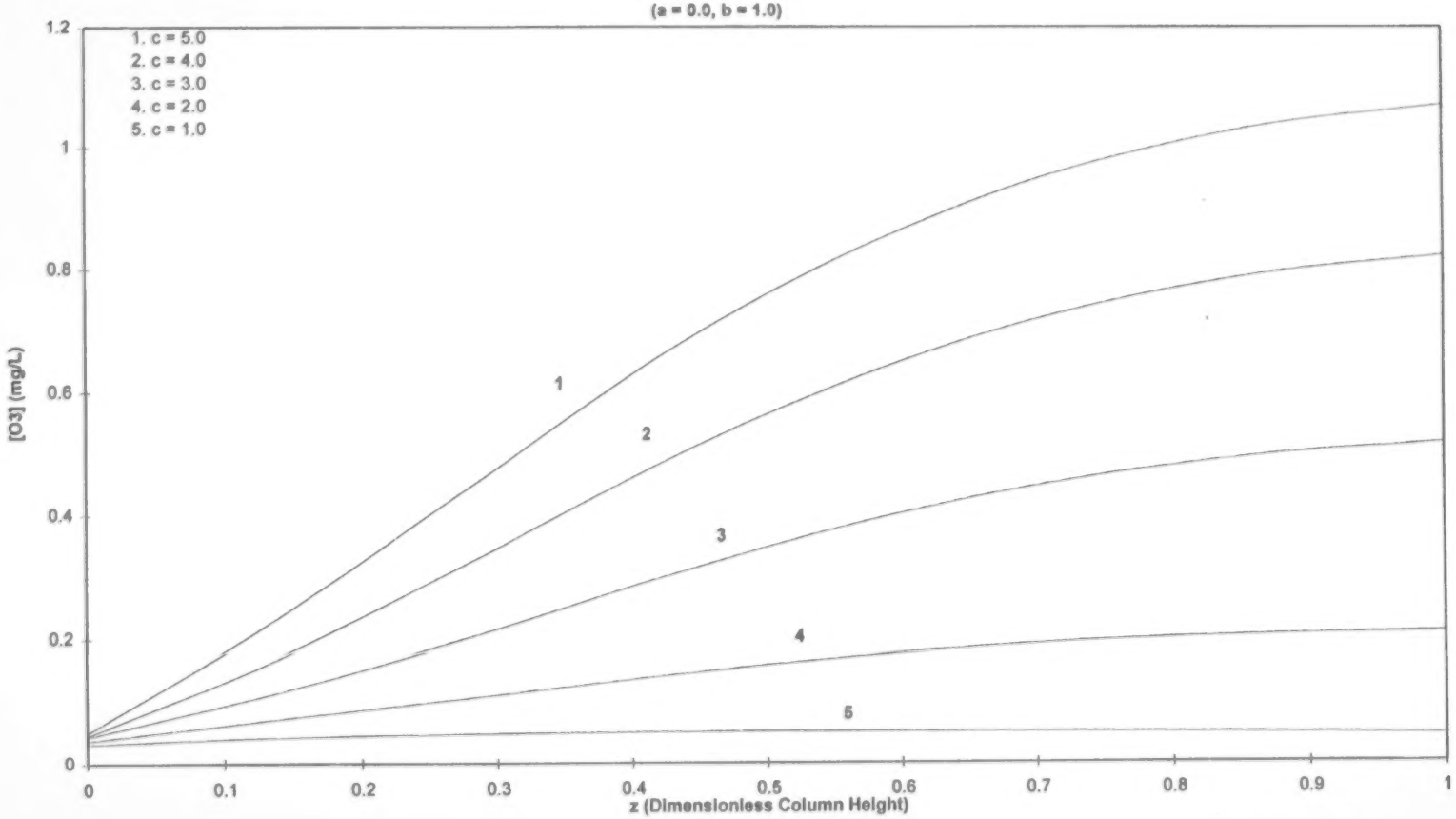

**Conclusions and Recommendations**

The results of this investigation should serve as a building block in the development of better technologies for the treatment of drinking water. With the increasing concerns regarding chlorination byproducts, ozone treatment is often the treatment alternative of choice. However, ozonation cannot be used effectively without a thorough understanding of its mechanisms and kinetics. While this research may not be able to conclusively define ozone decay kinetics due to experimental limitations, the kinetics presented here are shown to be an improvement over the commonly used first order descriptions.

This work follows on from that of Zhou (1995), in which the use of the back flow cell model was presented as an improvement over the axial dispersion model in both accuracy and simplicity. The model, along with the kinetic equation used in this research, was demonstrated to be able to provide good representations of bubble column concentration profiles in both cocurrent and countercurrent configurations using the kinetic parameters obtained through batch testing of the waters used. This research took those findings and attempted to determine if an empirical relationship existed between the kinetic parameters and various parameters related to water quality, and then to investigate whether such a relationship could be used to accurately predict concentration profiles using the back flow cell model.

Specific conclusions made are:

1) commonly used first order kinetics are not valid for waters containing natural organic material, due to a changing rate constant;

2) first order kinetics are applicable to the decay of ozone concentrations in pure Milli-Q water;

3) the proposed kinetic equation, which uses a specific ozone utilization constant which takes into account the changing quality of water during the course of ozonation, can be fitted to observed batch test data by utilizing a non-linear least squares method of varying the kinetic parameters "a", "b" and "c";

4) a measurable empirical relationship does exist between water quality and ozone decay kinetics, as measured in a batch reactor;

5) pH, total organic carbon, carbonate ion concentration, UV absorbance at 254 nm, total solids, bicarbonate ion concentration, magnesium hardness and calcium hardness were all determined to be significant parameters in the determination of ozone decay kinetics in natural waters;

6) the kinetic parameters "a", "b" and "c" were all observed to cause significant effects in both cocurrent and countercurrent concentration profiles, as generated by the back flow cell model, for a pilot-scale ozone column;

7) countercurrent concentration profiles were predicted relatively accurately by the back flow cell model, using kinetic parameters that were based on measured water quality properties;

8) the back flow cell model was unable to predict the s-bend observed in the measured concentration profiles near the bottom of some countercurrent column runs; and

9) cocurrent concentration profiles were predicted with varying degrees of success by the back flow cell model, using kinetic parameters that were based on measured water quality properties.

Based on these conclusions, and the situations experienced during the performance of this investigation, the following recommendations are made regarding future studies in this field:

1) further investigation should be undertaken regarding the use of declining utilization rate constants in ozone decay modelling;
2) any future work should first focus on the need for better observation resolution during the initial, rapid concentration decay phase of the ozonation process, possibly through the use of a 'wet wall' technique;
3) more work is required regarding the application of declining utilization rate constants in bubble column contactors and the assumptions made regarding hydrodynamics and the effects of water quality on mass transfer, especially in the cocurrent configuration;
4) further work is required to make the back flow cell model more readily useable in this type of investigation, rather than having the operator perform all of the iterative tasks; and
5) a future study, performed in the opposite order as this one (ie. fit the back flow cell model to observed profiles by changing cell $k_w$ values, and then using those results to predict batch test decay curves) may be of significant value.

**References**

American Water Works Research Foundation (AWWARF). 1991. *Ozone in Water Treatment: Application and Engineering. Cooperative Research Report.* Bruno Langlais, David A. Reckhow & Deborah R. Brink, eds., Lewis Publishers, Chelsea. pp. 11-132.

Beltran, F.J., Rivas, F.J. & Acado, B. 1993. Direct, radical and competitive reactions in the ozonation of water micropollutants. *J. Environ. Sci. Health, A28,* 9, p. 1947.

Beltran, F.J., Gomez-Serrano, V. & Duran, A. 1992. Degradation kinetics of p-nitrophenol ozonation in water. *Water Research, 26,* 1, p. 9.

Blum, D.J.W., Suffet, I.H. & Duguet, J.P. 1993. Estimation of hydroxyl radical reaction rate constants for organic chemicals in water. In *"Ozone in Water and Wastewater Treatment, Proceedings, Eleventh Ozone World Congress, San Francisco", 2,* p. S-20-6.

Brambilla, A., Bolzacchini, E., Meinardi, S., Orlandi, M., Polesello, S. & Rindone, B. 1995. Reactivity of organic micropollutants with ozone: a kinetic study. *Proceedings, 12th World Congress of the International Ozone Association, 15th to 18th May 1995, Lille, France,* Vol. 1, pp. 43-52.

Chang, B.-J. & Chian, E.S.K. 1981. A model study of ozone-sparged vessels for the removal of organics from water. *Water Research, 15;* p. 929.

Glaze, W.H. 1987. Drinking water treatment with ozone, *Environ. Sci. Technol., 21,* 3, p. 224.

Guittonneau, S., Glaze, W.H., Duguet, J.P., Wable, O. & Mallevialle, J. 1992. Characterization of natural water for potential to oxidize organic pollutants with ozone. *Ozone: Science and Engineering, 14,* p. 185.

Gurol, M.D. 1985. Factors controlling the removal of organic pollutants in ozone reactors. *Ozone in Water Treatment - Applications, Operations, and Technology,* AWWA, Denver, Colorado, p. 161.

Gurol, M.D. & Singer, P.C. 1983. Dynamics of the ozonation of phenol - II. Mathematical simulation. *Water Research, 17,* 9, p. 1173.

Hoigne, J. & Bader, H. 1979. Ozonation of water: selectivity and rate of oxidation of solutes. *Ozone: Science and Engineering, 1,* p. 73.

Hoigne, J. & Bader, H. 1983a. Rate constants of reactions of ozone with organic and inorganic compounds in water - Part I: Non-dissociating organic compounds. *Water Research, 17*, p. 173.

Hoigne, J. & Bader, H. 1983b. Rate constants of reactions of ozone with organic and inorganic compounds in water - Part II: Dissociating organic compounds. *Water Research, 17*, p. 185.

Kallas, J., Munter, R., Viiroja, A. & Korvits, M. 1995. Mathematical models, simulation and parameter estimation for water/wastewater treatment by ozone in semicontinuous, countercurrent and cocurrent columns. *Proceedings, 12th World Congress of the International Ozone Association, 15th to 18th May 1995, Lille, France,* Vol. 2, pp. 229-240.

Laplanche, A., Le Sauze, N., Martin, G. & Langlais, B. 1991. Simulation of ozone transfer in water. Comparison with a pilot unit. *Ozone: Science and Engineering, 13*, 5, p. 535.

Le Sauze, N., Laplanche, A., Martin, N. & Martin, G. 1993. Modeling of ozone transfer in a bubble column. *Water Research, 27*, 6, p. 1071.

Marinas, B.J., Liang, S. & Aieta, E.M. 1993. Modeling hydrodynamics and ozone residual distribution in a pilot-scale ozone bubble-diffuser contactor. *J. AWWA, 85*, 3, p. 91.

Roth, J.A. & Sullivan, D.E. 1983. Kinetics of ozone decomposition in water. *Ozone: Science and Engineering, 5*, p. 37.

Roustan, M., Wang, R. & Wolbert, D. 1995. Modeling hydrodynamics and mass transfer parameters in a continuous ozone bubble column. *Proceedings, 12th World Congress of the International Ozone Association, 15th to 18th May 1995, Lille, France,* Vol. 2, pp. 253-264.

Singer, P.C. & Gurol, M.D. 1983. Dynamics of the ozonation of phenol - I. Experimental observations, *Water Research, 17*, 9, p. 1163.

Smith, D.W. & Zhou, H. 1994. Theoretical analysis of ozone disinfection performance in a bubble column. *Ozone: Science and Engineering, 16*, p. 429.

Staehelin, J. & Hoigne, J. 1985. decomposition of ozone in water in the presence of organic solutes acting as promoters and inhibitors of radical chain reactions, *Environ. Sci. Technol., 19*, p. 1206.

Yurteri, C. & Gurol, M.D. 1988. Ozone consumption in natural waters: effects of background organic matter, pH and carbonate species. *Ozone: Science and Engineering, 10*, p. 277.

Yurteri, C. & Gurol, M.. Evaluation of kinetic parameters for the ozonation of organic micropollutants. *Wat. Sci. Tech., 21*, p. 465g.

Zhou, H. 1995. Investigation of Ozone Disinfection Kinetics and Contactor Performance Modeling. PhD Thesis, Department of Civil Engineering, University of Alberta, Edmonton, 327 p.

Zhou, H., Smith, D.W. & Stanley, S.J. 1994. Modeling of dissolved ozone concentration profiles in bubble columns. *Journal of Environmental Engineering, 120*, 4, p. 821.

# APPENDIX A

## BATCH TEST EXPERIMENTAL DATA

| Sample * | Initial Temp °C | Initial pH | Final pH |
|---|---|---|---|
| Rossdale .2 | 22.03 | 7.06 | 7.05 |
| Rossdale .4 | 21.17 | 7.52 | 7.53 |
| Rossdale .6 | 21.10 | 7.79 | 7.79 |
| Rossdale .8 | 20.67 | 7.94 | 7.78 |
| Pigeon .25 | 21.87 | 8.03 | 7.39 |
| Pigeon .50 | 20.87 | 8.22 | 7.91 |
| Pigeon .75 | 20.03 | 8.30 | 7.96 |
| Wabamun .25 | 21.20 | 7.84 | 7.49 |
| Wabamun .50 | 21.00 | 8.33 | 8.01 |
| Wabamun .75 | 19.27 | 8.15 | 7.90 |
| Slave .25 | 21.60 | 7.25 | 6.74 |
| Slave .50 | 20.73 | 7.56 | 7.07 |
| Slave .75 | 20.37 | 7.62 | 7.15 |
| Driedmeat .25 | 21.40 | 8.99 | 8.83 |
| Driedmeat .50 | 19.83 | 9.08 | 9.02 |
| Driedmeat .75 | 19.47 | 9.12 | 8.95 |
| Miquelon .25 | 20.67 | 9.56 | 9.56 |
| Miquelon .50 | 20.67 | 9.54 | 9.54 |
| Miquelon .75 | 20.37 | 9.54 | 9.54 |
| Hasse .25 | 21.07 | 7.89 | 7.16 |
| Hasse .50 | 21.23 | 8.31 | 7.90 |
| Hasse .75 | 19.93 | 8.29 | 8.06 |
| Red Deer .25 | 20.67 | 7.50 | 7.16 |
| Red Deer .50 | 20.73 | 7.80 | 7.55 |
| Red Deer .75 | 20.97 | 7.93 | 7.69 |

| Sample | Initial TOC (ppm) | Final TOC (ppm) | Initial $UV_{254}$ (absorb.) | Final $UV_{254}$ (absorb.) | Initial $UV_{280}$ (absorb.) | Final $UV_{280}$ (absorb.) |
|---|---|---|---|---|---|---|
| Rossdale .2 | 3.397 | 3.416 | 0.037 | 0.019 | 0.030 | 0.018 |
| Rossdale .4 | 6.550 | 6.562 | 0.059 | 0.040 | 0.049 | 0.035 |
| Rossdale .6 | 9.535 | 9.536 | 0.094 | 0.070 | 0.076 | 0.057 |
| Rossdale .8 | 12.836 | 12.443 | 0.128 | 0.088 | 0.101 | 0.071 |
| Pigeon .25 | 5.501 | 5.711 | 0.037 | 0.036 | 0.027 | 0.028 |
| Pigeon .50 | 10.387 | 10.366 | 0.067 | 0.052 | 0.047 | 0.041 |
| Pigeon .75 | 15.192 | 15.232 | 0.088 | 0.064 | 0.064 | 0.048 |
| Wabamun .25 | 9.029 | 9.221 | 0.047 | 0.024 | 0.036 | 0.017 |
| Wabamun .50 | 17.046 | 17.349 | 0.088 | 0.053 | 0.065 | 0.036 |
| Wabamun .75 | 24.862 | 24.909 | 0.146 | 0.086 | 0.101 | 0.062 |
| Slave .25 | 4.490 | 4.305 | 0.064 | 0.036 | 0.049 | 0.029 |
| Slave .50 | 8.850 | 8.708 | 0.109 | 0.073 | 0.075 | 0.055 |
| Slave .75 | 12.782 | 12.854 | 0.156 | 0.100 | 0.104 | 0.070 |
| Driedmeat .25 | 8.552 | 8.732 | 0.100 | 0.074 | 0.071 | 0.056 |
| Driedmeat .50 | 17.962 | 18.332 | 0.190 | 0.140 | 0.139 | 0.098 |
| Driedmeat .75 | 28.709 | 27.862 | 0.291 | 0.209 | 0.206 | 0.149 |
| Miquelon .25 | 27.623 | 29.11 | 0.207 | 0.161 | 0.099 | 0.079 |
| Miquelon .50 | 54.157 | 51.29 | 0.396 | 0.348 | 0.179 | 0.139 |
| Miquelon .75 | 76.857 | 74.39 | 0.591 | 0.500 | 0.274 | 0.219 |
| Hasse .25 | 7.476 | 7.901 | 0.045 | 0.028 | 0.031 | 0.020 |
| Hasse .50 | 14.674 | 15.01 | 0.086 | 0.069 | 0.057 | 0.044 |
| Hasse .75 | 21.600 | 21.54 | 0.130 | 0.103 | 0.086 | 0.066 |
| Red Deer .25 | 5.092 | 5.317 | 0.065 | 0.043 | 0.054 | 0.036 |
| Red Deer .50 | 9.859 | 9.820 | 0.125 | 0.094 | 0.109 | 0.073 |
| Red Deer .75 | 14.282 | 14.452 | 0.181 | 0.133 | 0.145 | 0.101 |

| Sample * | Initial $[CO_3^{2-}]$ (eq/L) | Final $[CO_3^{2-}]$ (eq/L) | Initial $[HCO_3^-]$ (eq/L) | Final $[HCO_3^-]$ (eq/L) |
|---|---|---|---|---|
| Rossdale .2 | 0 | 0 | .000527 | .000524 |
| Rossdale .4 | 0 | 0 | .000996 | .001040 |
| Rossdale .6 | .000086 | .000090 | .001333 | .001328 |
| Rossdale .8 | .000163 | .000094 | .001685 | .001792 |
| Pigeon .25 | .000113 | 0 | .000707 | .000980 |
| Pigeon .50 | .000164 | .000086 | .001338 | .001522 |
| Pigeon .75 | .000203 | .000136 | .001983 | .002114 |
| Wabamun .25 | .000109 | 0 | .000954 | .001178 |
| Wabamun .50 | .000228 | .000108 | .001727 | .001924 |
| Wabamun .75 | .000317 | .000262 | .002597 | .002664 |
| Slave .25 | 0 | 0 | .000503 | .000492 |
| Slave .50 | .000051 | .000024 | .000831 | .000882 |
| Slave .75 | .000084 | .000048 | .001201 | .001272 |
| Driedmeat .25 | .000215 | .000224 | .000815 | .000782 |
| Driedmeat .50 | .000459 | .000452 | .001584 | .001616 |
| Driedmeat .75 | .000671 | .000680 | .002379 | .002372 |
| Miquelon .25 | .002535 | .002398 | .003946 | .004080 |
| Miquelon .50 | .004797 | .004704 | .008037 | .008486 |
| Miquelon .75 | .007054 | .007086 | .012483 | .012342 |
| Hasse .25 | 0 | 0 | .000742 | .000772 |
| Hasse .50 | .000095 | .000100 | .001246 | .001256 |
| Hasse .75 | .000159 | .000156 | .001786 | .001814 |
| Red Deer .25 | .000028 | .000020 | .000738 | .000746 |
| Red Deer .50 | .000087 | .000096 | .001277 | .001270 |
| Red Deer .75 | .000131 | .000106 | .001898 | .001952 |

| Sample * | Initial TS (mg/L) | Final TS (mg/L) | Initial TSS (mg/L) | Final TSS (mg/L) | Initial TDS (mg/L) | Final TDS (mg/L) | Initial TVS (mg/L) | Final TVS (mg/L) | Initial VSS (mg/L) | Final VSS (mg/L) | Initial VDS (mg/L) | Final VDS (mg/L) |
|---|---|---|---|---|---|---|---|---|---|---|---|---|
| Rossdale .2 | 32.0 | 36 | 29.3 | 12 | 2.7 | 24 | 14.7 | 36 | -16.0 | 24 | 30.7 | 12 |
| Rossdale .4 | 61.3 | 128 | 22.7 | 72 | 38.7 | 56 | 29.3 | 44 | 2.7 | -4 | 26.7 | 48 |
| Rossdale .6 | 113.3 | 124 | 5.3 | 24 | 108.0 | 100 | 26.7 | 12 | 9.3 | -12 | 17.3 | 24 |
| Rossdale .8 | 196.0 | 188 | -300.0 | -164 | 496.0 | 352 | 61.3 | 36 | -264.0 | -108 | 325.3 | 144 |
| Pigeon .25 | 50.7 | 0 | 5.3 | -64 | 45.3 | 64 | 32.0 | -4 | 8.0 | -36 | 24.0 | 32 |
| Pigeon .50 | 73.3 | 124 | -34.7 | 16 | 108.0 | 108 | 48.0 | 76 | -13.3 | 36 | 61.3 | 40 |
| Pigeon .75 | 66.7 | 140 | -89.3 | -8 | 156.0 | 148 | 54.7 | 56 | -5.3 | -4 | 60.0 | 60 |
| Wabamun .25 | 102.0 | 76 | -490 | -244 | 592.0 | 320 | 66.0 | 40 | -292 | -104 | 358.0 | 144 |
| Wabamun .50 | 164.0 | 156 | -330.7 | -528 | 494.7 | 684 | 65.3 | 68 | -205.3 | -400 | 270.7 | 468 |
| Wabamun .75 | 258.7 | 240 | 49.3 | 16 | 209.3 | 224 | 138.7 | 88 | 85.3 | 28 | 53.3 | 60 |
| Slave .25 | 65.3 | 88 | 29.3 | 44 | 36.0 | 44 | 52.0 | 76 | 20.0 | 48 | 32.0 | 28 |
| Slave .50 | 46.7 | 80 | -8.0 | -44 | 54.7 | 124 | 78.7 | 68 | 60.0 | -12 | 18.7 | 80 |
| Slave .75 | 116.0 | 120 | 24.0 | 20 | 92.0 | 100 | 117.3 | 100 | 77.3 | 44 | 40.0 | 56 |
| Driedmeat .25 | 80.0 | 32 | 16.0 | -68 | 64.0 | 100 | 69.3 | 60 | 16.0 | 36 | 53.3 | 24 |
| Driedmeat .50 | 181.3 | 172 | -25.3 | -4 | 206.7 | 176 | 113.3 | 80 | 40.0 | -4 | 73.3 | 84 |
| Driedmeat .75 | 302.7 | 380 | -40.0 | 96 | 342.7 | 284 | 118.7 | 136 | -2.7 | 64 | 121.3 | 72 |
| Miquelon .25 | 1729.3 | 1716 | -20 | -24 | 1749.3 | 1740 | 193.3 | 240 | 6.7 | 36 | 186.7 | 204 |
| Miquelon .50 | 3464 | 3480 | -21.3 | -24 | 3485.3 | 3504 | 424.0 | 404 | 3.0 | 16 | 401.3 | 388 |
| Miquelon .75 | 5201.3 | 5192 | -57.3 | -76 | 5258.7 | 5268 | 548.0 | 600 | -4.0 | 72 | 552.0 | 528 |
| Hasse .25 | 96.0 | 68 | 26.7 | 20 | 69.3 | 48 | 98.7 | 44 | 45.3 | -16 | 53.3 | 60 |
| Hasse .50 | 130.7 | 112 | -36.0 | -52 | 166.7 | 164 | 64.0 | 60 | -2.7 | -16 | 66.7 | 76 |
| Hasse .75 | 177.3 | 252 | -60.0 | 16 | 237.3 | 236 | 92.0 | 84 | 4.0 | -56 | 88.0 | 140 |
| Red Deer .25 | 101.3 | 32 | 6.7 | 0 | 94.7 | 32 | 49.3 | -32 | 25.3 | -56 | 24.0 | 24 |
| Red Deer .50 | 125.3 | 80 | 21.3 | -16 | 104.0 | 96 | 46.7 | 16 | 14.7 | 4 | 32.0 | 12 |
| Red Deer .75 | 153.3 | 180 | -25.3 | -32 | 178.7 | 212 | 37.3 | 68 | -45.3 | 0 | 82.7 | 68 |

| Sample | Initial Ca Hardness ($mg/L\ CaCO_3$) | Final Ca Hardness ($mg/L\ CaCO_3$) | Initial Mg Hardness ($mg/L\ CaCO_3$) | Finai Mg Hardness ($mg/L\ CaCO_3$) |
|---|---|---|---|---|
| Rossdale .2 | 23.2 | 21.6 | 5.9 | 9.8 |
| Rossdale .4 | 46.1 | 44 | 10.4 | 24 |
| Rossdale .6 | 70.7 | 71.2 | 21.1 | 21 |
| Rossdale .8 | 96.5 | 103.0 | 31.5 | 18.2 |
| Pigeon .25 | 19.6 | 20.0 | 9.0 | 9.8 |
| Pigeon .50 | 40.6 | 41.2 | 17.5 | 18.2 |
| Pigeon .75 | 59.8 | 60.8 | 25.3 | 25.2 |
| Wabamun .25 | 16.8 | 19.2 | 12.8 | 10.8 |
| Wabamun .50 | 34.4 | 41.2 | 24.9 | 17.4 |
| Wabamun .75 | 43.0 | 44.4 | 47.0 | 43.8 |
| Slave .25 | 14.7 | 15.6 | 4.8 | 7.0 |
| Slave .50 | 32.1 | 31.8 | 9.5 | 10.0 |
| Slave .75 | 47.7 | 49.2 | 18.6 | 12.6 |
| Driedmeat .25 | 25.7 | 26.2 | 15.9 | 16.6 |
| Driedmeat .50 | 60.9 | 58.2 | 24.4 | 27.4 |
| Driedmeat .75 | 87.6 | 108.4 | 40.7 | 19.8 |
| Miquelon .25 | 27.1 | 26.8 | 208.7 | 204.8 |
| Miquelon .50 | 59.9 | 53.2 | 410.2 | 416.2 |
| Miquelon .75 | 82.1 | 83.0 | 626.3 | 627.2 |
| Hasse .25 | 28.4 | 28.8 | 32.3 | 32.2 |
| Hasse .50 | 56.2 | 56.6 | 67.5 | 67.4 |
| Hasse .75 | 85.1 | 85.8 | 100.8 | 100.6 |
| Red Deer .25 | 29.5 | 30.4 | 10.9 | 9.4 |
| Red Deer .50 | 64.4 | 61.4 | 20.6 | 20.8 |
| Red Deer .75 | 99.5 | 100 | 22.1 | 18.0 |

| Sample * | a | b | c |
|---|---|---|---|
| Rossdale .2 | .000242 | .003670 | 1.848 |
| Rossdale .4 | .003056 | .005577 | 3.333 |
| Rossdale .6 | .00473 | .01190 | 3.126 |
| Rossdale .8 | 0 | .03125 | 1.637 |
| Pigeon .25 | .001578 | .01049 | 4.087 |
| Pigeon .50 | 0 | .01502 | 1.912 |
| Pigeon .75 | .001752 | .01667 | 1.449 |
| Wabamun .25 | .002148 | .01886 | 3.155 |
| Wabamun .50 | 0 | .03927 | 1.834 |
| Wabamun .75 | 0 | .1478 | 2.945 |
| Slave .25 | .001478 | .003057 | 4.691 |
| Slave .50 | .001196 | .009401 | 1.581 |
| Slave .75 | 0 | .02664 | 1.661 |
| Hasse .25 | .000738 | .006905 | 1.598 |
| Hasse .50 | 0 | .02152 | 0.966 |
| Hasse .75 | 0 | .07225 | 1.672 |
| Red Deer .25 | .001028 | .004216 | 3.186 |
| Red Deer .50 | .000451 | .02005 | 1.757 |
| Red Deer .75 | 0 | .05848 | 2.023 |

# APPENDIX B

## BATCH TEST LOG(C/Co) VS TIME PLOTS

Figure B-1
Log C/Co vs t
Rossdale .8

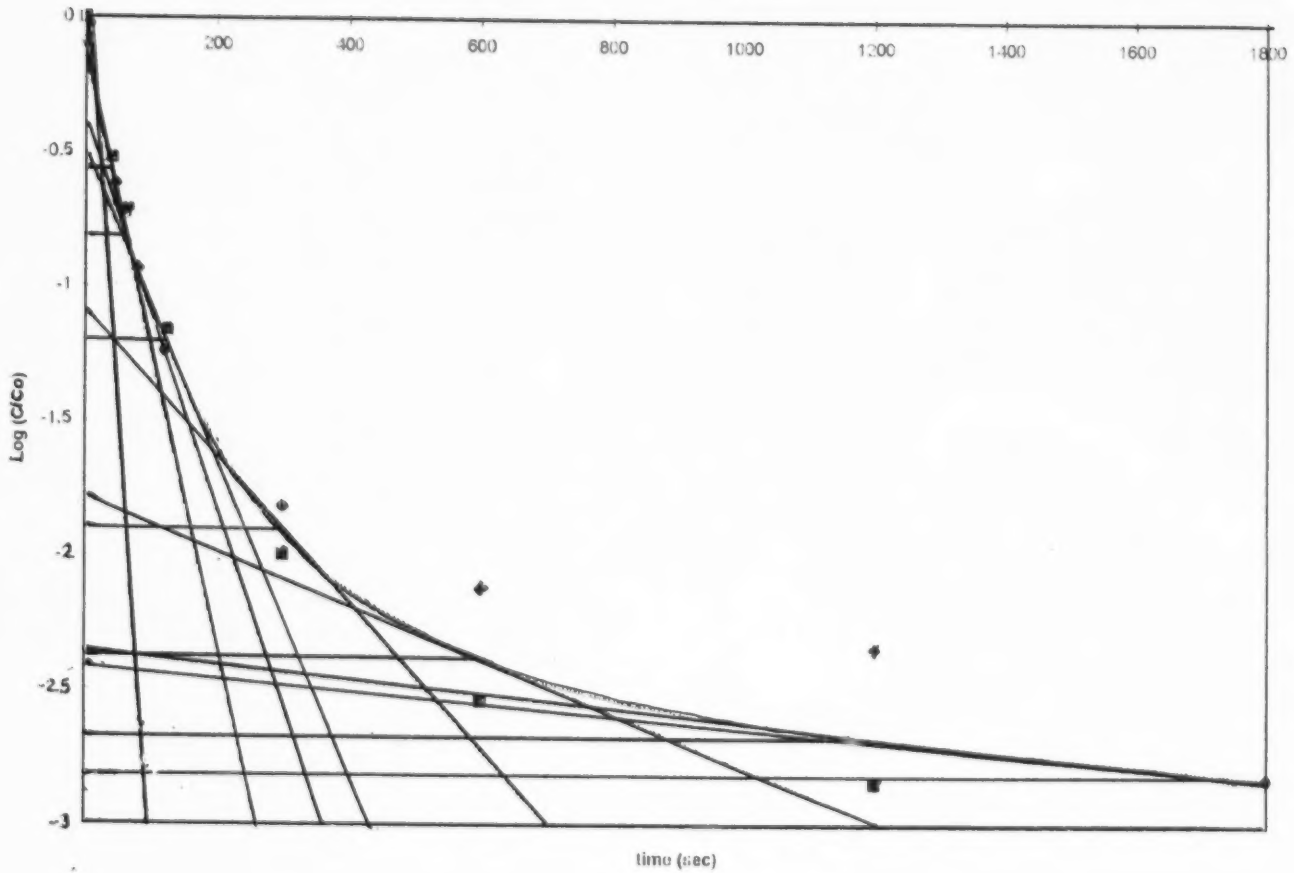

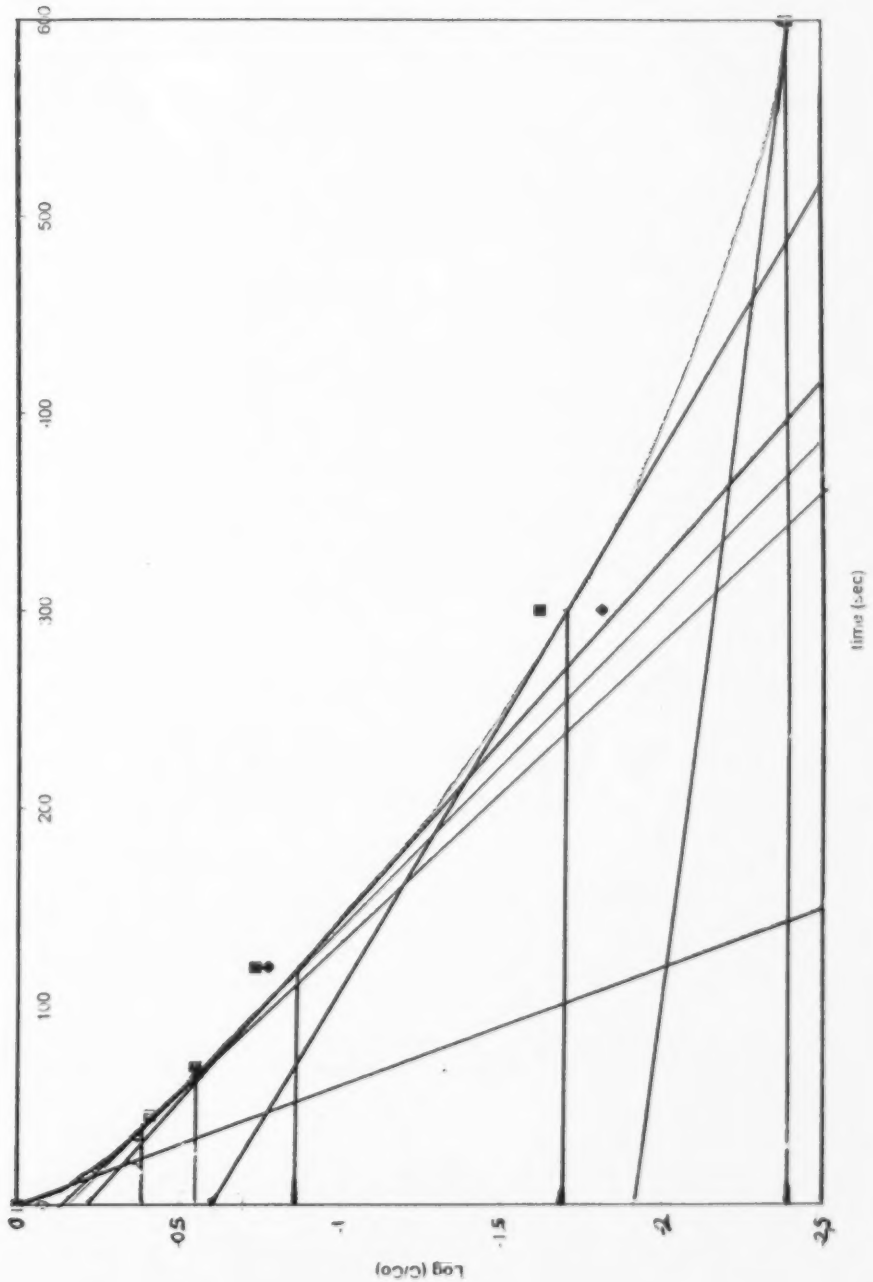


Figure B-2
Log C/Co vs t
Rossdale .6

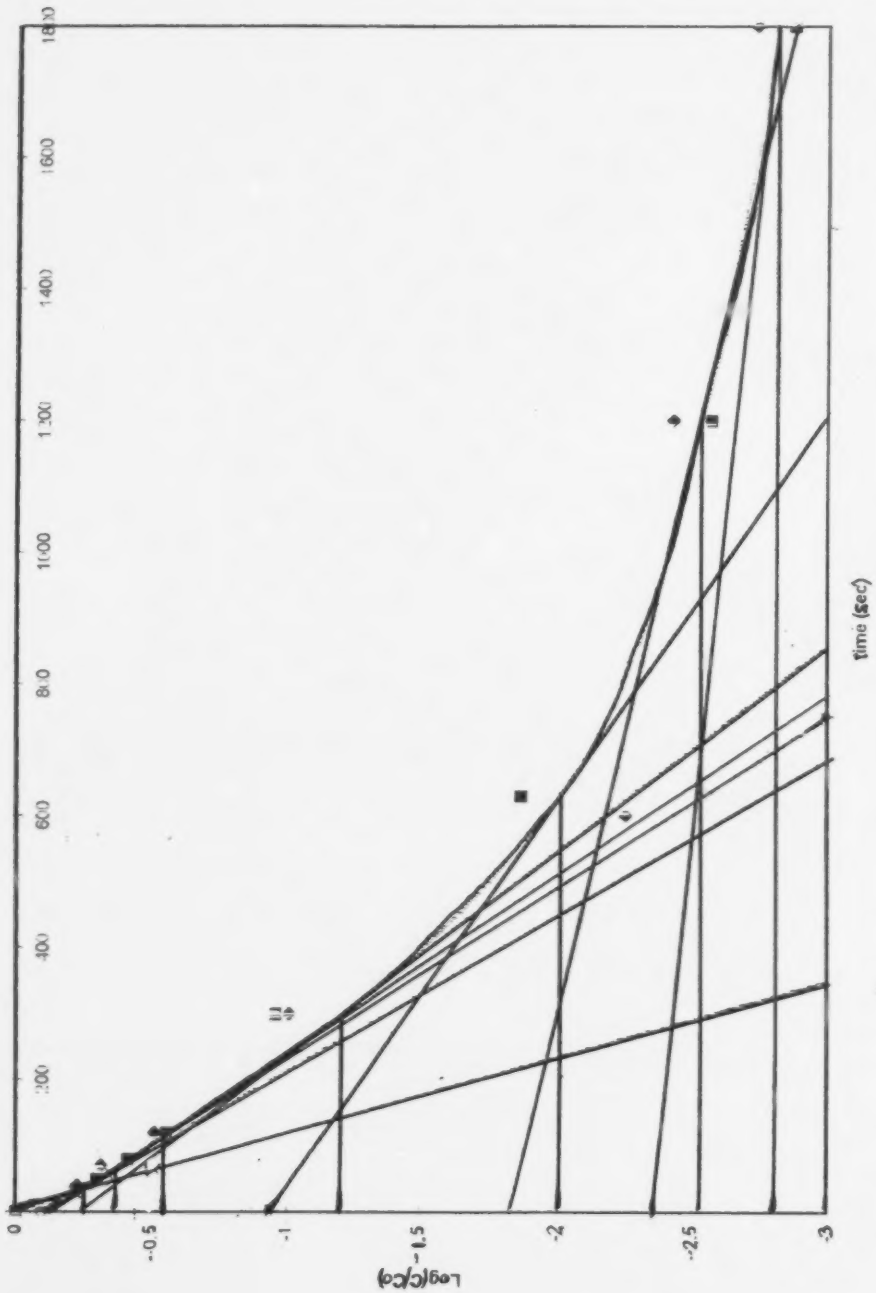


Figure B-3
Log C/Co vs t
Rossdale , 4

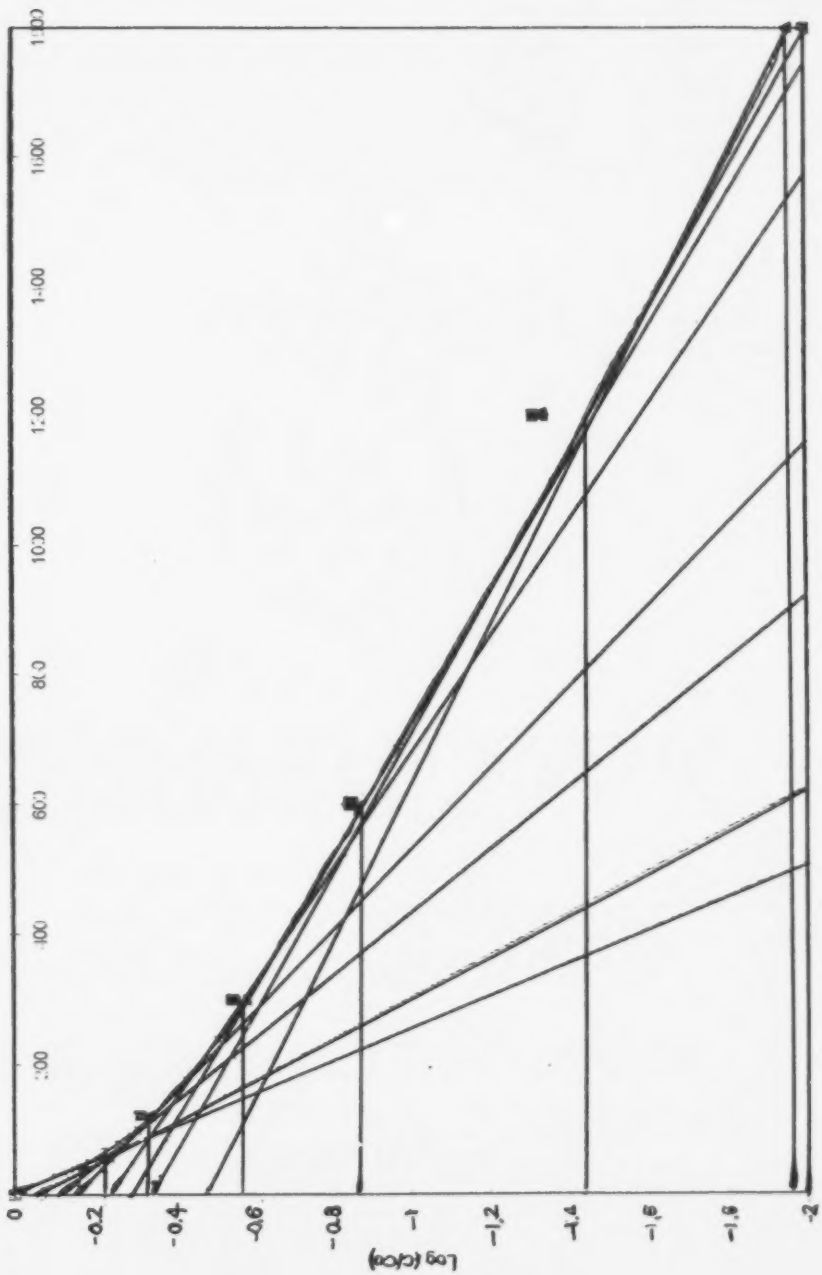


Figure B-4
Log C/Co vs t
Rossdale .2

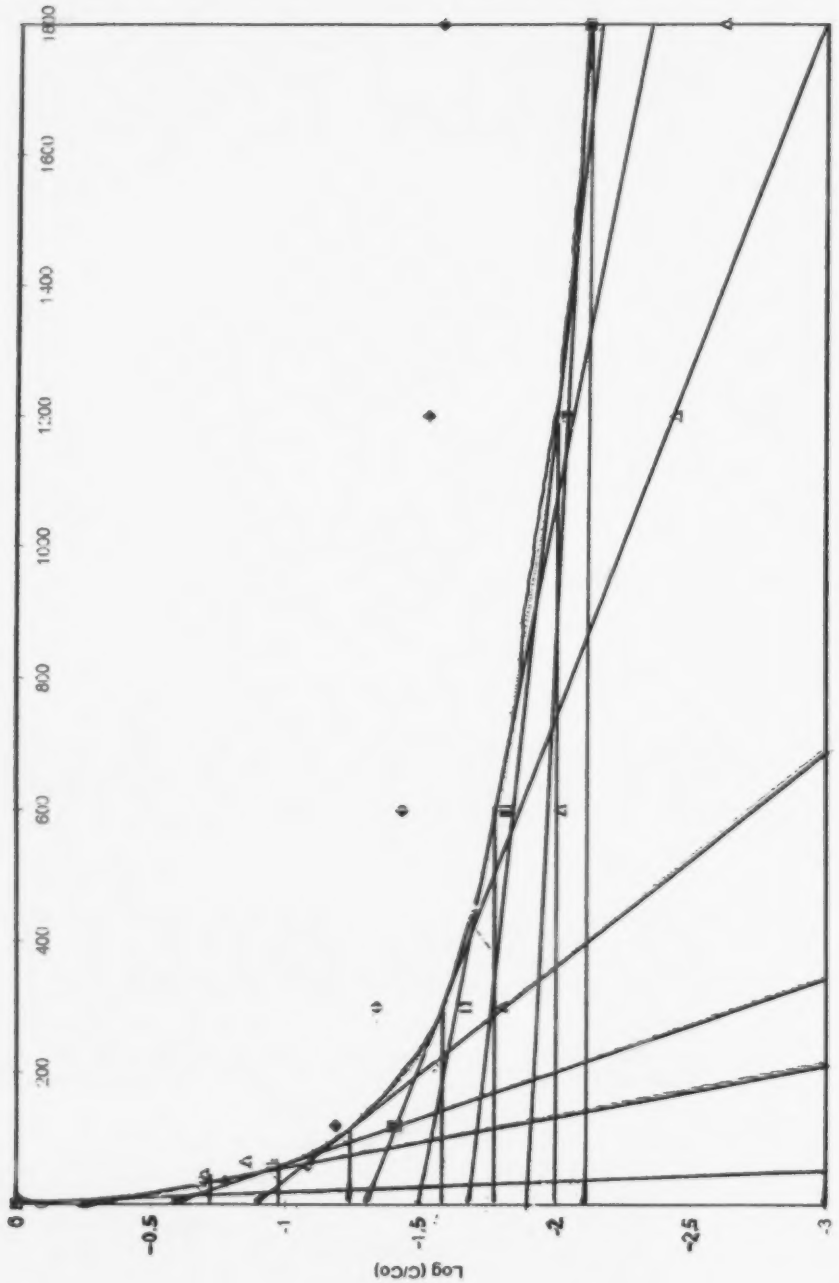


Figure B-5
Log C/Co vs t
Red Deer .75

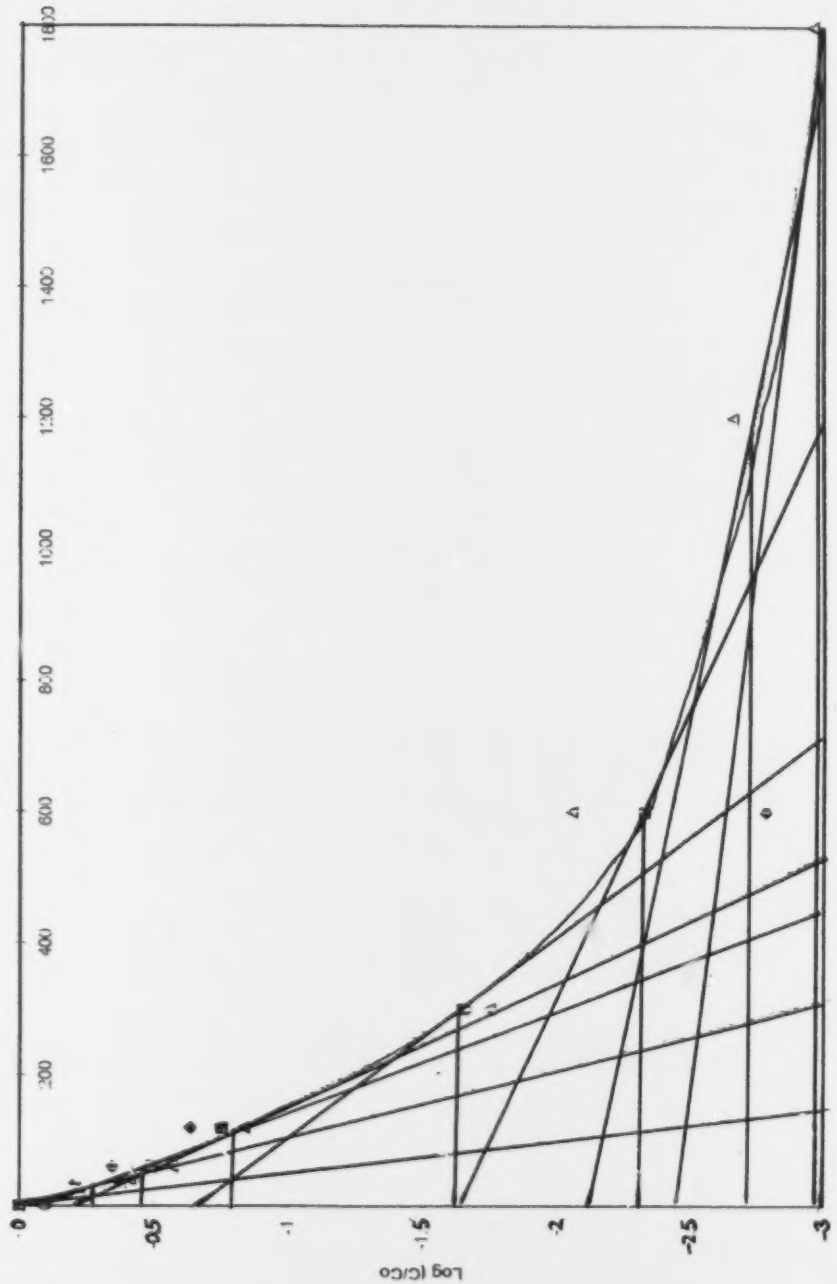


Figure B-6
Log C/Co vs t
Red Diver.50

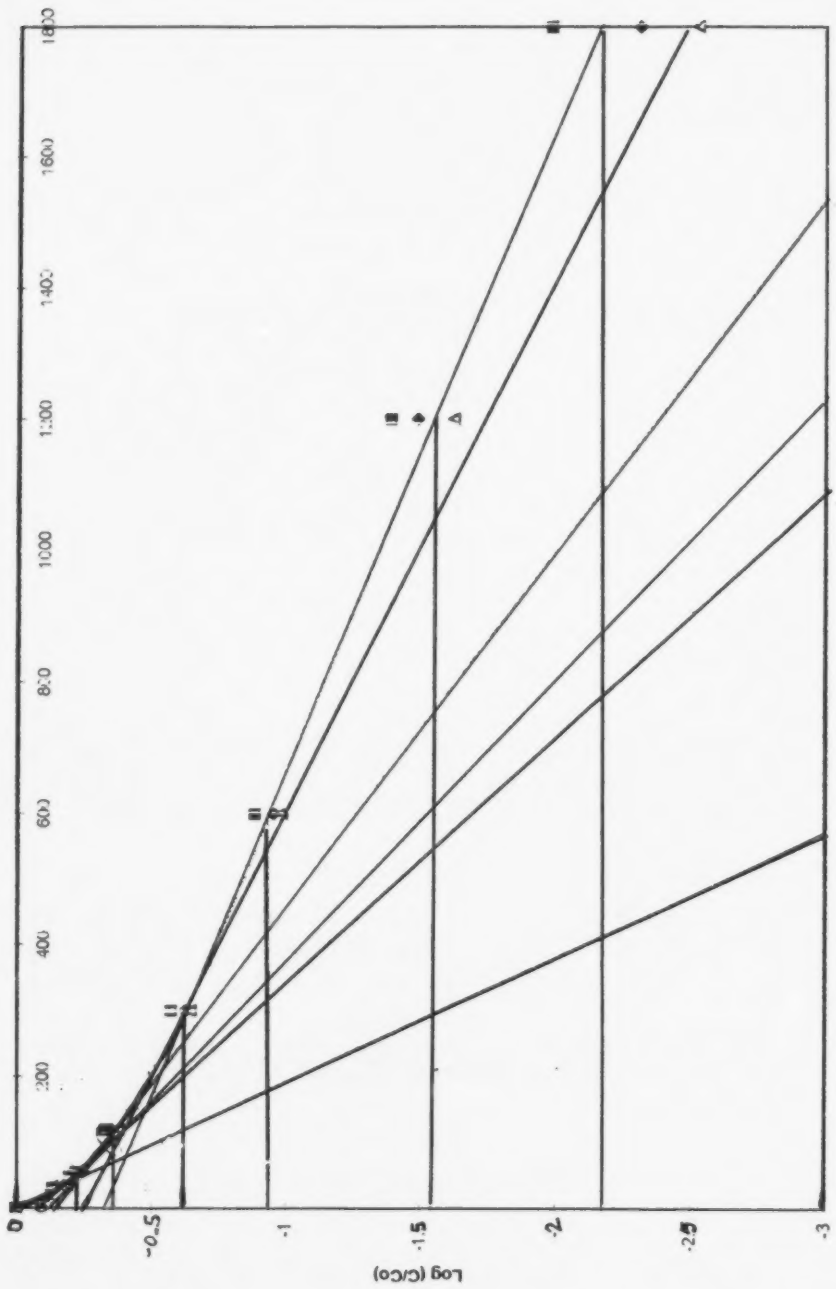


Figure B-7
Log C/Co vs t
Red Deer .25

Figure B-8
Log C/Co vs t
Slave Lake .75

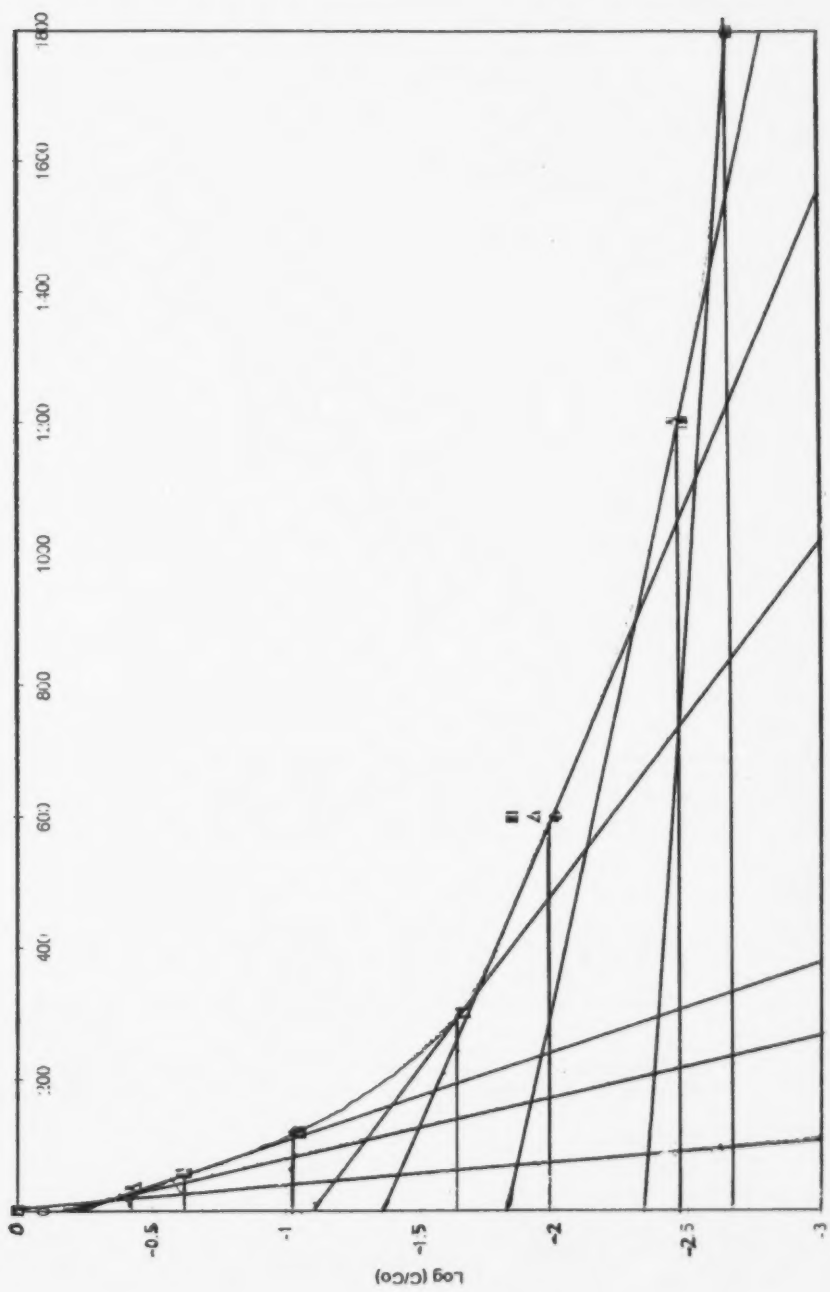

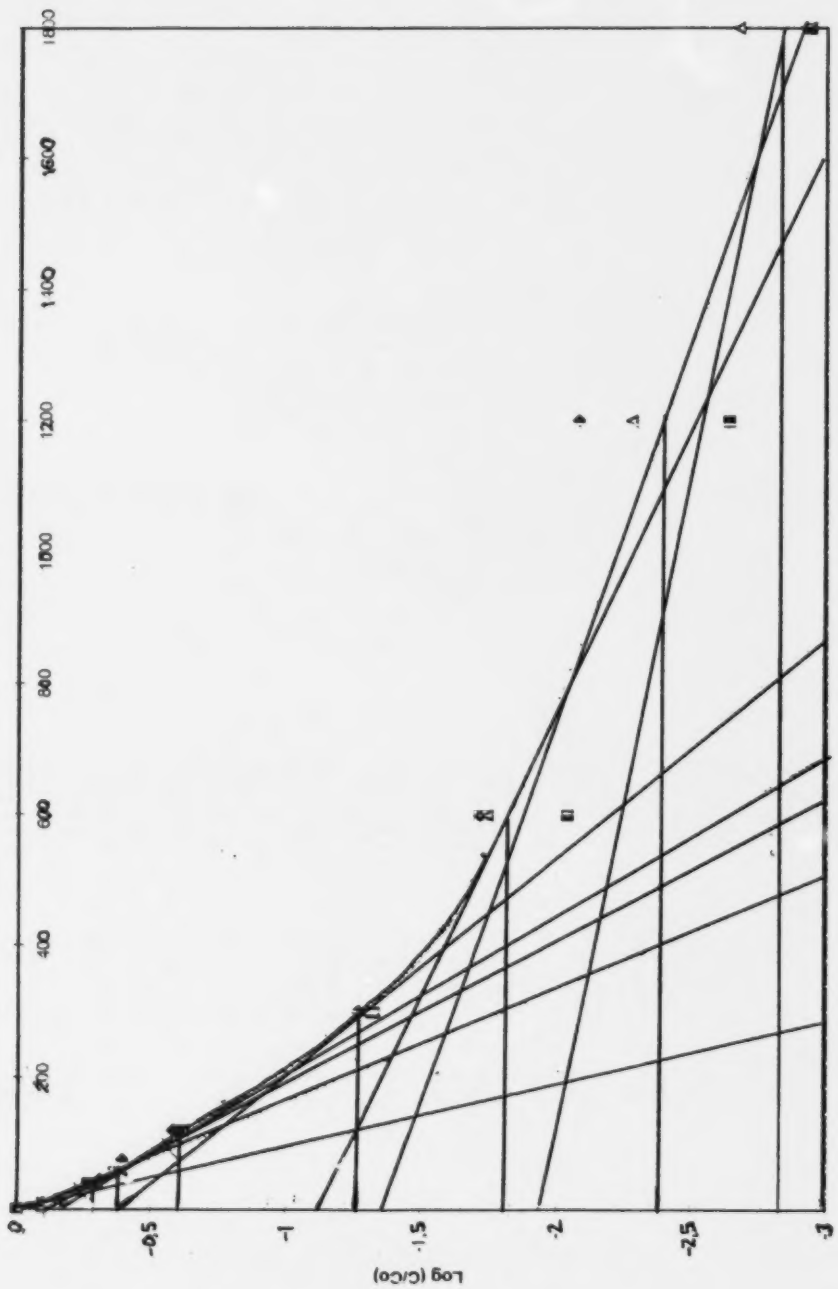


Figure B-9
Log C/Co vs t
Slave Lake .50

Figure B-10
Log C/Co vs t
Slave Lake .25

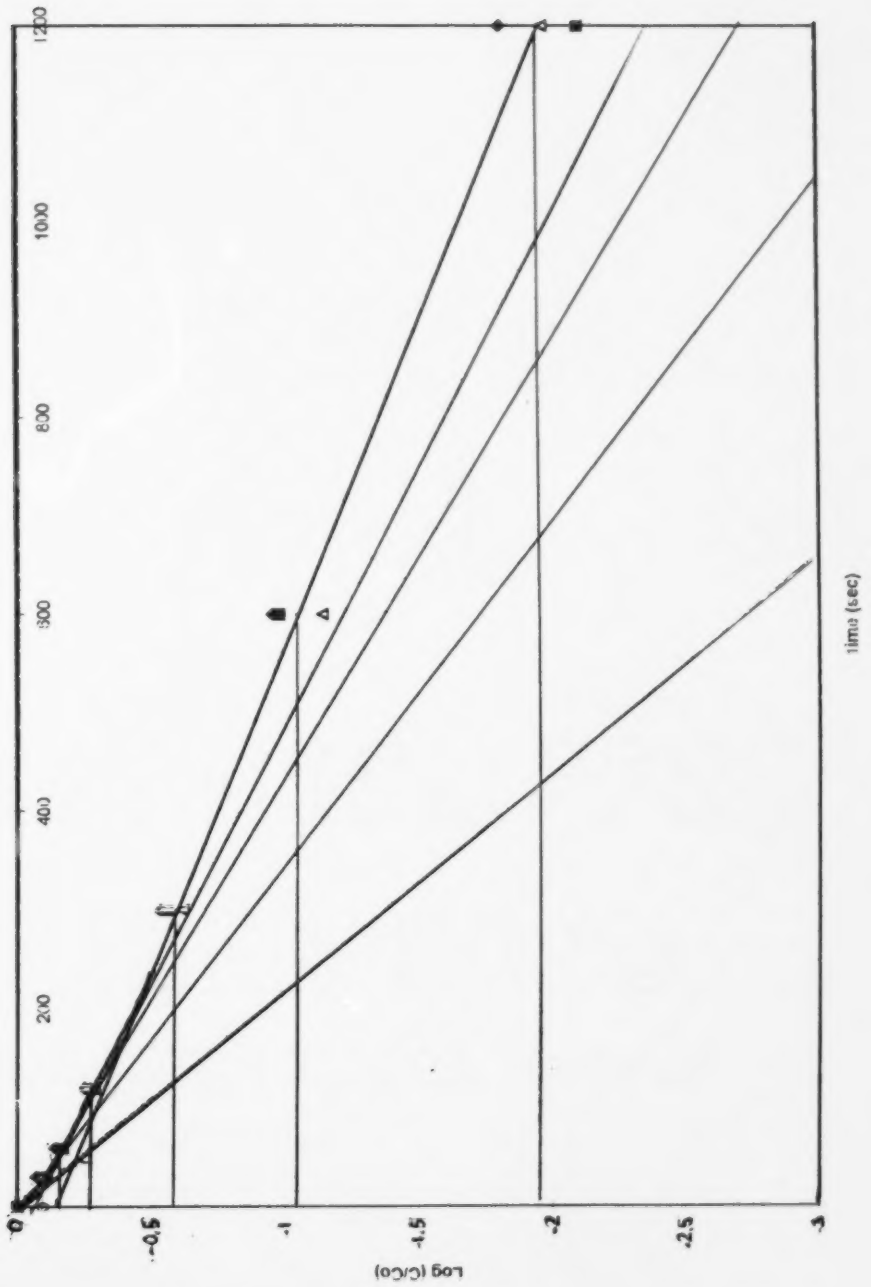

Figure B-11
Log C/Co vs t
Wabamun Lake .75

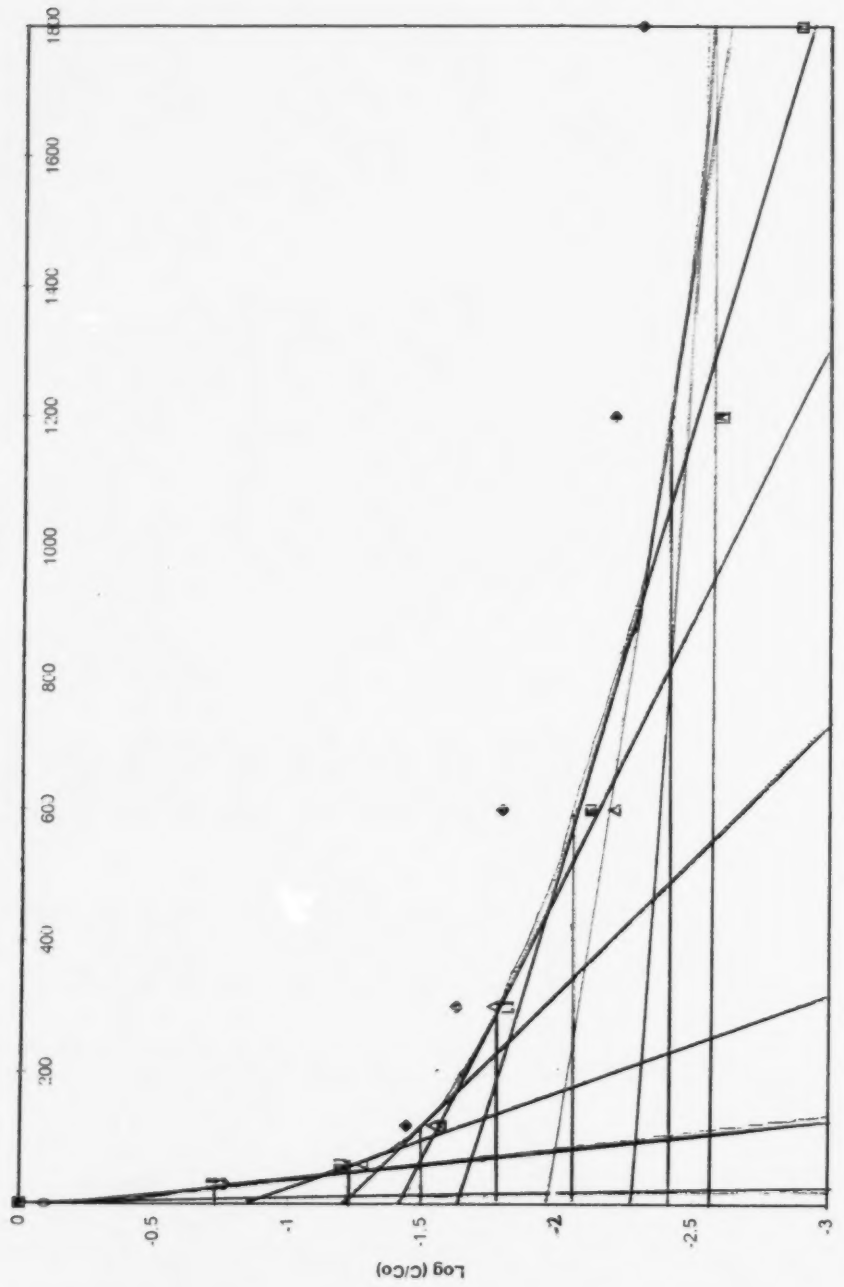

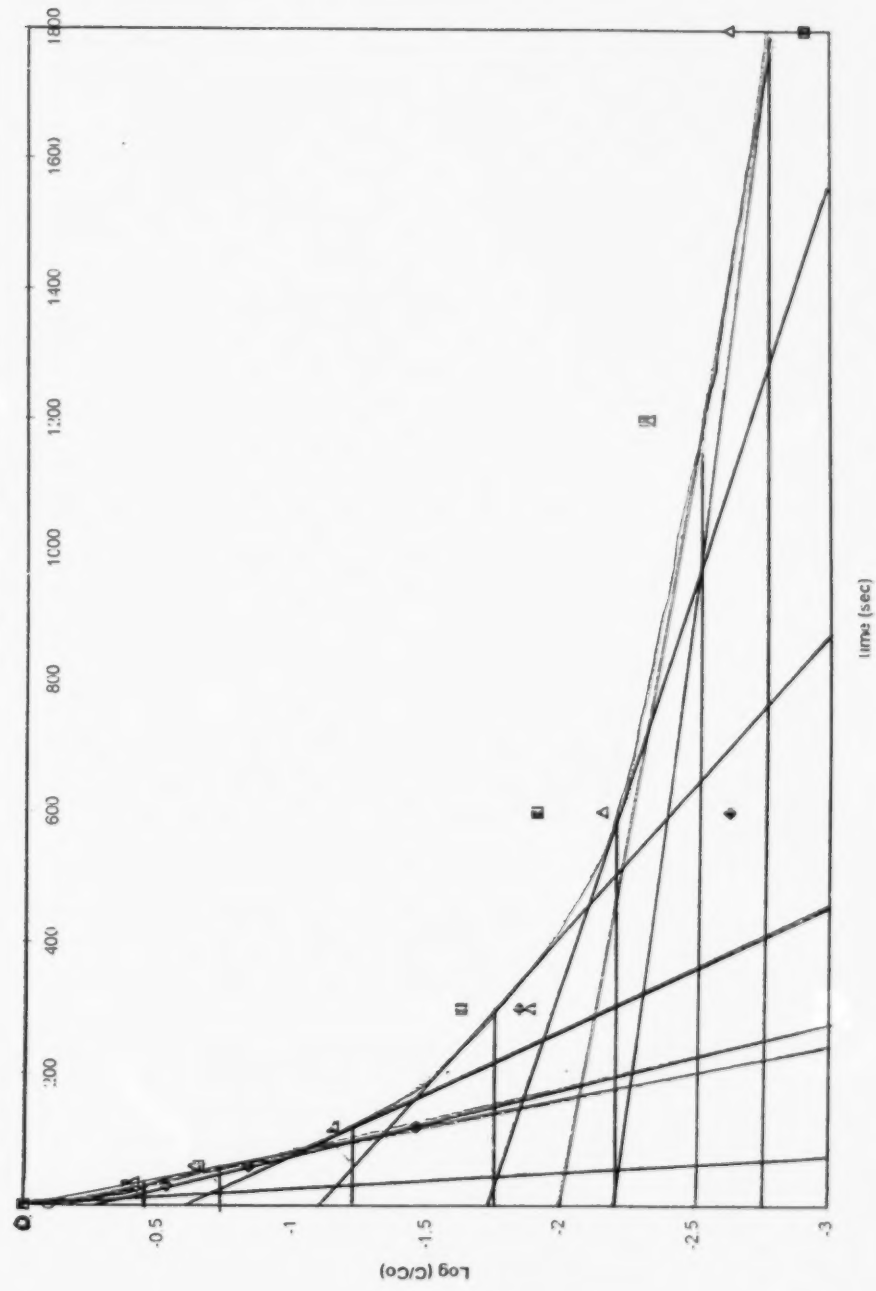


Figure B-12
Log C/Co vs: t
Wabamun Lake .50

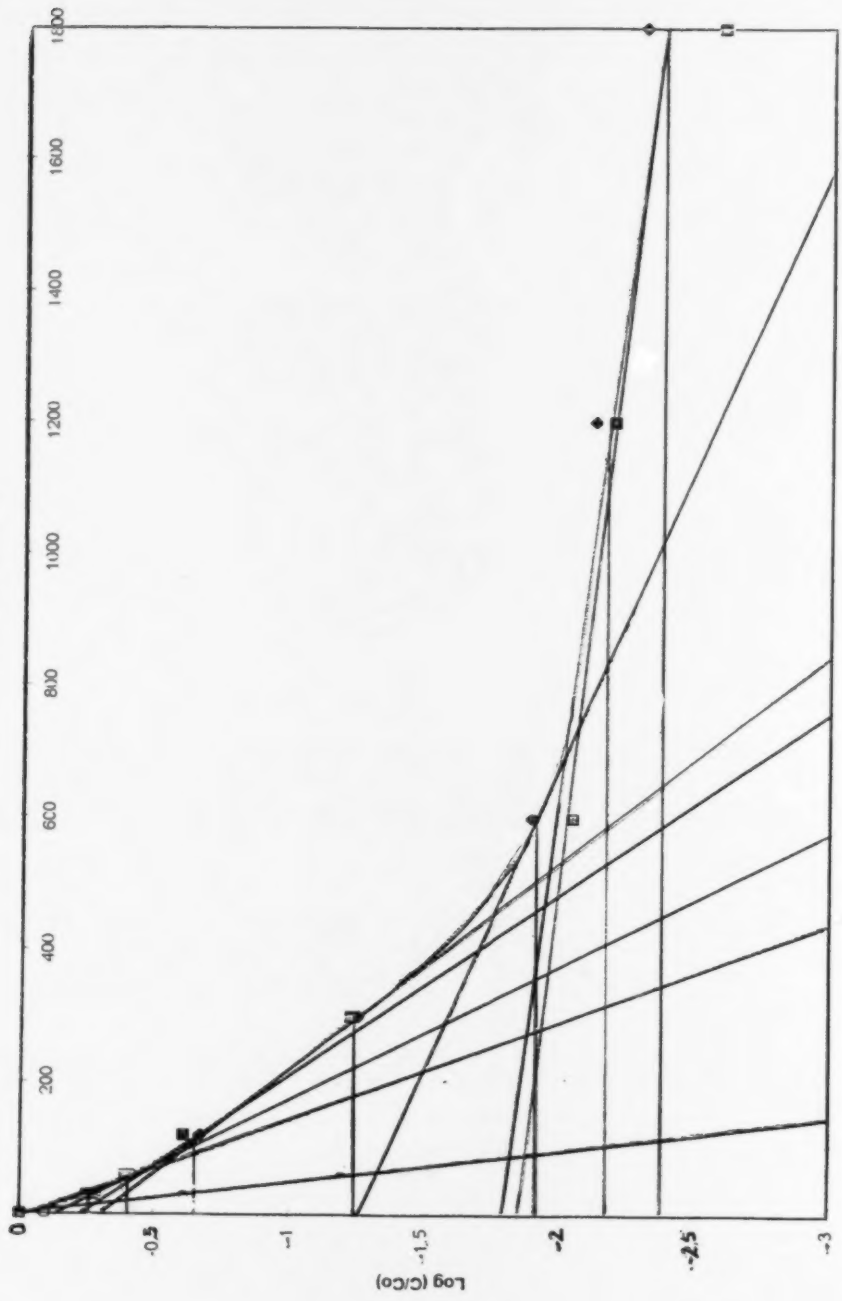


Figure B-13
Log C/Co vs t
Wabamun Lake .25

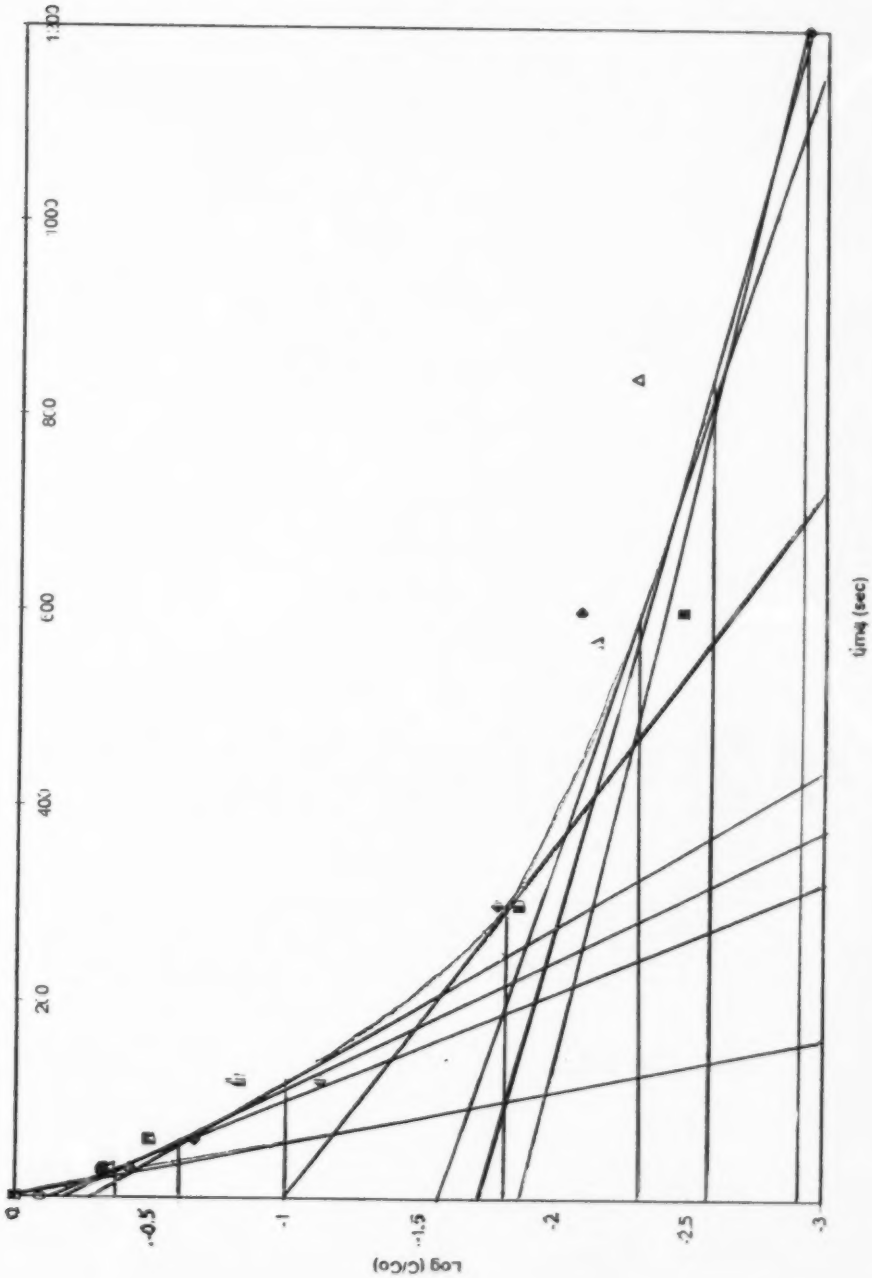


Figure B-14
Log C/Co vs t
Pigeon Lake .75

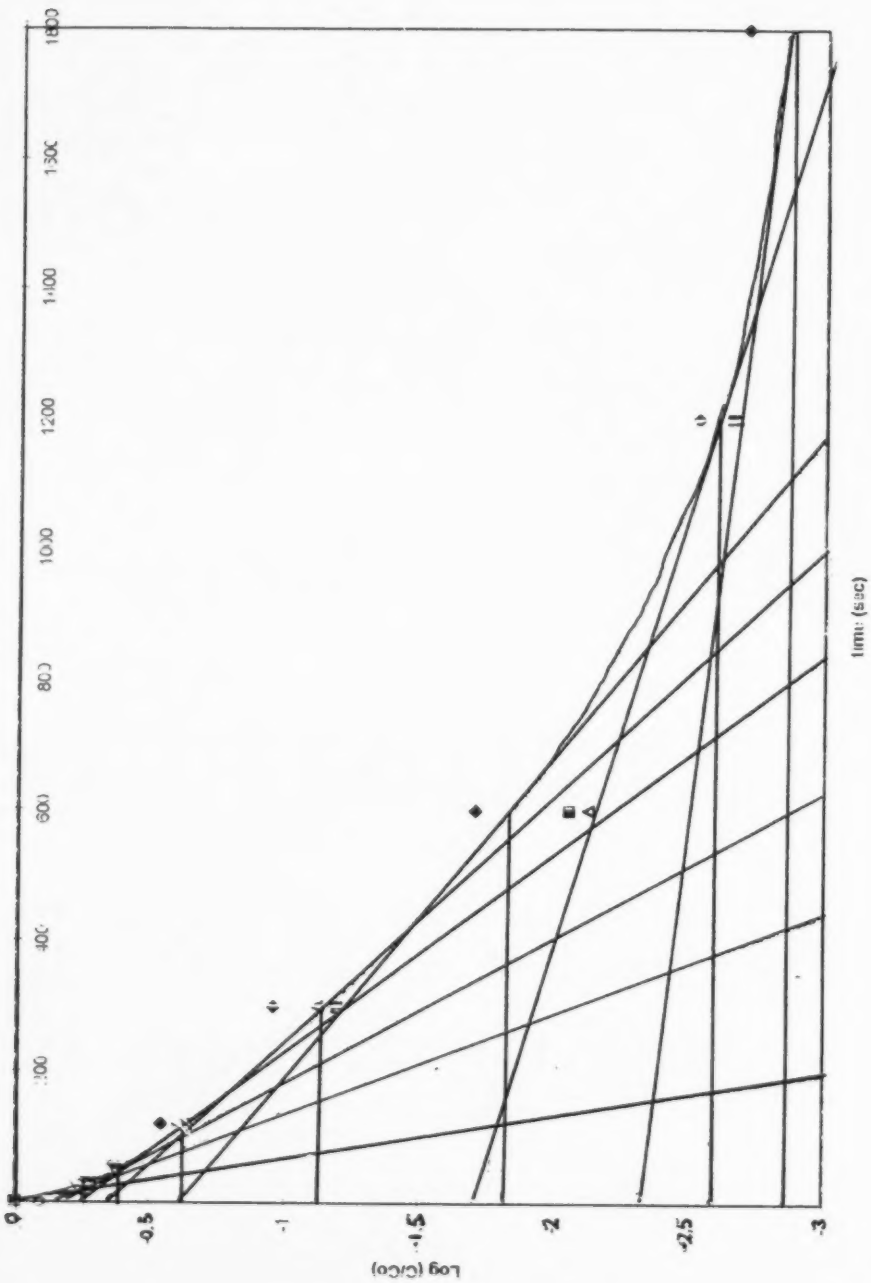


Figure B-15
Log C/Co vs t
Pigeon Lake .50

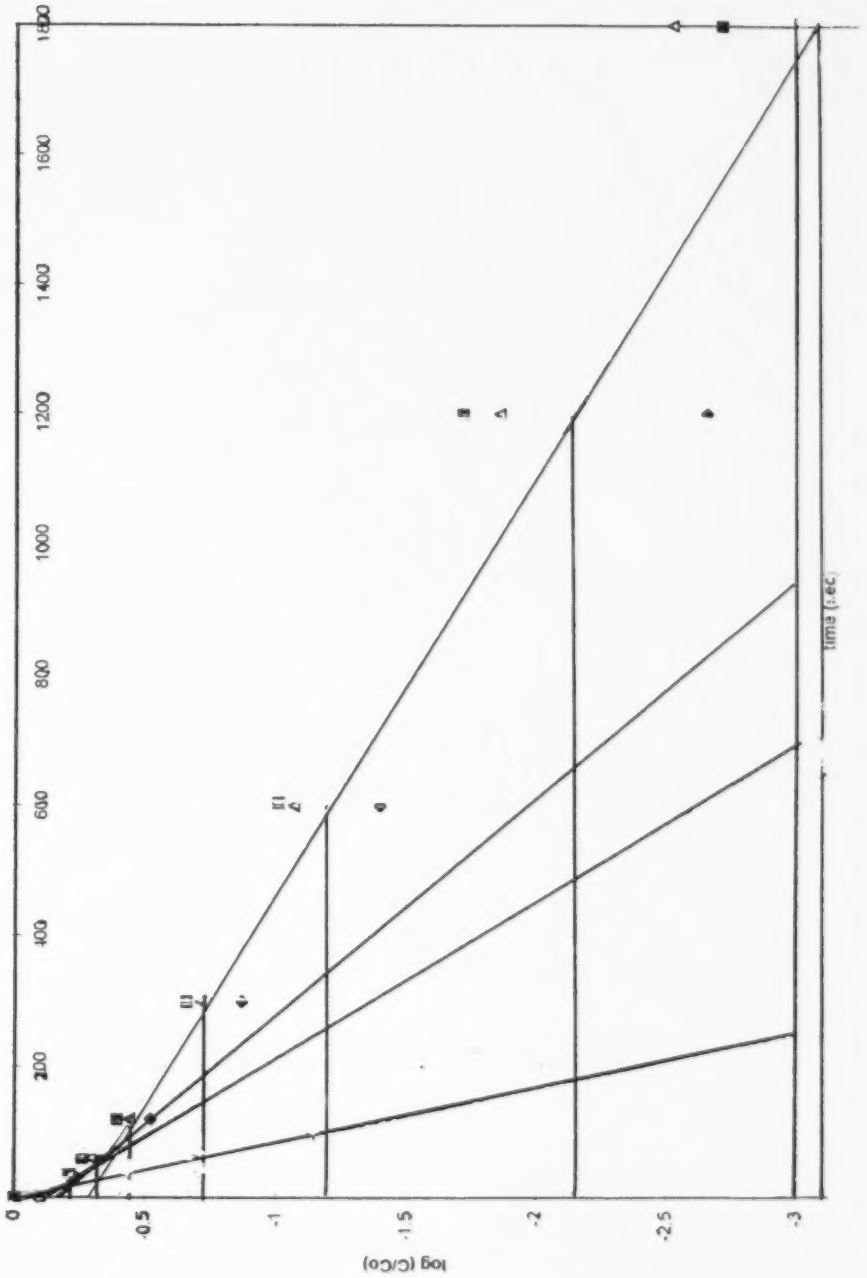


Figure B-16
Log C/Co vs t
Pigeon Lake .25

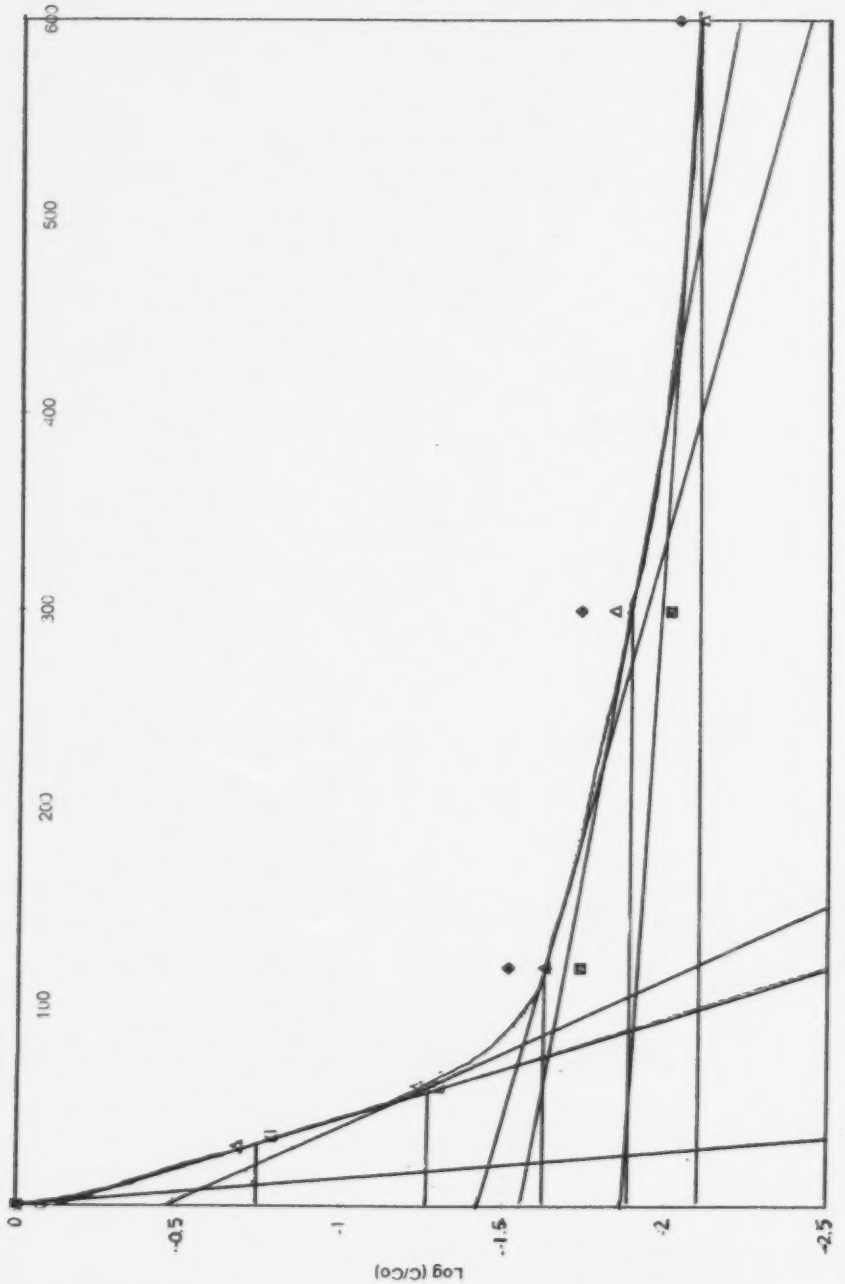


Figure B-17
Log C/Co vs t
Hasse Lake .75

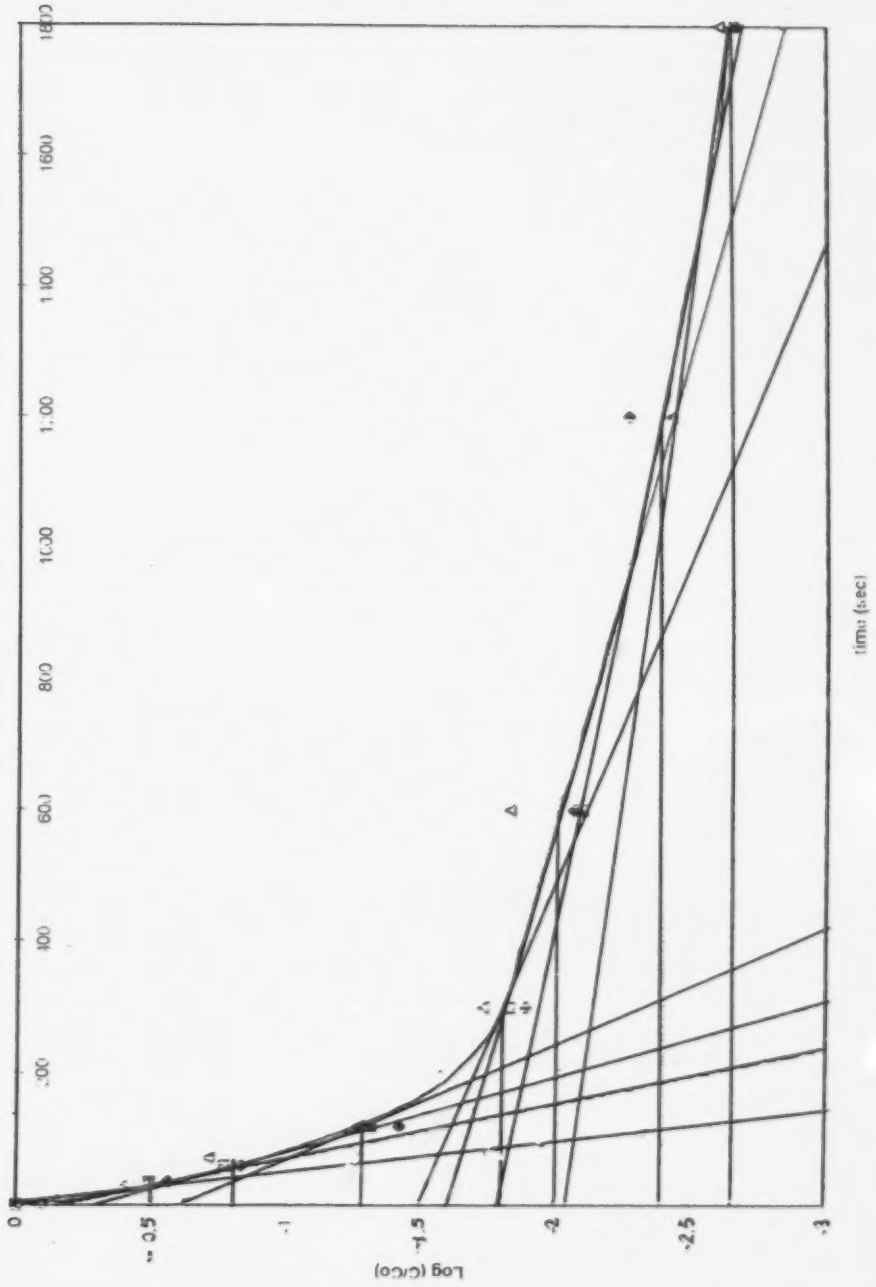


Figure B-18
Log C/Co vs t
Hasse Lake .50

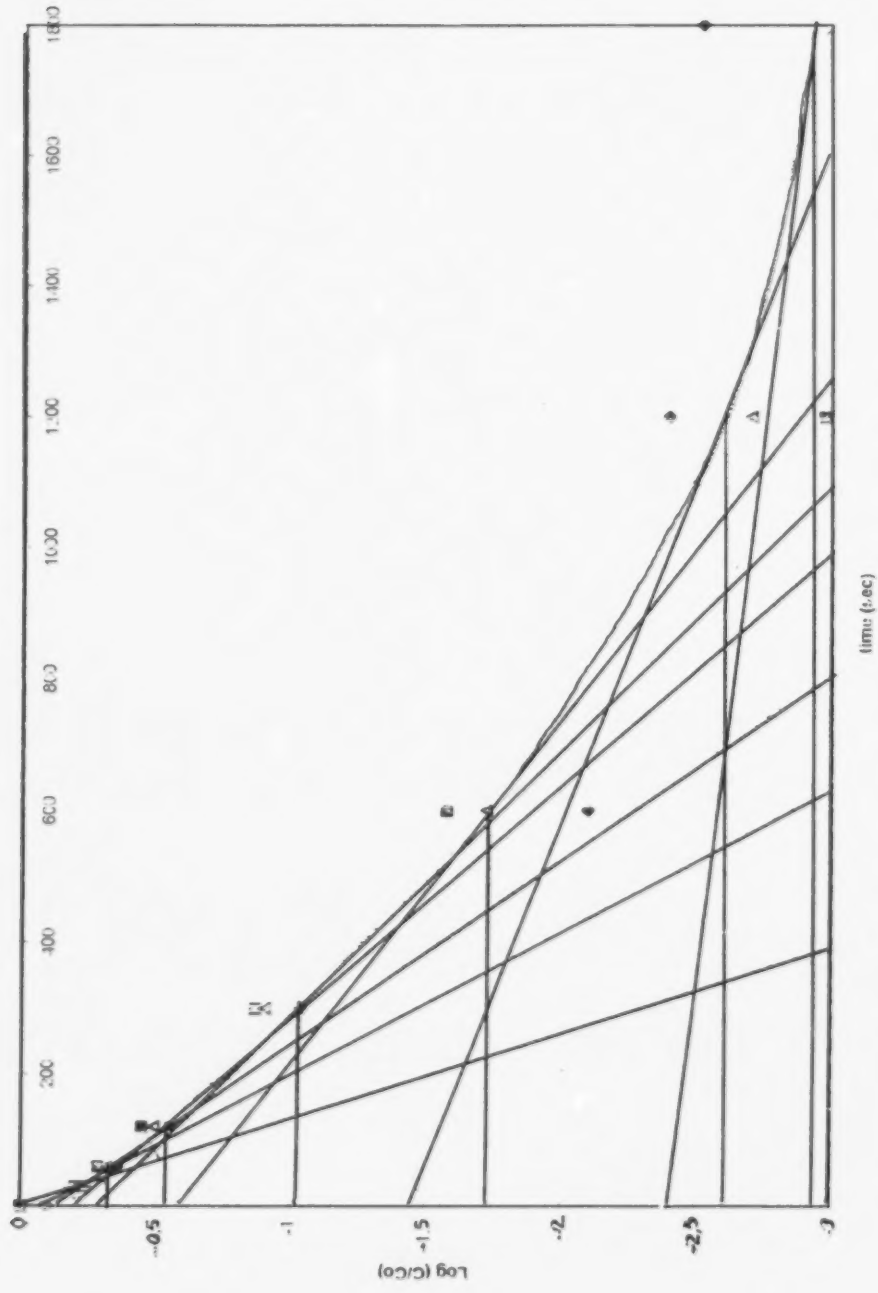


Figure B-19
Log C/Co vs t
Hasse Lake .25

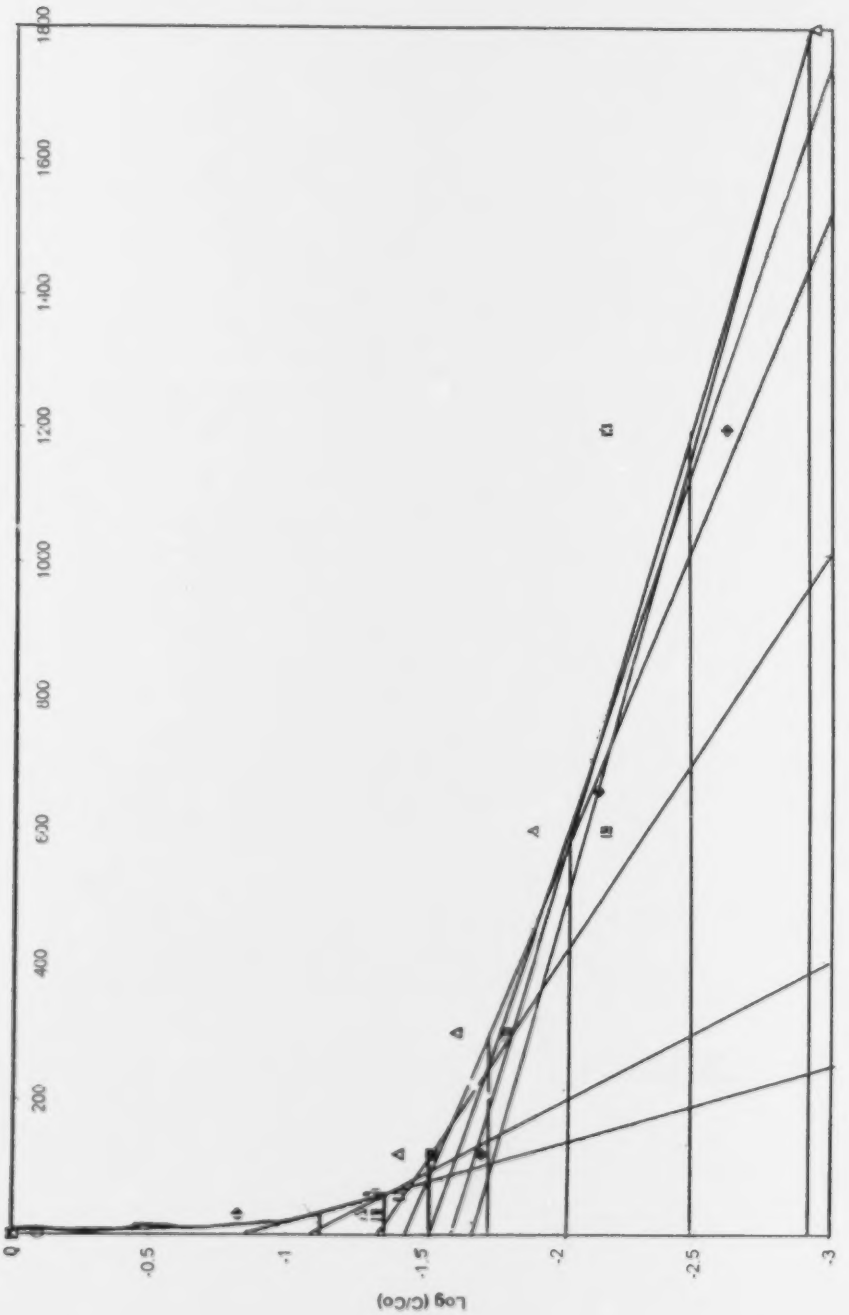


Figure B-20
Log C/Co vs t
Driedmeat Lake .75

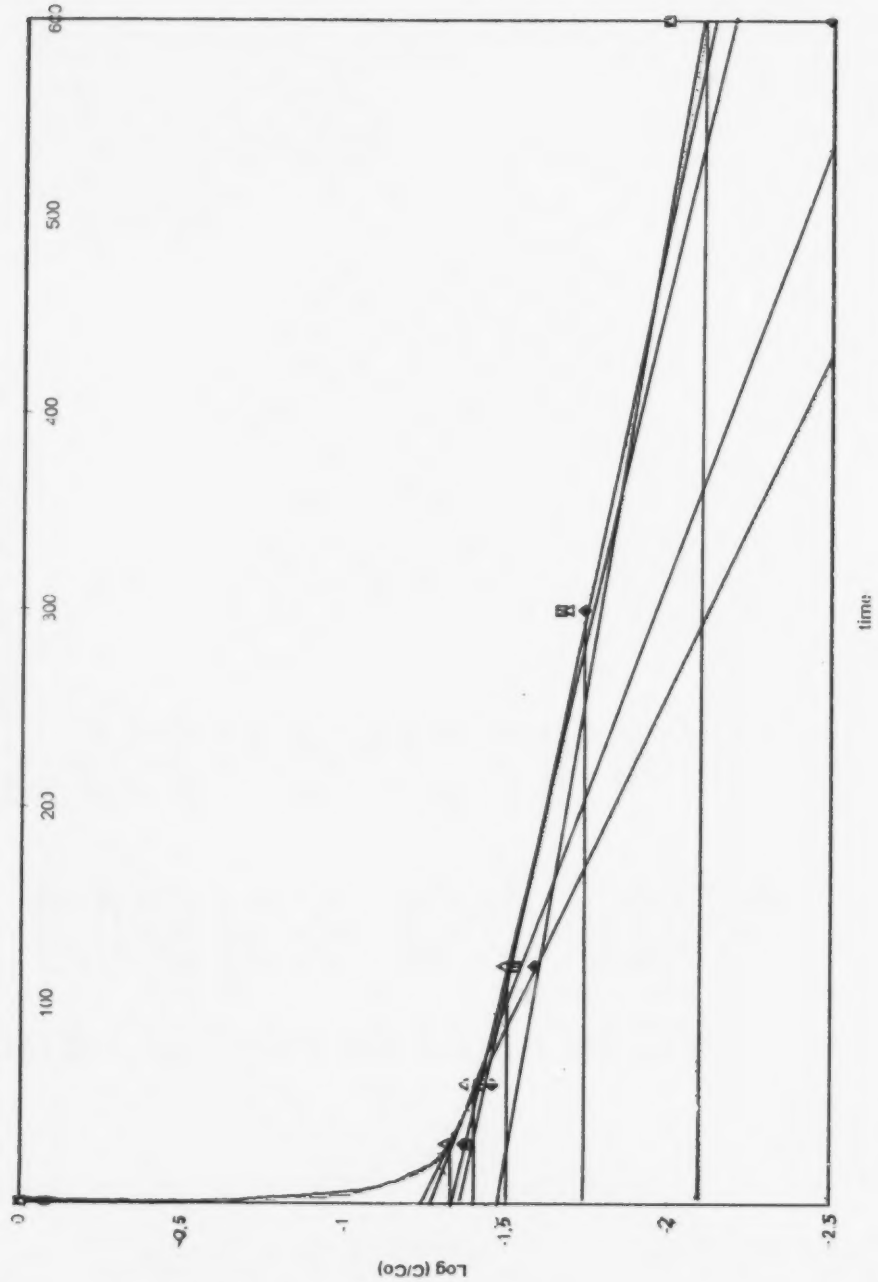


Figure B-21
Log C/Co vs t
Driedmeat Lake ,50

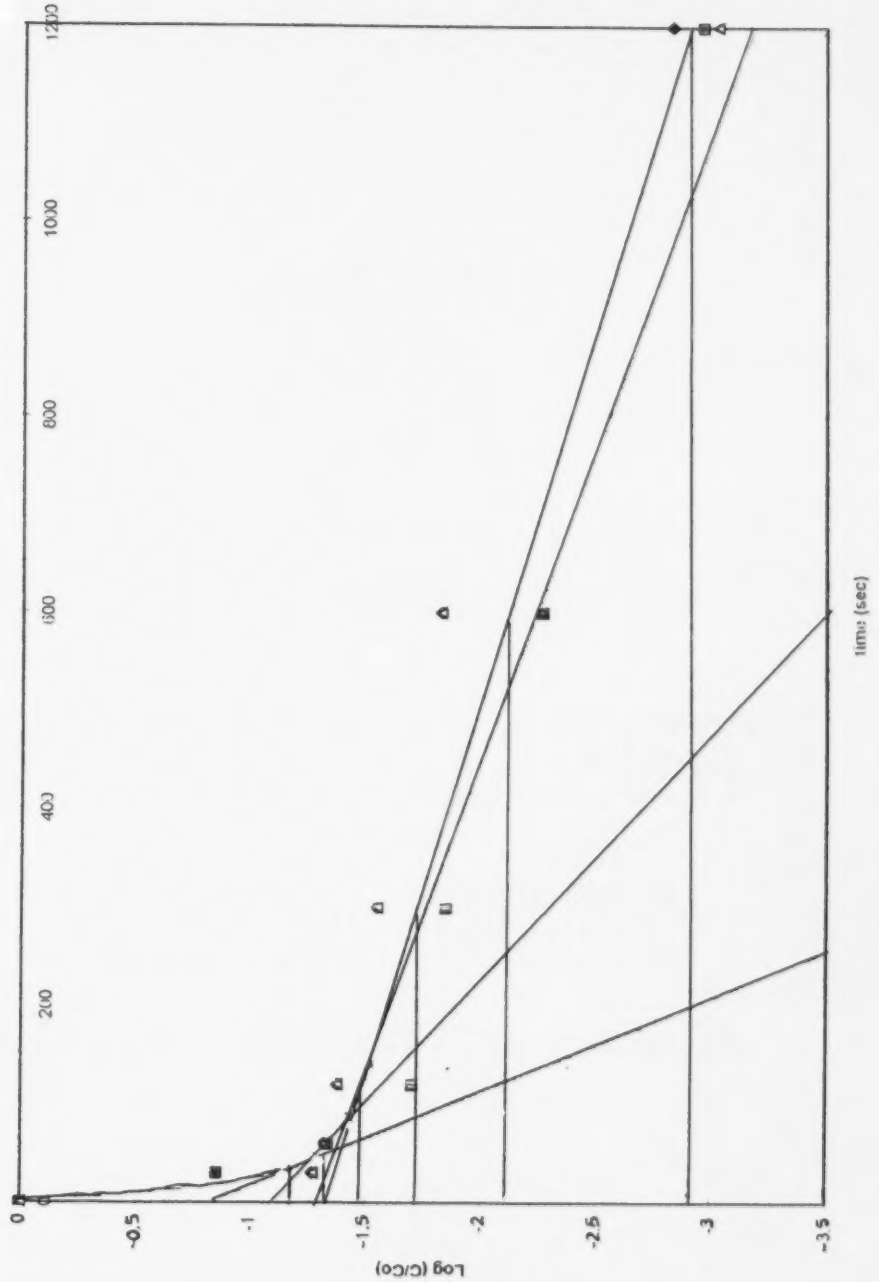


Figure B-22
Log C/Co vs t
Driedmeat Lake .25

# APPENDIX C

## BATCH TEST $K_w$ VS $\Delta O_3$ PLOTS

**Figure C-1 : Fitted kw Curve for Wabamun Lake .25**

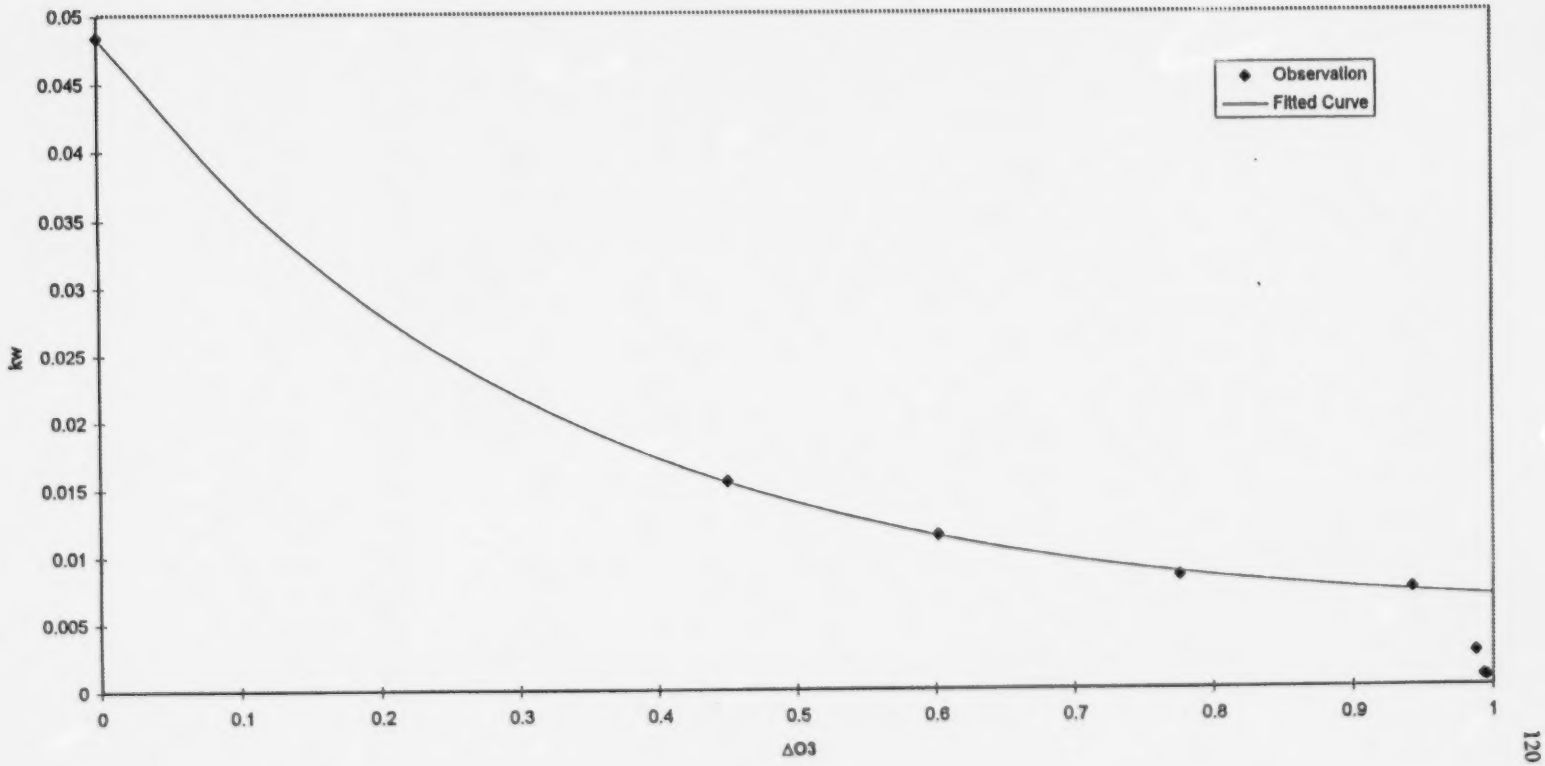

**Figure C-2 : Fitted kw Curve for Wabamun Lake .50**

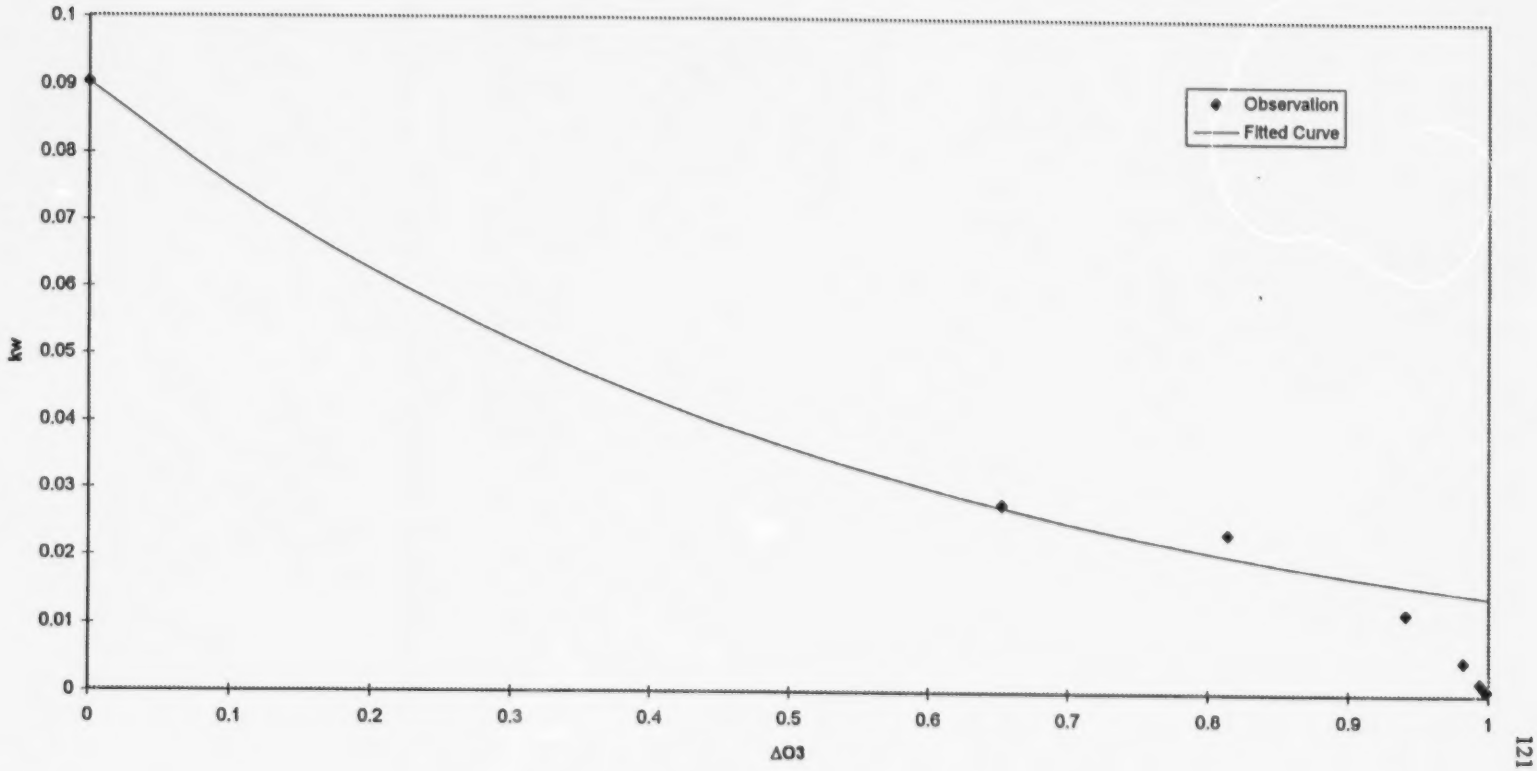

**Figure C-3 : Fitted kw Curve for Wabamun Lake .75**

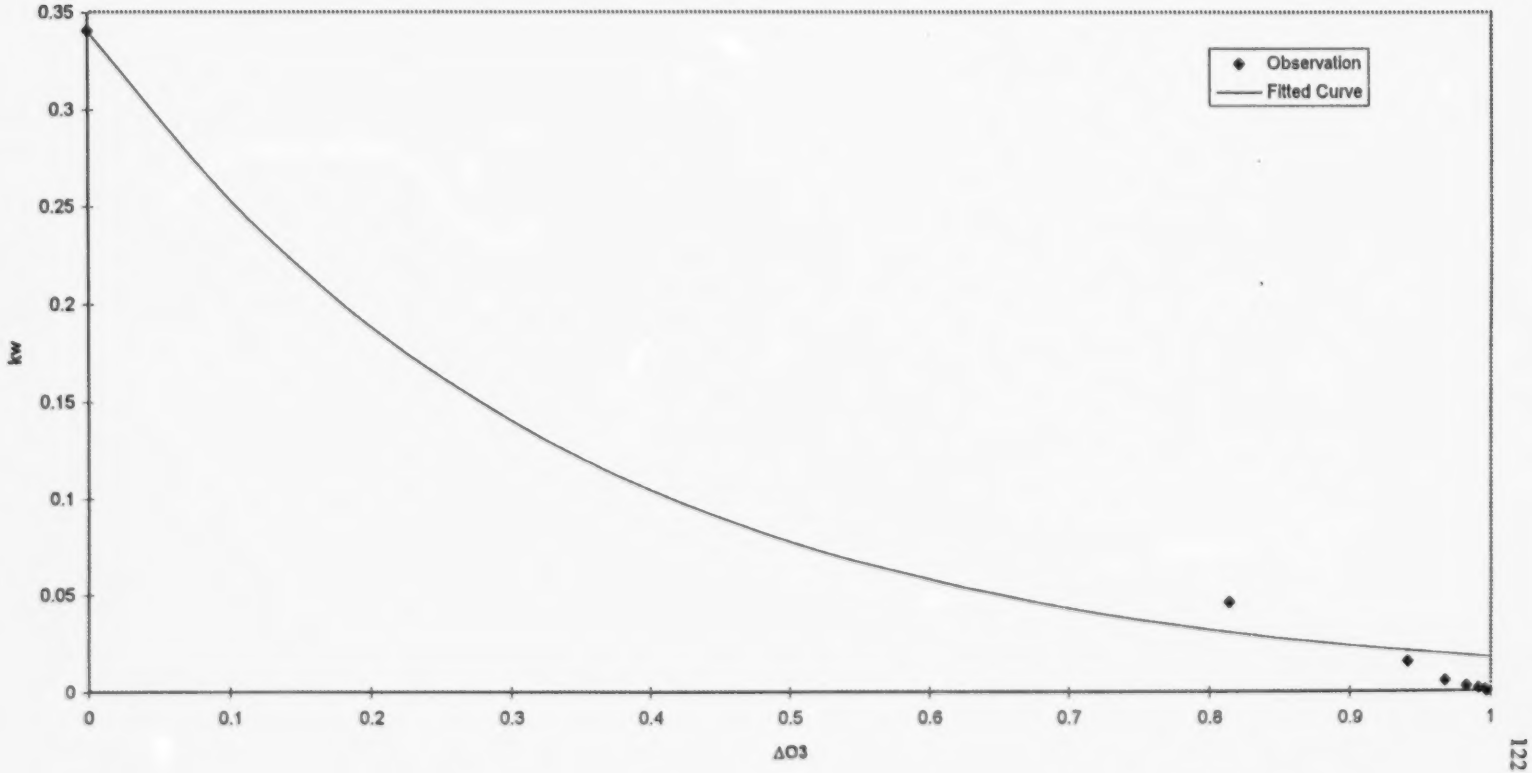

**Figure C-4 : Fitted kw Curve for Slave Lake .25**

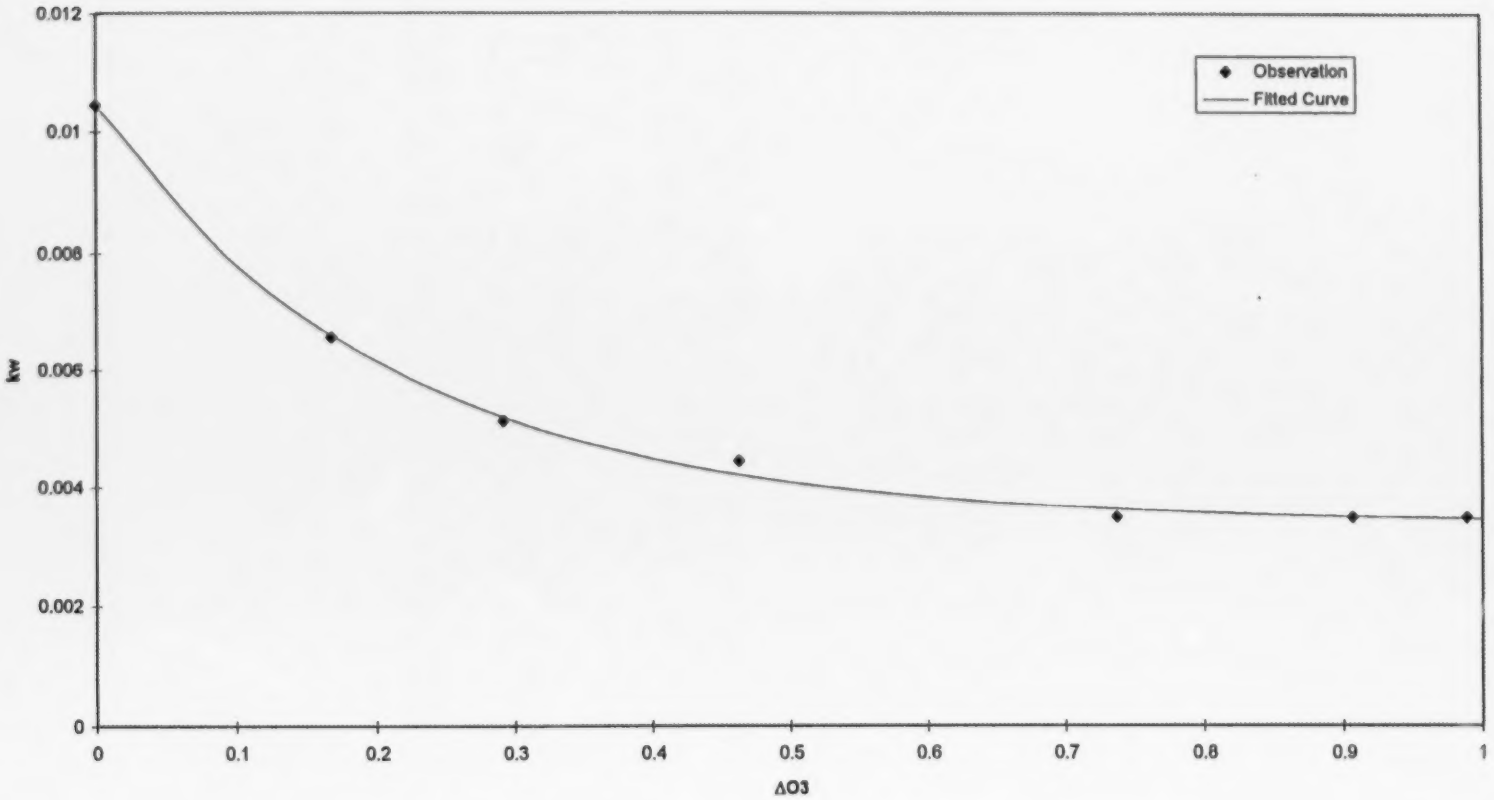

**Figure C-5 : Fitted kw Curve for Slave Lake .50**

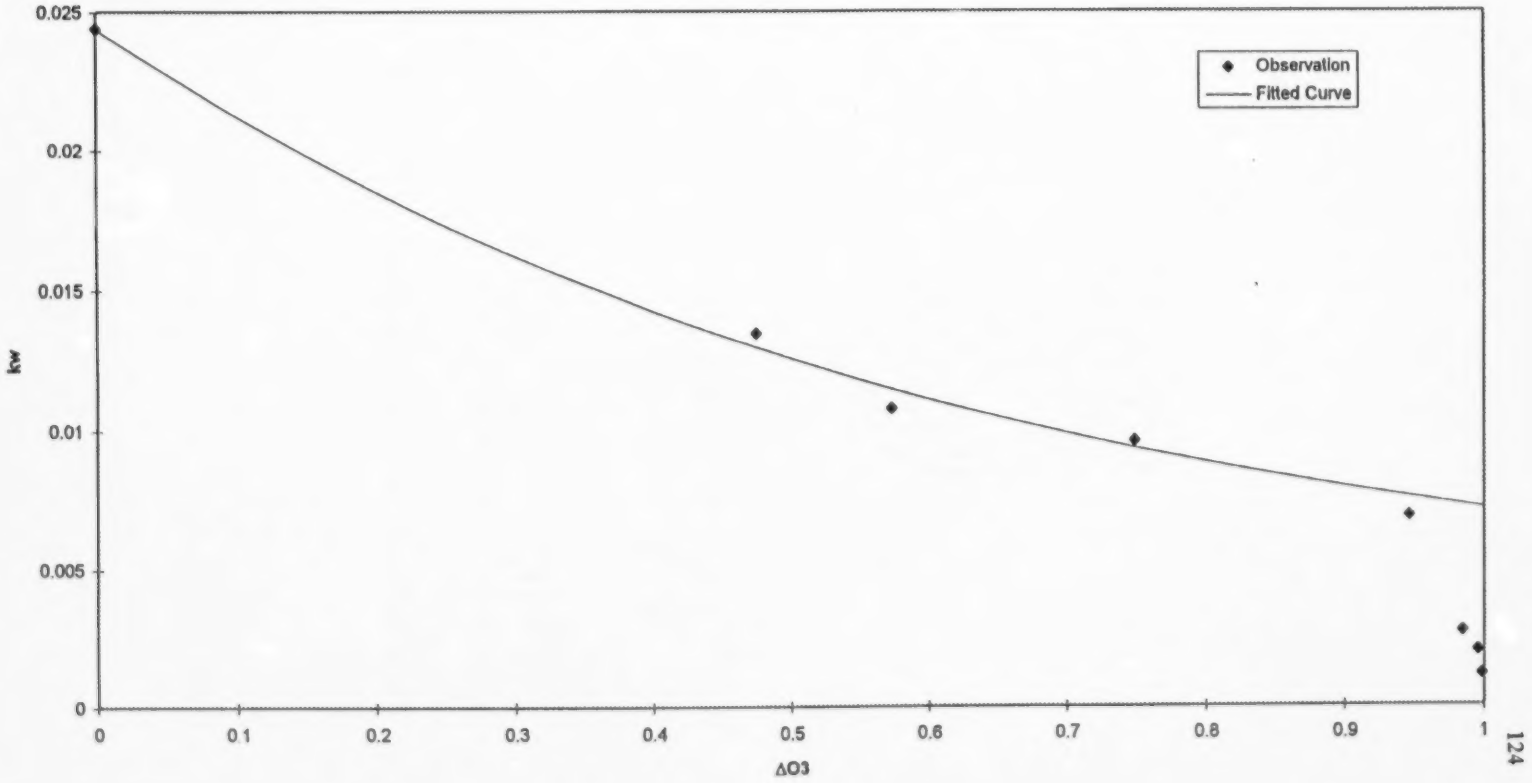

**Figure C-6 : Fitted kw Curve for Slave Lake .75**

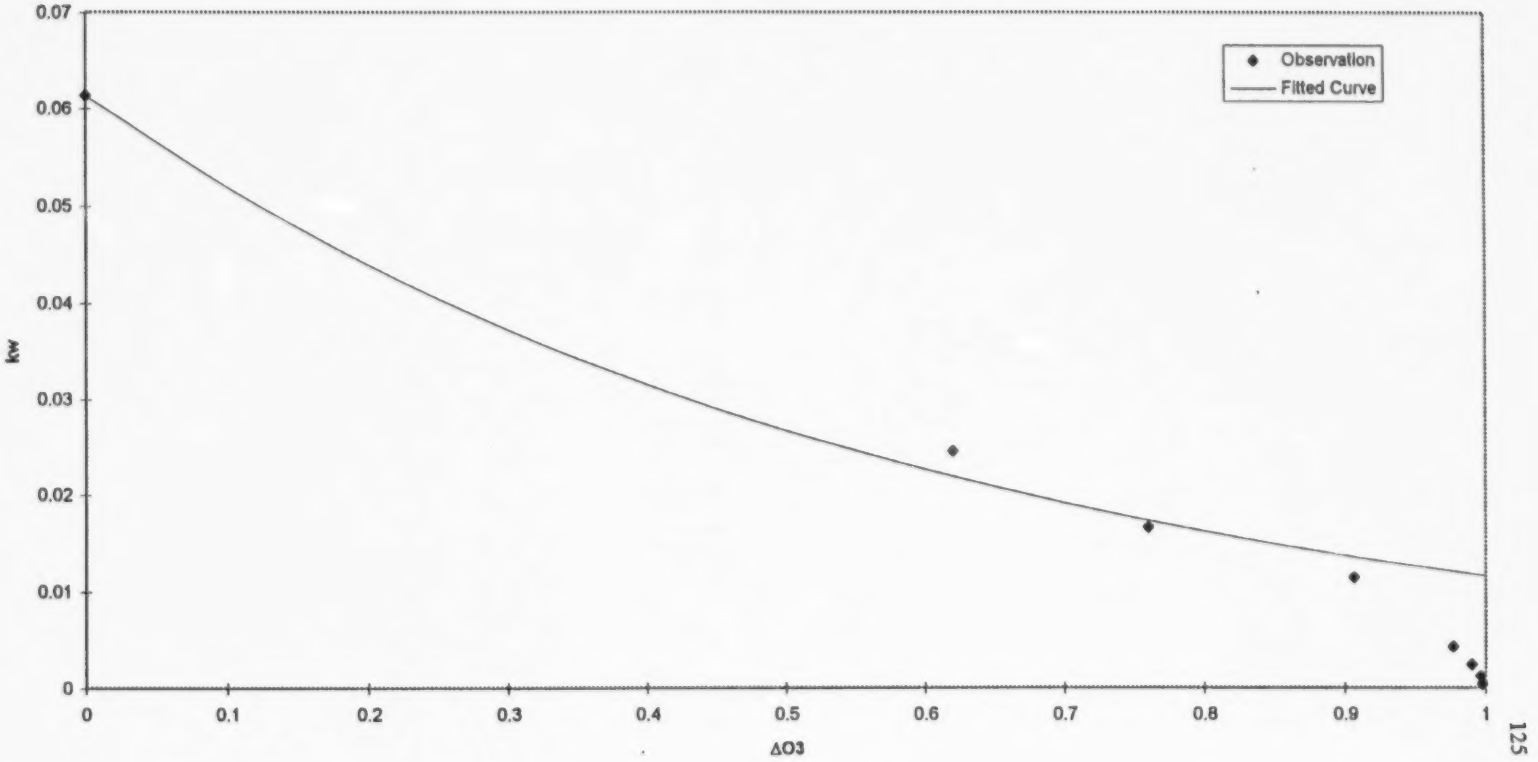

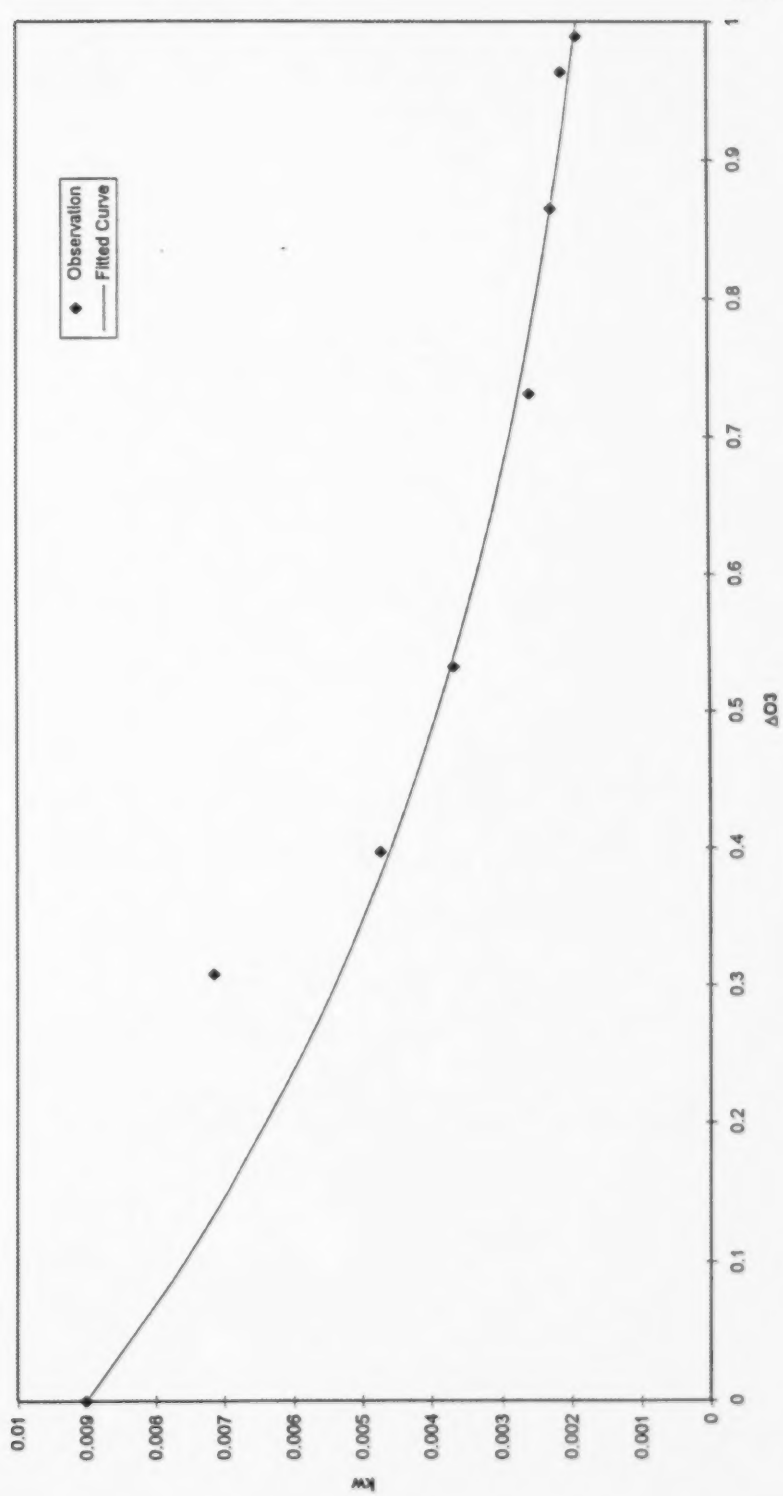


Figure C-7 : Fitted kw Curve for Rossdale .2

Figure C-8 : Fitted kw Curve for Rossdale .4

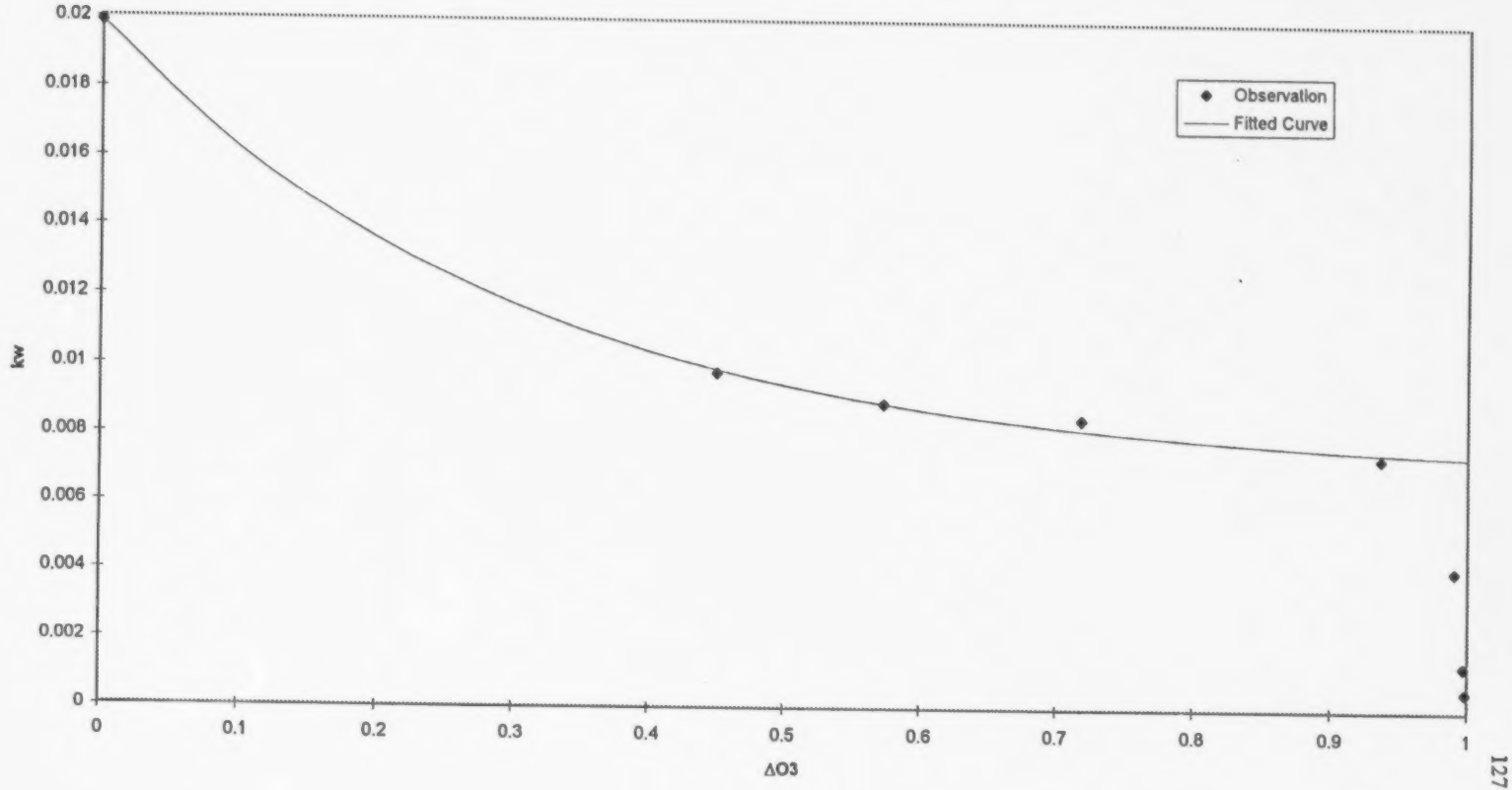

Figure C-9 : Fitted kw Curve for Rossdale .6

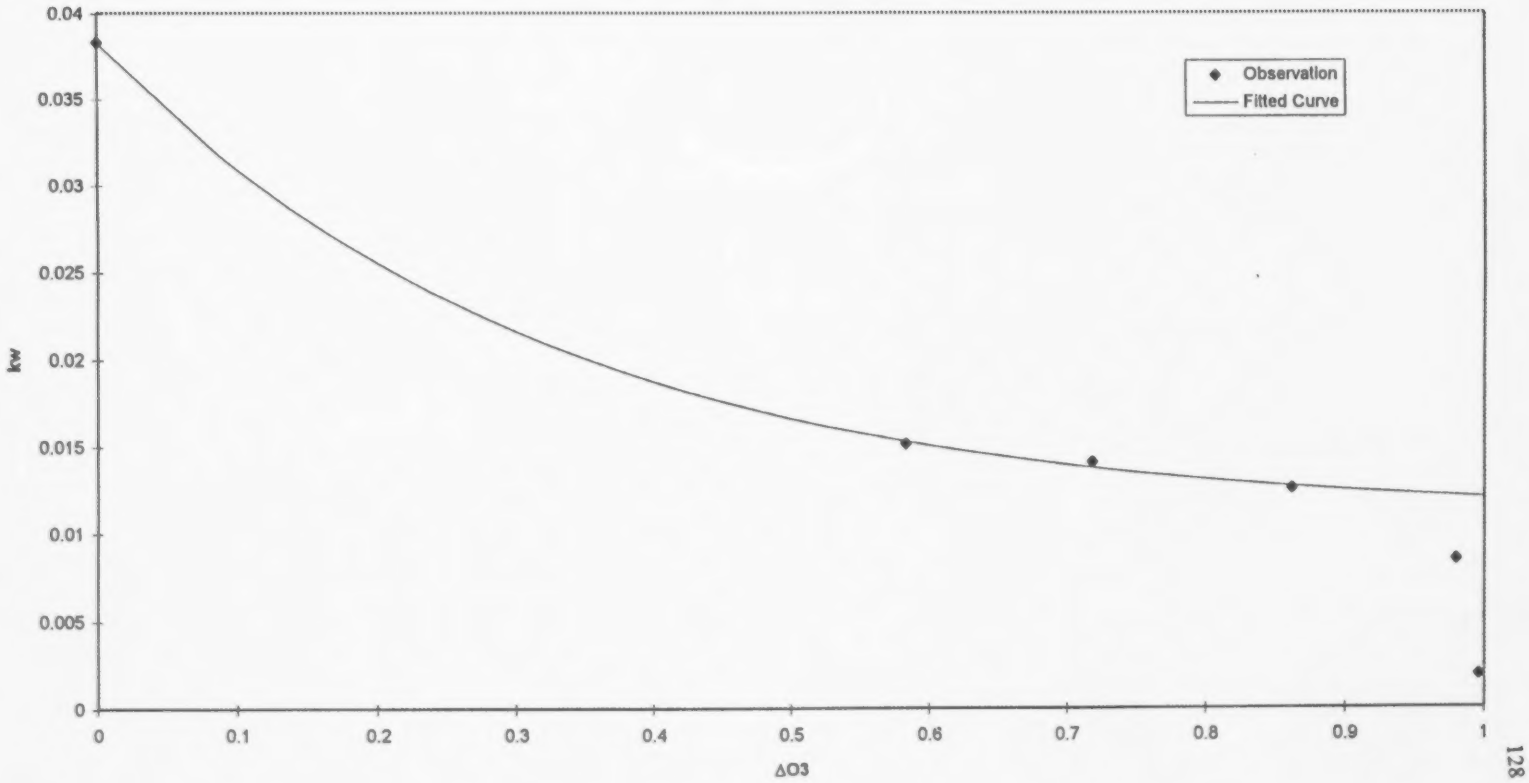

Figure C-10 : Fitted kw Curve for Rossdale .8

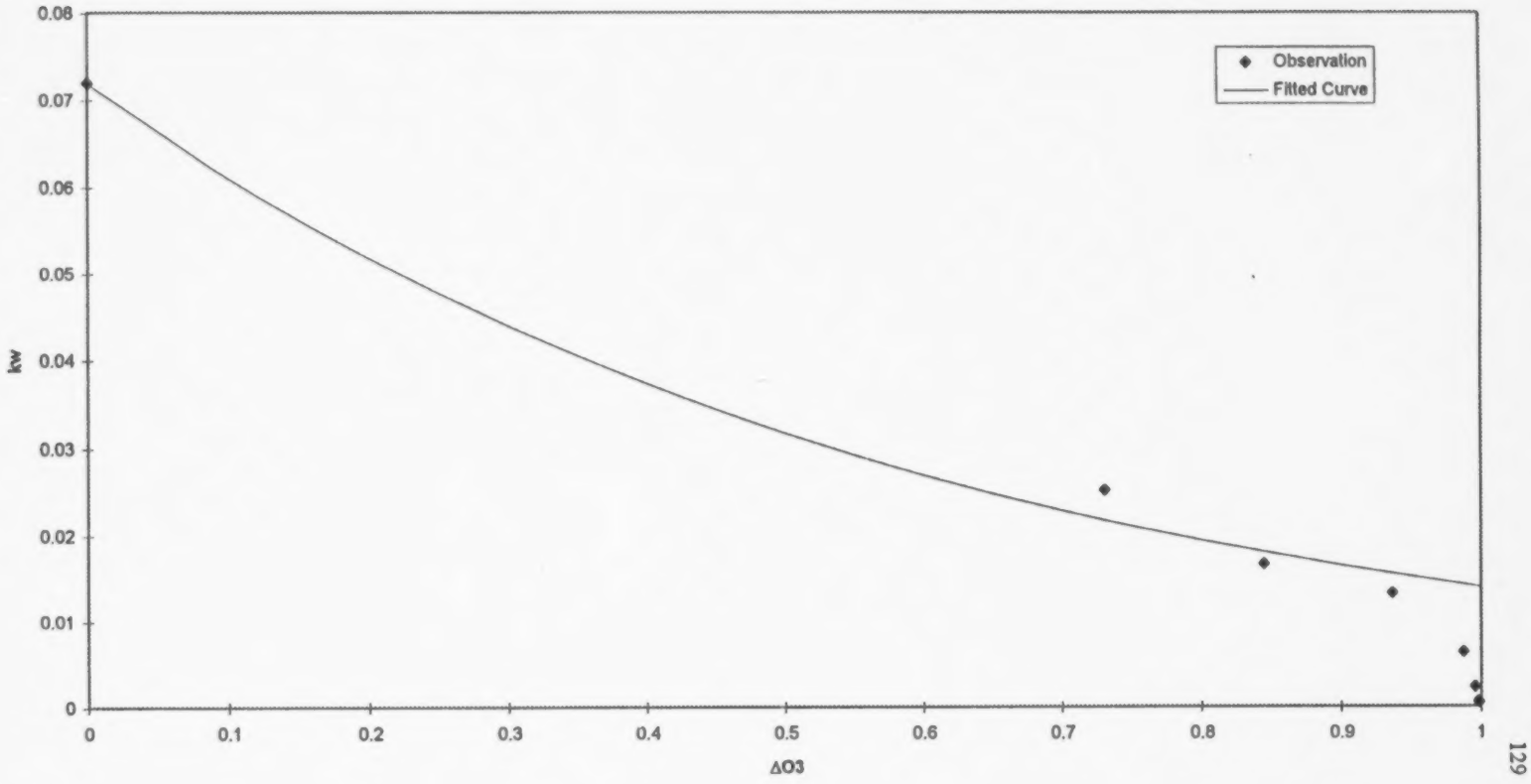

Figure C-11 : Fitted kw Curve for Red Deer .25

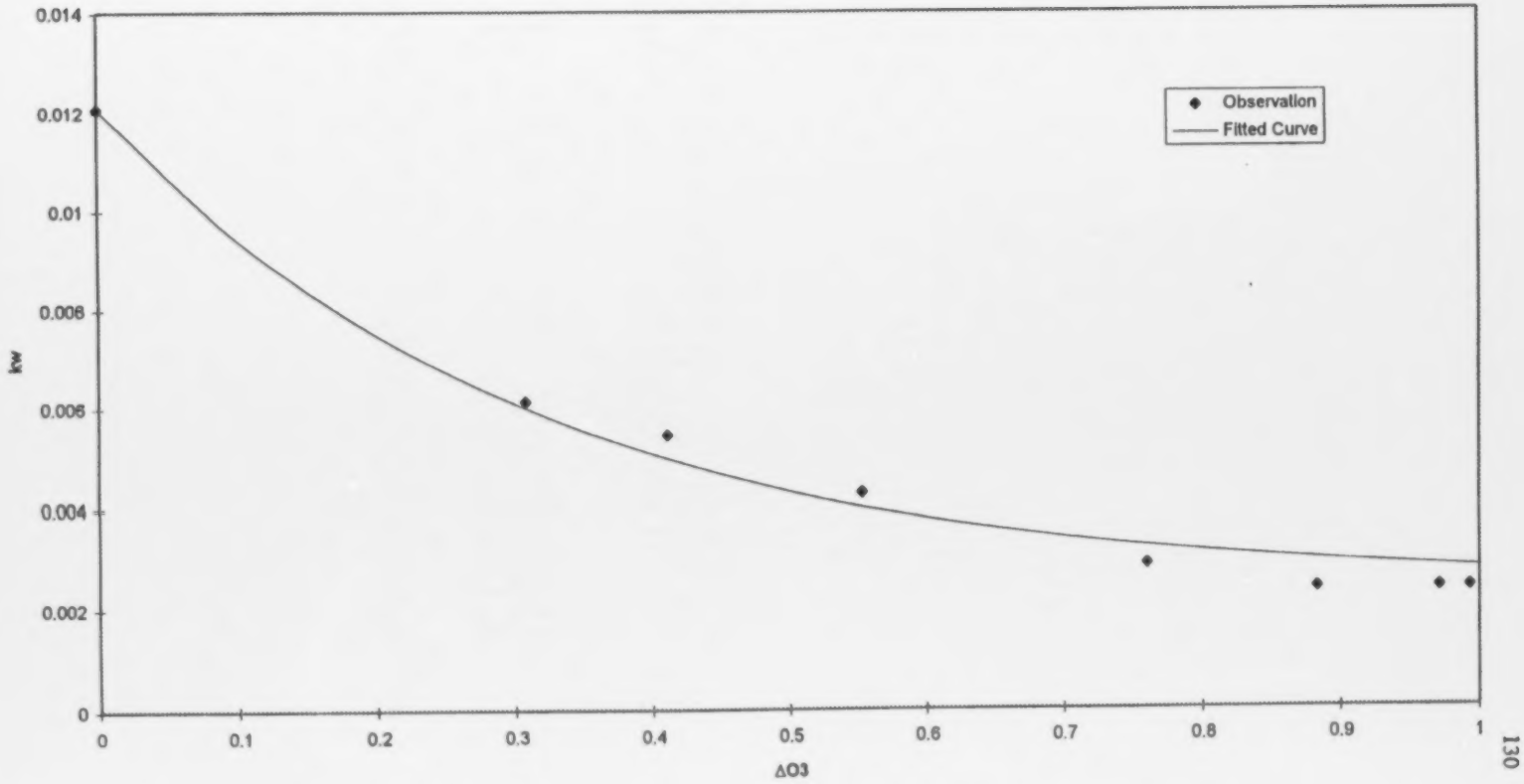

Figure C-12 : Fitted kw Curve for Red Deer .50

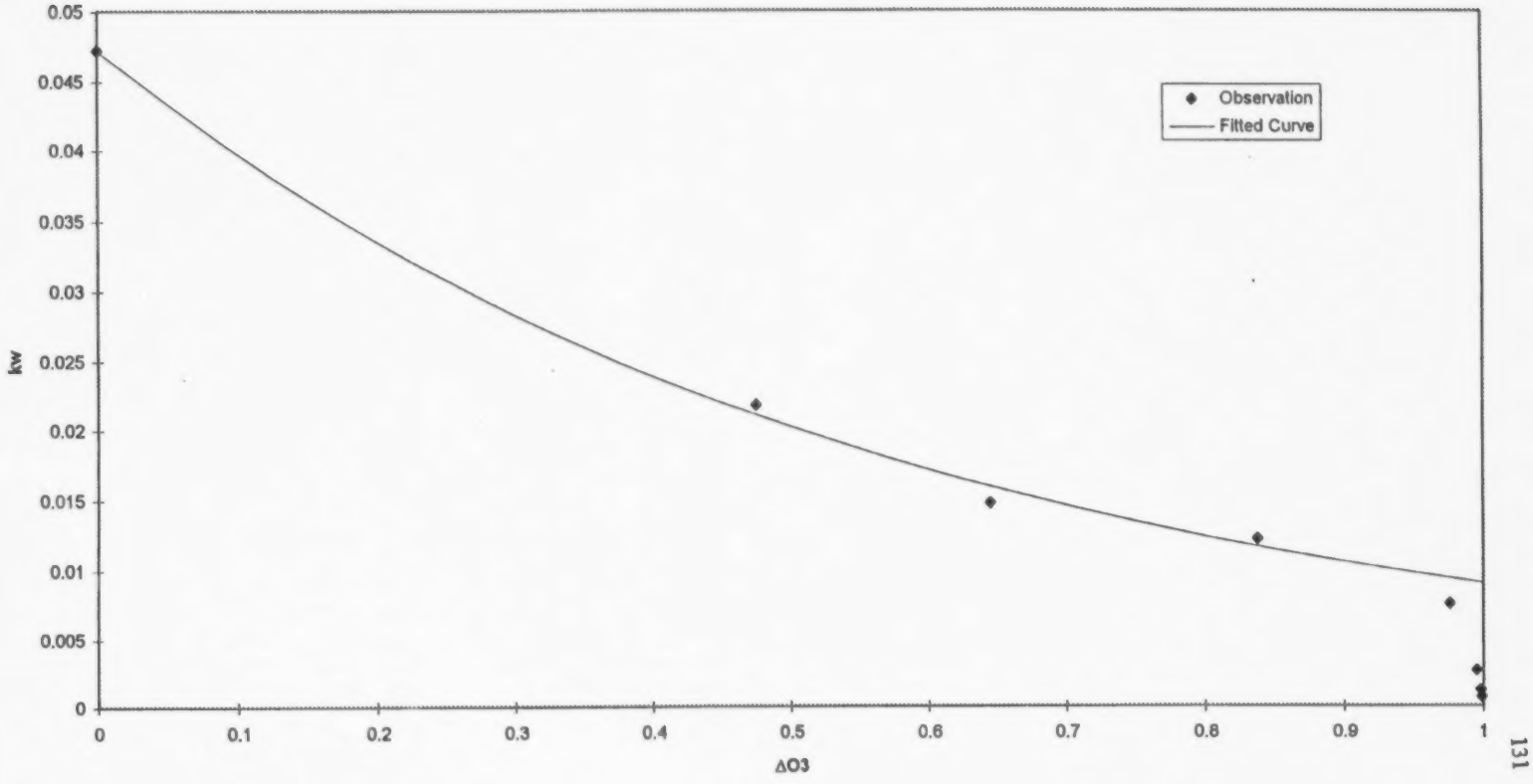

Figure C-13 : Fitted kw Curve for Red Deer .75

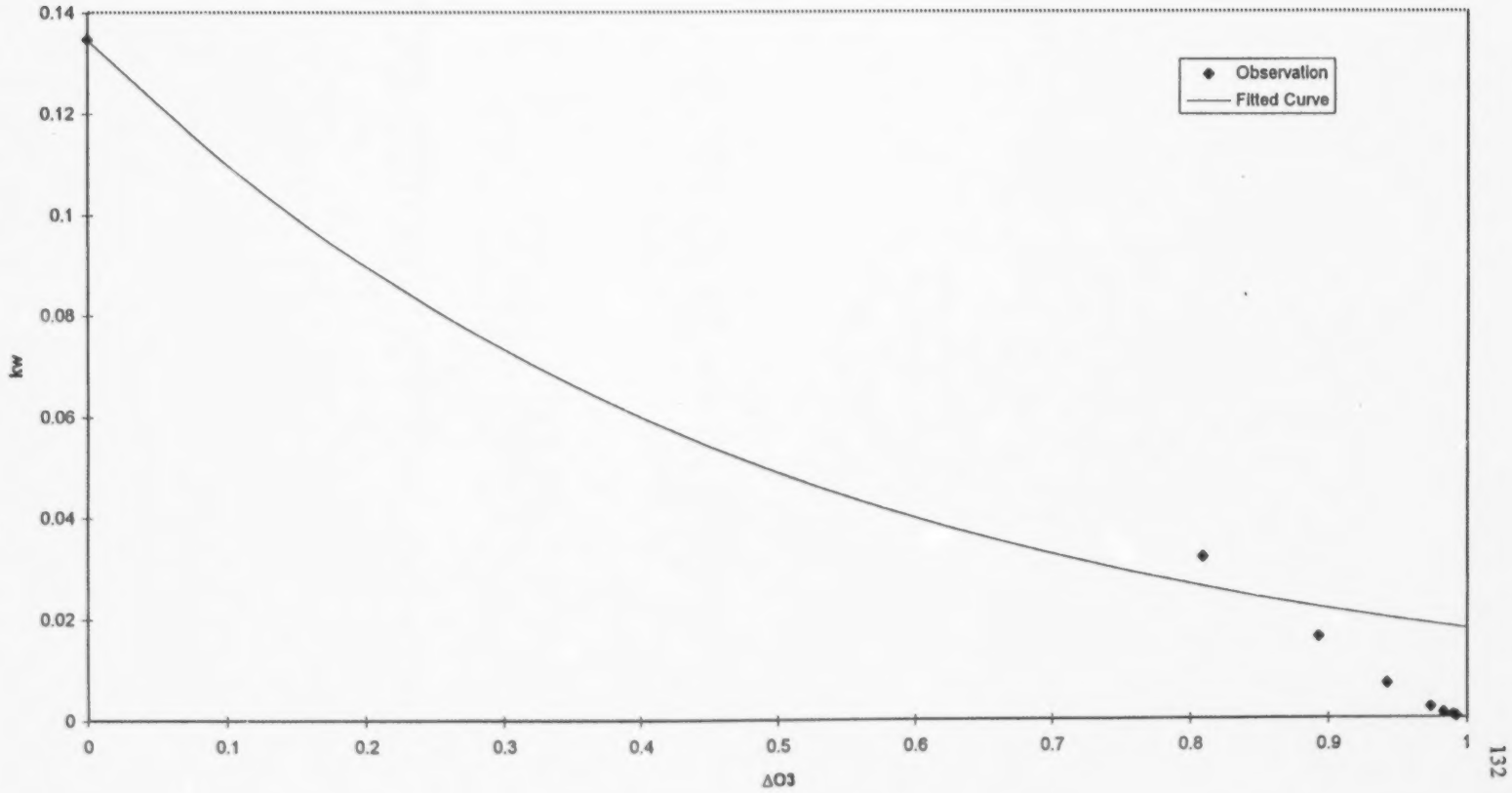

Figure C-14 : Fitted kw Curve for Pigeon Lake .25

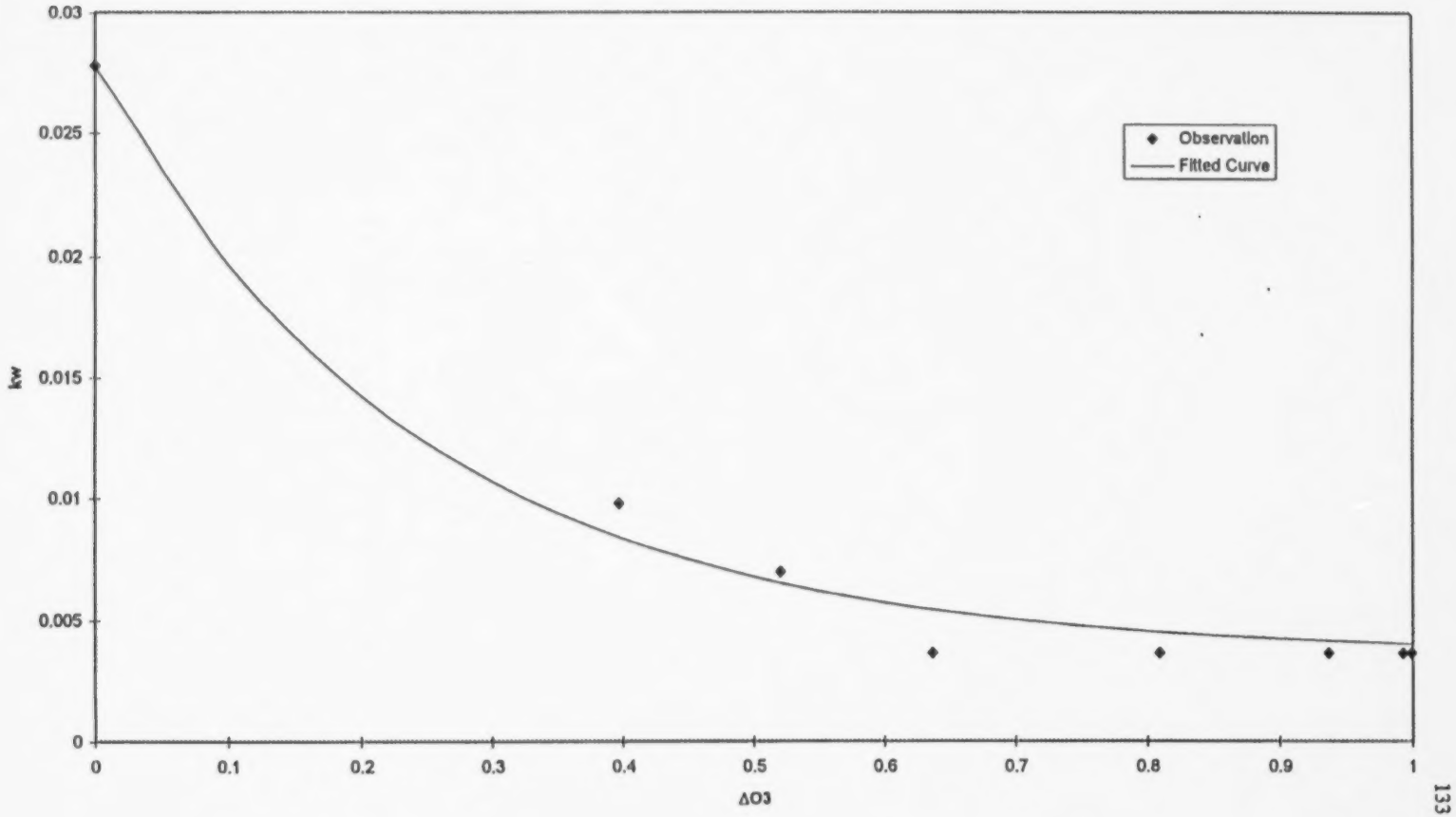

Figure C-15 : Fitted kw Curve for Pigeon Lake .50

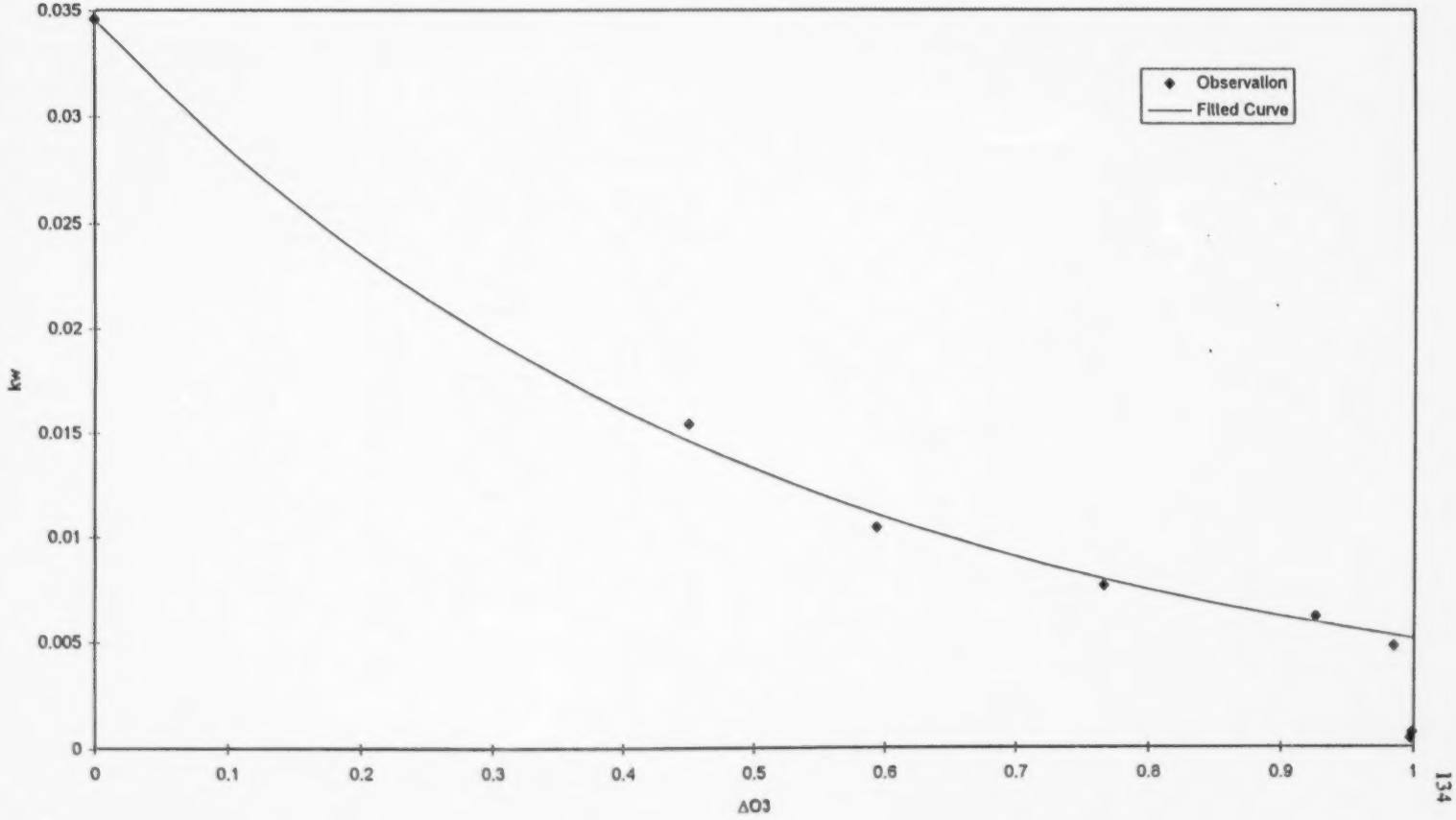

Figure C-16 : Fitted kw Curve for Pigeon Lake .75

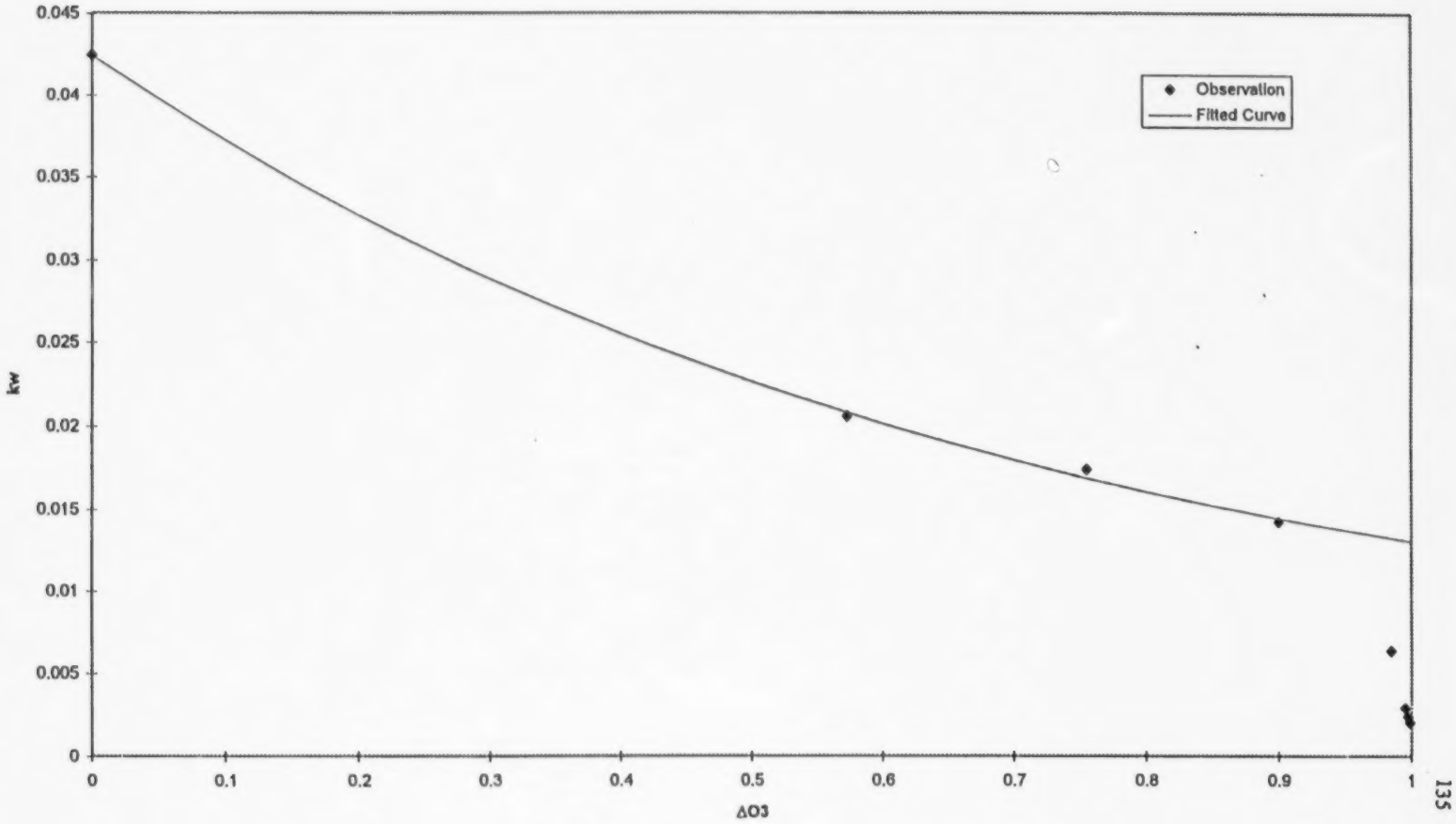

Figure C-17 : Fitted kw Curve for Hasse Lake .25

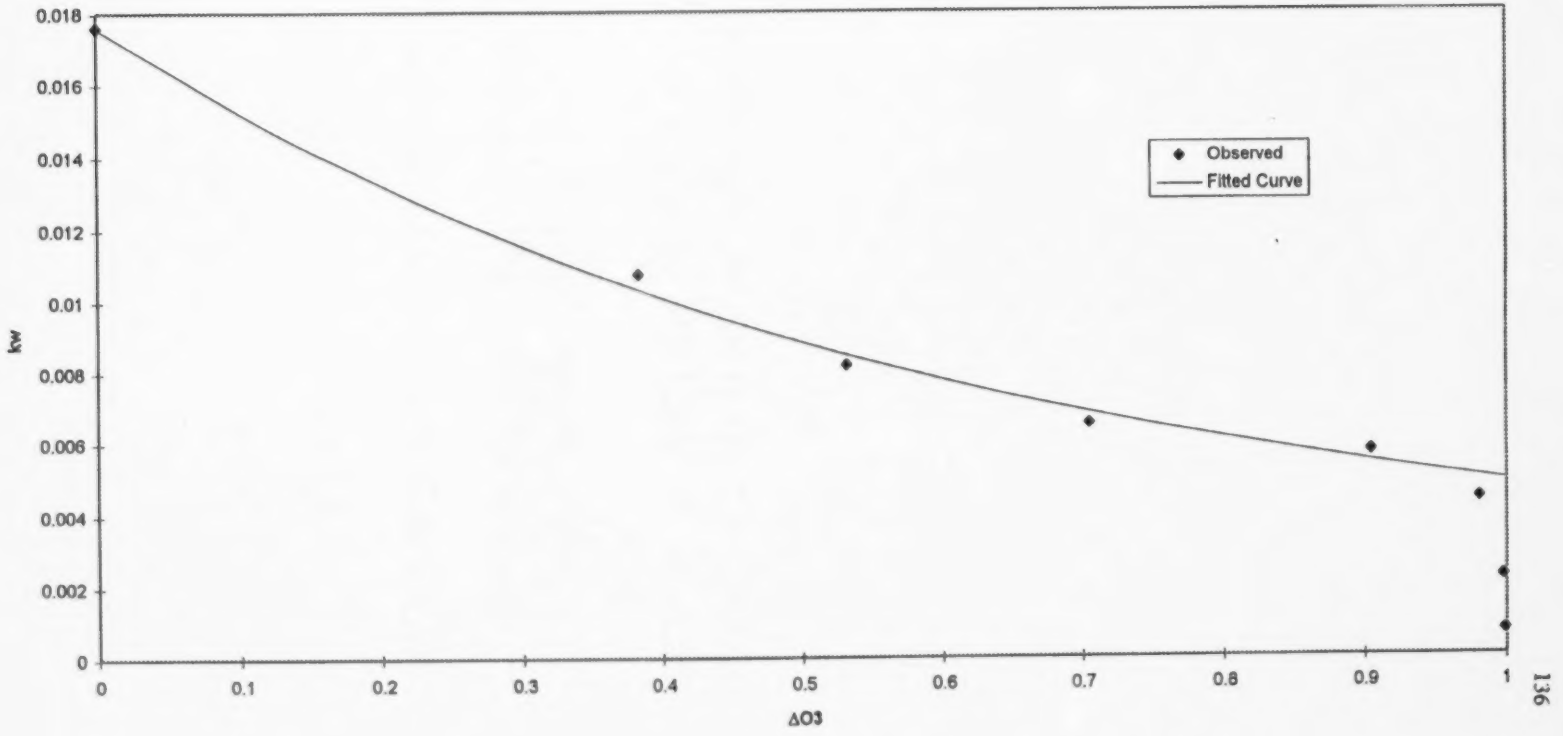

Figure C-18 : Fitted kw Curve for Hasse Lake .50

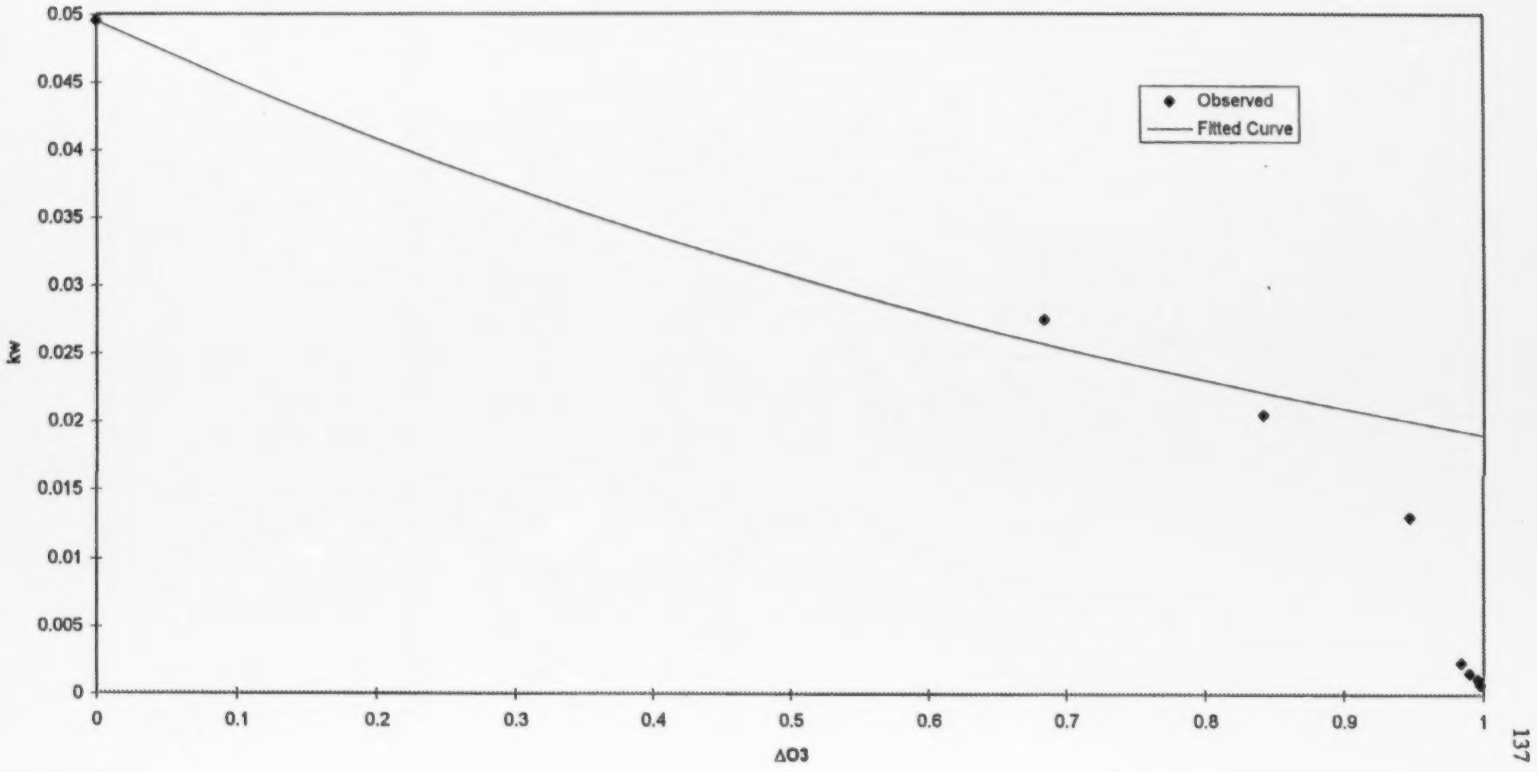

**Figure C-19 : Fitted kw Curve for Hasse Lake .75**

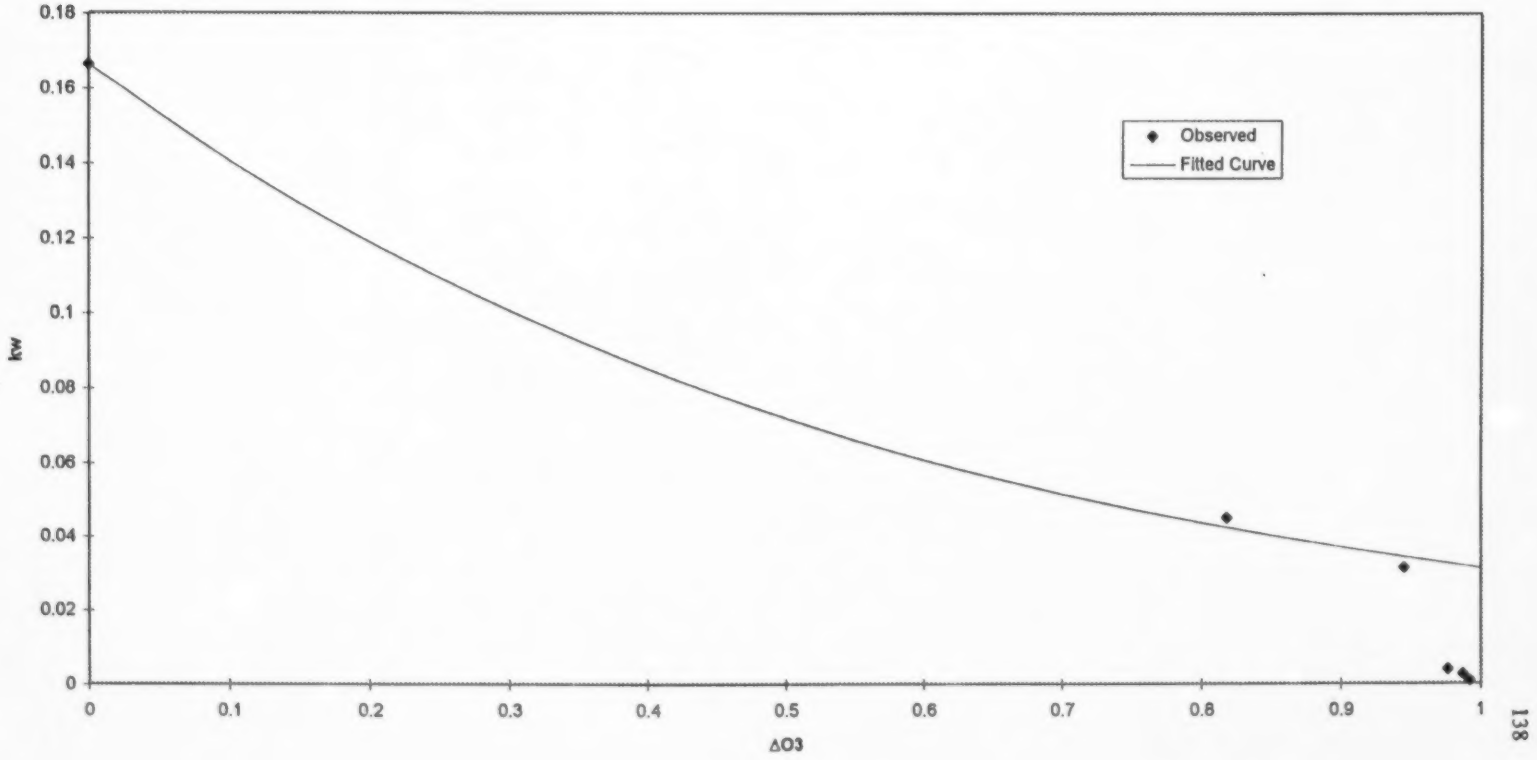

# APPENDIX D

## PILOT SCALE EXPERIMENTAL DATA

| Sample | Config. | Bar. Press (mm Hg) | $H_2O$ Flow (L/min) | Gas Flow (L/min) | $O_3$% (%) | $O_3$ Gen P. (psi) |
|---|---|---|---|---|---|---|
| Rossdale | ↑↓ | 711.5 | 2.61 | 0.82 | 1.734 | 6.0 |
| Rossdale | ↑↑ | 711.5 | 2.86 | 0.71 | 1.675 | 6.0 |
| Red Deer | ↑↓ | 704.9 | 2.93 | 0.92 | 1.75 | 6.25 |
| Red Deer | ↑↑ | 704.9 | 2.93 | 0.92 | 2.80 | 6.0 |
| Slave Lake | ↑↓ | 704.9 | 2.79 | 0.81 | 1.86 | 6.6 |
| Slave Lake | ↑↑ | 704.9 | 2.86 | 1.08 | 1.61 | 6.5 |
| Hasse Lake | ↑↓ | 704.9 | 2.79 | 0.91 | 1.69 | 6.7 |
| Hasse Lake | ↑↑ | 704.9 | 2.79 | 1.05 | 1.62 | 6.6 |
| Wabamun Lake | ↑↓ | 704.9 | 2.79 | 0.85 | 1.65 | 6.7 |
| Wabamun Lake | ↑↑ | 704.9 | 2.79 | 0.91 | 1.65 | 6.7 |
| Pigeon Lake | ↑↓ | 700.0 | 2.73 | 1.00 | 2.53 | 6.3 |
| Pigeon Lake | ↑↑ | 700.0 | 2.86 | 0.91 | 2.22 | 6.1 |
| Miquelon Lake | ↑↓ | 700.0 | 2.86 | 0.84 | 2.49 | 6.5 |
| Miquelon Lake | ↑↑ | 700.0 | 2.73 | 0.82 | 2.56 | 6.4 |
| Driedmeat Lake | ↑↓ | 695.9 | 2.73 | 0.92 | 2.47 | 6.4 |
| Driedmeat Lake | ↑↑ | 695.9 | 2.73 | 0.92 | 2.46 | 6.2 |

| Sample | Config. | Temp. (°C) | pH | TOC (ppm) | $UV_{254}$ (absorb.) | $UV_{280}$ (absorb.) |
|---|---|---|---|---|---|---|
| Rossdale | ↑↓ | 21.6 | 7.74 | 8.505 | .083 | .063 |
| Rossdale | ↑↑ | 21.5 | 7.74 | 8.285 | .083 | .061 |
| Red Deer | ↑↓ | 24.0 | 7.78 | 10.619 | .085 | .066 |
| Red Deer | ↑↑ | 24.0 | 7.78 | 10.477 | .089 | .070 |
| Slave Lake | ↑↓ | 24.0 | 7.73 | 11.495 | .090 | .063 |
| Slave Lake | ↑↑ | 23.9 | 7.59 | 11.173 | .090 | .063 |
| Hasse Lake | ↑↓ | 24.1 | 8.14 | 17.461 | .115 | .081 |
| Hasse Lake | ↑↑ | 23.6 | 8.16 | 16.820 | .110 | .075 |
| Wabamun Lake | ↑↓ | 24.0 | 8.14 | 18.601 | .097 | .070 |
| Wabamun Lake | ↑↑ | 24.0 | 8.20 | 17.741 | .097 | .067 |
| Pigeon Lake | ↑↓ | 24.2 | 7.96 | 13.471 | .059 | .044 |
| Pigeon Lake | ↑↑ | 24.1 | 7.96 | 11.606 | .061 | .045 |
| Miquelon Lake | ↑↓ | 24.3 | 9.54 | 47.885 | .381 | .162 |
| Miquelon Lake | ↑↑ | 24.2 | 9.56 | 50.285 | .373 | .158 |
| Driedmeat Lake | ↑↓ | 23.7 | 9.04 | 18.372 | .178 | .134 |
| Driedmeat Lake | ↑↑ | 23.8 | 9.02 | 17.052 | .188 | .135 |

| Sample | Config. | $[CO_3^{2-}]$ (eq/L) | $[HCO_3^-]$ (eq/L) |
|---|---|---|---|
| Rossdale | ↑↓ | .000074 | .001112 |
| Rossdale | ↑↑ | .000074 | .001112 |
| Red Deer | ↑↓ | .00007 | .001382 |
| Red Deer | ↑↑ | .00005 | .001368 |
| Slave Lake | ↑↓ | .000014 | .000928 |
| Slave Lake | ↑↑ | .000014 | .000934 |
| Hasse Lake | ↑↓ | .000124 | .0012 |
| Hasse Lake | ↑↑ | .000108 | .001216 |
| Wabamun Lake | ↑↓ | .000176 | .00183 |
| Wabamun Lake | ↑↑ | .000164 | .001863 |
| Pigeon Lake | ↑↓ | .000118 | .001406 |
| Pigeon Lake | ↑↑ | .000098 | .001476 |
| Miquelon Lake | ↑↓ | .005146 | .007906 |
| Miquelon Lake | ↑↑ | .00508 | .008042 |
| Driedmeat Lake | ↑↓ | .00047 | .001564 |
| Driedmeat Lake | ↑↑ | .000452 | .00157 |

| Sample | Config. | TS (mg/L) | TSS (mg/L) | TDS (mg/L) | TVS (mg/L) | VSS (mg/L) | VDS (mg/) |
|---|---|---|---|---|---|---|---|
| Rossdale | ↑↓ | 116 | -196 | 312 | 36 | -116 | 152 |
| Rossdale | ↑↑ | 120 | -188 | 308 | 28 | -80 | 108 |
| Red Deer | ↑↓ | 92 | -8 | 100 | 64 | 44 | 20 |
| Red Deer | ↑↑ | 104 | 20 | 84 | 56 | 24 | 32 |
| Slave Lake | ↑↓ | 92 | 28 | 64 | 68 | 48 | 20 |
| Slave Lake | ↑↑ | 88 | 40 | 48 | 60 | 16 | 44 |
| Hasse Lake | ↑↓ | 200 | 36 | 164 | 76 | 8 | 68 |
| Hasse Lake | ↑↑ | 80 | -76 | 156 | 108 | 48 | 60 |
| Wabamun Lake | ↑↓ | 112 | -60 | 172 | 92 | 56 | 36 |
| Wabamun Lake | ↑↑ | 128 | -20 | 148 | 100 | 28 | 72 |
| Pigeon Lake | ↑↓ | 88 | -24 | 112 | 52 | -24 | 76 |
| Pigeon Lake | ↑↑ | 84 | -20 | 104 | 56 | -24 | 80 |
| Miquelon Lake | ↑↓ | 3480 | -132 | 3612 | 380 | -72 | 452 |
| Miquelon Lake | ↑↑ | 3544 | -36 | 3580 | 364 | -12 | 376 |
| Driedmeat Lake | ↑↓ | 232 | 88 | 144 | 80 | -8 | 88 |
| Driedmeat Lake | ↑↑ | 212 | -36 | 248 | 80 | -8 | 88 |

| Sample | Config. | $[Ca^{2+}]$ (mg/L $CaCO_3$) | $[Mg^{2+}]$ (mg/L $CaCO_3$) |
|---|---|---|---|
| Rossdale | ↑↓ | 61.6 | 18.4 |
| Rossdale | ↑↑ | 57.6 | 19.4 |
| Red Deer | ↑↓ | 72.0 | 11.4 |
| Red Deer | ↑↑ | 68.2 | 10.4 |
| Slave Lake | ↑↓ | 33.0 | 10.2 |
| Slave Lake | ↑↑ | 31.0 | 10.4 |
| Hasse Lake | ↑↓ | 58.4 | 66.6 |
| Hasse Lake | ↑↑ | 57.4 | 66.6 |
| Wabamun Lake | ↑↓ | 34.0 | 17.8 |
| Wabamun Lake | ↑↑ | 34.2 | 18.6 |
| Pigeon Lake | ↑↓ | 40.0 | 19.2 |
| Pigeon Lake | ↑↑ | 39.8 | 18.2 |
| Miquelon Lake | ↑↓ | 61.4 | 425.4 |
| Miquelon Lake | ↑↑ | 60.2 | 423.8 |
| Driedmeat Lake | ↑↓ | 70.2 | 14.6 |
| Driedmeat Lake | ↑↑ | 70.8 | 16.2 |

| Sample | Config. | a | b | c |
|---|---|---|---|---|
| Rossdale | ↑↓ | 0 | 0.0134 | 2.310 |
| Rossdale | ↑↑ | 0 | 0.0130 | 2.726 |
| Red Deer | ↑↓ | 0 | 0.0312 | 2.776 |
| Red Deer | ↑↑ | 0 | 0.0313 | 3.034 |
| Slave Lake | ↑↓ | 0 | 0.0290 | 1.861 |
| Slave Lake | ↑↑ | 0 | 0.0256 | 2.239 |
| Hasse Lake | ↑↓ | 0 | 0.130 | 2.658 |
| Hasse Lake | ↑↑ | 0 | 0.0672 | 1.805 |
| Wabamun Lake | ↑↓ | 0 | 0.105 | 2.785 |
| Wabamun Lake | ↑↑ | 0 | 0.102 | 3.824 |
| Pigeon Lake | ↑↓ | 0 | 0.0409 | 3.020 |
| Pigeon Lake | ↑↑ | 0 | 0.0326 | 5.371 |
| Miquelon Lake | ↑↓ | 0 | 1.20E+12 | 1.16E+18 |
| Miquelon Lake | ↑↑ | 0 | 1.33E+12 | 6.98E+17 |
| Driedmeat Lake | ↑↓ | 0 | 0.864 | 2.480 |
| Driedmeat Lake | ↑↑ | 0 | 0.772 | 3.783 |

# APPENDIX E

## FORTRAN PROGRAM LISTING FOR PREDICTING DISSOLVED OZONE PROFILES IN NATURAL WATERS

*Reproduced with permission from Zhou (1995).*

```
C            DECLARE VARIABLES
C   ITMAX = MAXIMUM ALLOWABLE NUMBER OF ITERATION;
C   N = NUMBER OF EQUATIONS TO BE SOLVED;
C   ERREL = STOPPING CRITERION (RELATIVE ERROR BETWEEN TWO
C            SUCCESSIVE APPROXIMATIONS);
C   FNORM = A SCALAR WHICH IS F(1)**2+F(2)**2+...+F(N)**2.
C
    INTEGER ITMAX, N, L, M
    REAL ERREL
    PARAMETER (N=30,L=10,M=6)
C
    INTEGER K, NOUT, NINTV, J, JMAX
    REAL FCN, FNORM, X(N), XGUESS(N), DA(10), STG, STL, XO, R, A, CSVAL,
   &        BREAK(L), CSCOEF(4,L), T(L), W(L), Z(M), Y(M), HT,
   &        CO, BOT, TOP, SSR, EPS, DELT, S(L), G(M), BOT2, TOP2
    COMMON /DATAIN/ DA, STG, STL, XO, R, A
    INTRINSIC FLOAT
    EXTERNAL FCN, LSJAC, NEQNJ, UMACH, SSET, CSAKM, CSVAL,
C            SET VALUES OF OZONE CONC. AND INITIAL GUESSES
C
    READ (5,'(3E12.3)') CO, DELT, EPS
    READ (5,'(5E12.4)') (DA(I), I=1,10)
    READ (5,'(5E12.4)') STG, STL, XO, R, A
    READ (5,'(4F12.3)') (Z(I), I=1,M)
    READ (5,'(3F12.4)') (XGUESS(I), XGUESS(L+I),
   &        XGUESS(2*L+I), I=1,L)
    JMAX=10
    J=0
C
    CALL UMACH (2, NOUT)
    WRITE (NOUT,'(9X,A,9X,A,/)')'SSR','STG'
  100 CONTINUE
    J=J+1
C   ------------------------------------------------
C            CALL NEQNJ SUBROUTINE FOR DETERMINATION OF O3
    ERREL=1.0E-4
    ITMAX=100
C            FIND THE SOLUTION
    CALL NEQNJ (FCN, LSJAC, ERREL, N, ITMAX, XGUESS, X,
   &        FNORM)
C   ------------------------------------------------
C            CALL CSAKM SUBROUTINE FOR INTERPOLATION OF GAS O3
    T(1)=0.05
    DO 50 I=2,L
    T(I)=T(I-1)+0.1
   50 CONTINUE
    DO 51 I=1,L
    S(I)=X(L+1)
   51 CONTINUE
    CALL CSAKM (L, T, S, BREAK, CSCOEF)
    NINTV=L-1
    DO 52 I=1,M
    HT=FLOAT(I)/FLOAT(M+1)
```

```
      G(I)=CSVAL(HT, NINTV, BREAK, CSCOEF)
   52 CONTINUE
      HT=0.0
      BOT2=CSVAL(HT, NINTV, BREAK, CSCOEF)
      HT=1.0
      TOP2=CSVAL(HT, NINTV, BREAK, CSCOEF)
C     ------------------------------------------------------------
C     CALL CSAKM SUBROUTINE FOR INTERPOLATION OF AQ. O3
      T91)=0.05
      DO 30 I=2,L
      T(I)=T(I-1)+0.1
   30 CONTINUE
      DO 31 I=1,L
      W(I)=X(2*L+1)
   31 CONTINUE
      CALL CSAKM (L, T, W, BREAK, CSCOEF)
      NINTV=L-1
      DO 32 I=1,M
      HT=FLOAT(I)/FLOAT(M+1)
      Y(I)=CSVAL(HT, NINTV, BREAK, CSCOEF)*CO
   32 CONTINUE
C             CALCULATE DISSOLVED OZONE AT THE BOTTOM
      HT=0.0
      BOT=CSVAL(HT, NINTV, BREAK, CSCOEF)*CO
C             CALCULATE DISSOLVED OZONE AT THE TOP
      HT=1.0
      TOP=CSVAL(HT, NINTV, BREAK, CSCOEF)*CO
C     ------------------------------------------------------------
C             PERFORM THE LEAST SQUARE REGRESSION
      SSR=0.0
      DO 40 I=1,M
      SSR=SSR+(Z(I)-Y(I))**2
   40 CONTINUE
      WRITE (NOUT,'(E12.4, A, E12.4)') SSR, ',', STG
C     ------------------------------------------------------------
C             OUTPUT
      IF (SSR .LE. EPS) THEN
        WRITE (NOUT,'(//, 13X, A, //, 2X, A, 6X, A, 13X, A)')
     &          'THE SOLUTION OF EQUATIONS',
     &          'NO OF CSTR,', 'GASEOUS,', 'AQUEOUS,'
        WRITE (NOUT, '(3X, I4, A, 9X, E10.3, A, 10X, E10.3)')
     &          (K,',',X(L+K),',',X(2*L+K), K=1,L)
        WRITE (NOUT, 99) FNORM
   99 FORMAT (/,15X,'FNORM =', 1X,E10.3,//)
C
        WRITE (NOUT,'(/,7X,A,8X,A,7X,A,7X,A,9X,A,8X,A)')
     &          'DA,','STG,','STL,','XO,','R,','A'
        WRITE (NOUT,'(1X,5(F10.4,A))') DA(1),',',DA(DA(2),',',
     &          DA(3),',',DA(4),',',DA(5),',',DA(6),',',
     &          DA(7),',',DA(8),',',DA(9),',',DA(10),','
        WRITE (NOUT,'(1X,5(F10.4,A))')
     &          STG,',',STL,',',XO,',',R,',',A
        WRITE (NOUT,'(//,5X,A,8X,A,8X,A,8X,A)')
     &          'Z,','Z(I),','Y(I),','G(I)'
```

```
      WRITE (NOUT,'(3X,A,13X,F12.3,A,F12.3)')'0.0,,',BOT,
     &       ',',BOT2
      WRITE (NOUT,(1X,F5.2,A,F12.3,A,F12.3,A,F12.3)')
     &       (I/7.0,',',Z(I),',',Y(I),',',G(I), I=1,M)
      WRITE (NOUT,'3X,A,13X,F12.3,A,F12.3)')'1.0,,',TOP,
     &       ',',TOP2
      WRITE (NOUT,(//,7X,A,7X,A)') 'J=,','SSR=,'
      WRITE (NOUT,'(6X,I4,A,E12.3)')J, ',', SSR
     ELSE IF (J .GE. JMAX) THEN
      WRITE (NOUT,'(5X,A,8X,A,8X,A)')
     &       '#,','Z(I),','Y(I)'
      WRITE (NOUT,'(2X,I4,A,F12.3,A,F12.3)')
     &       (I,',',Z(I),',',Y(I), I=1,M)
      WRITE (NOUT,'(3X,A)')'PARAMETER ERROR'
       ELSE
            STG = (1.0+DELT)*STG
            STL = (1.0+DELT)*STL
            GO TO 100
     END IF
     CONTINUE
     END
C    ------------------------------------------------------------
C            USER-SUPPLIED SUBROUTINE
     SUBROUTINE FCN (X, F, N)
     INTEGER N, L
     REAL X(N), F(N), DA(10), STG, STL, XO, R, A
     COMMON /DATAIN/ DA, STG, STL, XO, R, A
C            (0,1,0,1) FOR COCURRENT FLOW;
C            (1,0,1,0) FOR COUNTERCURRENT FLOW.
     DATA A1, A2, A3, A4/1.0, 0.0, 1.0, 0.0/
     L=10
      F(1) = 1.0-(1.0+A)*X(1)*X(L+1)-STG*((1+A)*X(L+1)
     &       -X(2*L+1))
C
     DO 10 I=2,L
      F(I)=(1+A*(I-1))*X(I-1)*X(L+I-1)-(1+A*1)*X(I)
     &       *X(L+I)-STG*((1+A*I)*X(L+1)-X(2*L+I))
     10 CONTINUE
      F(L+1)=1.-(1.+A)*X(1)-STG*XO*((1+A)*X(L+1)
     &       -X(2*L+1))
     DO 11 I=L+2,2*L
      F(I) = (1.+A*(I-1-L))*X(I-1-L)-(1.+A*(I-L))*X(I-L)
     &       -STG*XO*((1.+A*(I-L))*X(I)-X(L+I))
     11 CONTINUE
      F(2*L+1) = -(1.+R+STL+DA(1))*X(2*L+1)+(A1+R)
     &       *X(2*L+2)+STL*(1.+A*1.)*X(L+1)
     DO 12 I=2*L+2,3*L-1
      F(I) = (A2+R)*X(I-1)-(1.+2*R+STL+DA(I-2*L))*X(I)+(A3
     &       +R)*X(I+1)+STL*(1.+A*(I-2*L))*X(I-L)
     12 CONTINUE
      F(3*L) = (A4+R)*X(3*L-1)-(1.+R+STL+DA(10))*X(3*L)
     &       +STL*(1.+A*L)*X(2*L)
     RETURN
     END
```

```
C  ------------------------------------------------------
C            USER-SUPPLIED SUBROUTINE TO COMPUTE JACOBIAN
      SUBROUTINE LSJAC (N, X, FJAC)
      INTEGER N,L
      REAL X(N), FJAC(N,N), DA(10), STG, STL, XO, R, A
      COMMON /DATAIN/ DA, STG, STL, XO, R, A
      EXTERNAL SSET
C            (0, 1, 0, 1) FOR COCURRENT FLOW;
C            (1, 0, 1, 0) FOR COUNTERCURRENT FLOW.
      DATA A1, A2, A3, A4/1.,0.,1.,0./
C
      L=10
      CALL SSET (N**2, 0.0, FJAC, 1)
        FJAC(1,1) = -(1.0+A)*X(L+1)
        FJAC(1, L+1) = -(1.+A)*X(1)-STG*(1.+A)
        FJAC(1,2*L+1) = STG
       DO 20 I=2,L
        FJAC(I,I-1) = (1.+A*9I-1))*X(L+I-1)
        FJAC(I,I) = -(1.+A*I)*X(L+I)
        FJAC(I,L+I-1) = (1.+A*(I-1))*X(I-1)
        FJAC(I,L+1) = -(1+A*I)*X(I)-STG*(1.+A*I)
        FJAC(I,2*L+I) = STG
      20 CONTINUE
        FJAC(L+1,1) = -(1.+A)
        FJAC(L+1,L+1) = -STG*XO*(1.+A)
        FJAC(L+1,2*L+1) = STG*XO
       DO 21 I=L+2,2*L
        FJAC(I,I-1-L) = 1.+A*(I-1-N)
        FJAC(I,I-L) = -(1.+A*(I-N))
        FJAC(I,I) = -STG*XO*(1.+A*(I-N))
        FJAC(I,L+1) = STG*XO
      21 CONTINUE
        FJAC(2*L+1,L+1) = STL*(1.+A*1.)
        FJAC(2*L+1,2*L+1) = -(1.+R+STL+DA(1))
        FJAC(2*L+1,2*L+2) = A1+R
       DO 22 I=2*L+2,3*L-1
        FJAC(I,I-L) = STL*(1.+A*(I-2*L))
        FJAC(I,I-1) = A2+R
        FJAC(I,I) = -(1.+2*R+STL+DA(I-2*L))
        FJAC(I,I+1) = A3+R
      22 CONTINUE
        FJAC(3*L,2*L) = STL*(1.+A*L)
        FJAC(3*L,3*L-1) = A4+R
        FJAC(3*L,3*L) = -(1.+R+STL+DA(L))
       RETURN
       END
```

# APPENDIX F

## DETAILED DERIVATION OF BACK FLOW CELL MODEL

*Adapted with permission from Zhou (1995).*

STEP 1: Dissolved Ozone

At steady state, the mass balance with respect to the amount of dissolved ozone within a CSTR yields:

$$O_{3aq,in} - O_{3aq,out} + \text{mass transfer} - \text{reaction} = 0 \quad (1)$$

Substituting, this gives:

(for j = 1)

$$Q_L C_0 + Q_B C_{L,2} + k_L a(C^*_{L,1} - C_{L,1})\frac{V}{N} - k_w C_{L,1}\varepsilon_L \frac{V}{N} - (Q_L + Q_B)C_{L,1} = 0 \quad (2)$$

where $Q_B$ is the backflow rate, N is the number of CSTRs in series, and V is the total volume of the reactor. Other symbols are as defined previously.

(for $2 \le j \le N-1$)

$$(Q_L + Q_B)C_{L,j-1} + Q_B C_{L,j+1} + k_L a(C^*_{L,j} - C_{L,j})\frac{V}{N} - k_w C_{L,j}\varepsilon_L \frac{V}{N} - (Q_L + 2Q_B)C_{L,j} = 0 \quad (3)$$

(for j = N)

$$(Q_L + Q_B)C_{L,N-1} + k_L a(C^*_{L,N} - C_{L,N})\frac{V}{N} - k_w C_{L,N}\varepsilon_L \frac{V}{N} - (Q_L + Q_B)C_{L,N} = 0 \quad (4)$$

STEP 2: Gaseous Ozone

The mass balance with respect to gaseous ozone in a CSTR under steady state yields:

$$O_{3g,in} - O3_{g,out} - \text{mass transfer} = 0 \quad (5)$$

Substituting, we get:

$$Q_{G,j-1}C_{G,j-1} - Q_{G,j}C_{G,j} + k_L a(C^*_{L,j} - C_{L,j})\frac{V}{N} = 0 \quad (6)$$

STEP 3: Total Gas

Ozone generators generally produce a product gas that is a few percent ozone, while the remainder consists of air or oxygen, depending on the input gas. Treating this remainder as an inert carry-gas, a the following mass balance equation can be generated:

$$Q_{G,j-1}C_{T,j-1} - Q_{G,j}C_{T,j} - k_L a(C^*_{L,j} - C_{L,j})\frac{V}{N} = 0 \quad (7)$$

where $C_T$ is the total mole concentration of all gases in the gas phase. Note that unlike $Q_L$, $Q_{G,j}$ changes with height as a result of hydrostatic pressure decreases and gaseous ozone depletion.

STEP 4: Relationships of $P_j$, $C_T$, $C_G$ and $C_L^*$ with the number of mixed cells j

a) $P_j$ vs j

$$P_j = P_T + \rho g \varepsilon_L (L - \frac{j}{N} L) \tag{8}$$

$$P_0 = P_T + \rho g \varepsilon_L L \tag{9}$$

where $P_T$ is the total pressure at the surface of columns, and $P_o$ is the total pressure at the column bottom. The above two equations mean that the hydraulic head $P_j$ decreases linearly with j as long as the liquid holdup $\varepsilon_L$ is constant.

b) $C_T$ and $C_G$ vs j

As ozonation is normally operated at room temperature and pressure, it is reasonable to assume that the gas phase follows the behaviour of an ideal gas. Therefore:

$$PV = nRT \tag{10}$$

where n is the moles of gas. For the total mole concentration of all gases:

$$C_{T,j} = \frac{n_{T,j}}{V} = \frac{P_j}{RT} \tag{11}$$

For the ozone gas:

$$C_{G,j} = \frac{n_{G,j}}{V} = \frac{P_j y_j}{RT} \tag{12}$$

c) $C_L^*$ vs j

The saturation concentration of dissolved ozone in equilibrium with ozone is governed by Henry's Law:

$$p = Py = HC_L^* \tag{13}$$

Applying the above equation for ozone absorption, it yields:

$$C_{L,j}^* = \frac{P_j}{H} y_j \tag{14}$$

where $y_j$ is the molar ratio of ozone in the gas phase.

At the bottom of the column, the saturation concentration of dissolved ozone is:

$$C_{L,0}^{*} = \frac{P_0}{H} y_0 \tag{15}$$

STEP 5: Simplification of Mass Balance Equations Using Dimensionless Parameters

a) Basic Dimensionless Parameters:

$$z = \frac{j - 0.5}{L} \tag{16}$$

$$\alpha = -\frac{\rho g \varepsilon_L L}{NP_0} \tag{17}$$

$$r = \frac{Q_B}{Q_L} \tag{18}$$

$$St_L = \frac{k_L a L}{Nu_L} \tag{19}$$

$$St_G = \frac{k_L a L}{Nu_{G,0}} \frac{RT}{H} \tag{20}$$

$$D_a = \frac{k_w \varepsilon_L L}{Nu_L} \tag{21}$$

$$D_b = \frac{k_M \varepsilon_L L}{Nu_L} \tag{22}$$

$$X = \frac{C_L}{C_0^{*}} \tag{23}$$

$$Y = \frac{y}{y_0} \tag{24}$$

$$q_G = \frac{Q_{G,j}}{Q_{G,0}} \tag{25}$$

b) Simplification of basic terms:

Replacing with $\alpha$, the relationships of $P_j$, $C_T$, $C_G$ and $C_L^{*}$ with j can be simplified as follows:

$$P_j = P_T + \rho g \varepsilon_L L - \frac{\rho g \varepsilon_L L_j}{N} = P_0(1+\alpha j) \tag{26}$$

$$C_{Tj} = \frac{P_0(1+\alpha j)}{RT} \tag{27}$$

$$C_{Gj} = \frac{P_0(1+\alpha j)y_j}{RT} \tag{28}$$

$$C^*_{Lj} = \frac{P_0(1+\alpha j)}{H} y_j \tag{29}$$

$$\frac{C^*_{Lj}}{C^*_{L,0}} = \frac{P_j y_j}{P_0 y_0} = \frac{P_0(1+\alpha j)}{P_0}\frac{y_j}{y_0} = (1+\alpha j)Y_j \tag{30}$$

c) Simplification of BFCM

To simplify the BFCM for dissolved ozone, equations 2 to 5 were first divided by $Q_L C^*_{L,0}$:

$$\frac{C_0}{C^*_{L,0}} + \frac{Q_B}{Q_L}\frac{C_{L,2}}{C^*_{L,0}} + k_L a\left(\frac{C^*_{L,1}}{C^*_{L,0}} - \frac{C_{L,1}}{C^*_{L,0}}\right)\frac{V}{Q_L N} - k_w \frac{C_{L,1}}{C^*_{L,0}}\varepsilon_L \frac{V}{Q_L N} - \left(1+\frac{Q_B}{Q_L}\right)\frac{C_{L,1}}{C^*_{L,0}} = 0 \quad (j = 1) \tag{31}$$

$$\left(1+\frac{Q_B}{Q_L}\right)\frac{C_{L,j-1}}{C^*_{L,0}} + \frac{Q_B}{Q_L}\frac{C_{L,j+1}}{C^*_{L,0}} + k_L a\left(\frac{C^*_{L,j}}{C^*_{L,0}} - \frac{C_{L,j}}{C^*_{L,0}}\right)\frac{V}{Q_L N} - k_w \frac{C_{L,j}}{C^*_{L,0}}\varepsilon_L \frac{V}{Q_L N} - \left(1+\frac{2Q_B}{Q_L}\right)\frac{C_{L,j}}{C^*_{L,0}} = 0 \quad (2 \le j \le N\text{-}1) \tag{32}$$

$$\left(1+\frac{Q_B}{Q_L}\right)\frac{C_{L,N-1}}{C^*_{L,0}} + k_L a\left(\frac{C^*_{L,N}}{C^*_{L,0}} - \frac{C_{L,N}}{C^*_{L,0}}\right)\frac{V}{Q_L N} - k_w \frac{C_{L,N}}{C^*_{L,0}}\varepsilon_L \frac{V}{Q_L N} - \left(1+\frac{Q_B}{Q_L}\right)\frac{C_{L,N}}{C^*_{L,0}} = 0 \quad (j = N) \tag{33}$$

Because $V/Q_L = L/u_L$, the three equations above can be transformed as:

$$\frac{C_0}{C^*_{L,0}} + \frac{Q_B}{Q_L}\frac{C_{L,2}}{C^*_{L,0}} + \frac{k_L a L}{u_L N}\left(\frac{C^*_{L,1}}{C^*_{L,0}} - \frac{C_{L,1}}{C^*_{L,0}}\right) - \frac{k_w \varepsilon_L L}{u_L N}\frac{C_{L,1}}{C^*_{L,0}} - \left(1+\frac{Q_B}{Q_L}\right)\frac{C_{L,1}}{C^*_{L,0}} = 0 \quad (j = 1) \tag{34}$$

$$\left(1+\frac{Q_B}{Q_L}\right)\frac{C_{L,j-1}}{C^*_{L,0}} + \frac{Q_B}{Q_L}\frac{C_{L,j+1}}{C^*_{L,0}} + \frac{k_L a L}{u_L N}\left(\frac{C^*_{L,j}}{C^*_{L,0}} - \frac{C_{L,j}}{C^*_{L,0}}\right) - \frac{k_w \varepsilon_L L}{u_L N}\frac{C_{L,j}}{C^*_{L,0}} - \left(1+\frac{2Q_B}{Q_L}\right)\frac{C_{L,j}}{C^*_{L,0}} = 0 \quad (2 \le j \le N\text{-}1) \tag{35}$$

$$\left(1+\frac{Q_B}{Q_L}\right)\frac{C_{L,N-1}}{C^*_{L,0}} + \frac{k_L a L}{u_L N}\left(\frac{C^*_{L,N}}{C^*_{L,0}} - \frac{C_{L,N}}{C^*_{L,0}}\right) - \frac{k_w \varepsilon_L L}{u_L N}\frac{C_{L,N}}{C^*_{L,0}} - \left(1+\frac{Q_B}{Q_L}\right)\frac{C_{L,N}}{C^*_{L,0}} = 0$$

$$(j = N) \qquad (36)$$

Substituting the dimensionless quantities and basic terms developed previously into these three equations, we obtain:

$$X_0 - (1 + r + St_L + D_a)X_1 + rX_2 + St_L(1 + \alpha)Y_1 = 0 \qquad (j = 1) \quad (37)$$

$$(1 + r)X_{j-1} - (1 + 2r + St_L + D_a)X_j + rX_{j+1} + St_L(1 + \alpha j)Y_j = 0 \qquad (2 \le j \le N\text{-}1) \quad (38)$$

$$(1 + r)X_{N-1} - (1 + r + St_L + D_a)X_N + St_L(1 + \alpha N)Y_N = 0 \qquad (j = N) \quad (39)$$

For the gaseous ozone, Equation 6 was first divided by the ($Q_{G,0}$ $P_0$ $y_0$) and then combined with Equation 28:

$$\frac{Q_{Gj-1}}{Q_{G,0}} \frac{P_0(1 + \alpha(j-1))y_{j-1}}{RTP_0y_0} - \frac{Q_{Gj}}{Q_{G,0}} \frac{P_0(1 + \alpha j)y_j}{RTP_0y_0} - k_L a \left(\frac{C^*_{Lj}}{P_0y_0} - \frac{C_{Lj}}{P_0y_0}\right) \frac{V}{Q_{G,0}N} = 0 \qquad (40)$$

Noting $V/Q_{G,0} = L/u_{G,0}$ and $P_0y_0 = HC^*_{L,0}$, Equation 40 can be transformed as:

$$\frac{Q_{Gj-1}}{Q_{G,0}} \frac{(1 + \alpha(j-1))y_{j-1}}{y_0} - \frac{Q_{Gj}}{Q_{G,0}} \frac{(1 + \alpha j)y_j}{y_0} - \frac{k_L aRTL}{HNu_{G,0}} \left(\frac{C^*_{Lj}}{C^*_{L,0}} - \frac{C_{Lj}}{C^*_{L,0}}\right) = 0 \qquad (41)$$

Substituting the dimensionless quantities and basic terms developed above into Equation 41, one obtains:

$$q_{Gj-1}Y_{j-1}[1 + \alpha(j-1)] - q_{Gj}Y_j(1 + \alpha j) - St_G[(1 + \alpha j)Y_j - X_j] = 0 \qquad (42)$$

For the total gas, Equation 7 was first divided by ($Q_{G,0}$ $P_0$) and then combined with Equation 27:

$$\frac{Q_{Gj-1}}{Q_{G,0}} \frac{P_0(1 + \alpha(j-1))}{RTP_0} - \frac{Q_{Gj}}{Q_{G,0}} \frac{P_0(1 + \alpha j)}{RTP_0} - k_L a \left(\frac{C^*_{Lj}}{P_0} - \frac{C_{Lj}}{P_0}\right) \frac{V}{Q_{G,0}N} = 0 \qquad (43)$$

Noting $V/Q_{G,0} = L/u_{G,0}$ and $P_0 = HC^*_{L,o}/y_0$, Equation 43 can be transformed as:

$$\frac{Q_{Gj-1}}{Q_{G,0}}[1 + \alpha(j-1)] - \frac{Q_{Gj}}{Q_{G,0}}(1 + \alpha j) - \frac{k_L aLRTy_0}{u_{G,0}NH} \left(\frac{C^*_{Lj}}{C^*_{L,0}} - \frac{C_{Lj}}{C^*_{L,0}}\right) = 0 \qquad (44)$$

Substituting the dimensionless quantities and basic terms developed above into Equation 44, one obtains:

$$q_{Gj-1}[1 + \alpha(j-1)] - q_{Gj}(1 + \alpha j) - St_G y_0[(1 + \alpha j)Y_j - X_j] = 0 \qquad (45)$$

STEP 6: Zero-Index Variables

Based on the definitions of variables (Equations 23 to 25), the zero-index variables are:

$$Y_0 = 1 \tag{46}$$

$$X_0 = 1 \tag{47}$$

$$q_{G,0} = 1 \tag{48}$$

NOTE: As a similar approach could be used to derive the countercurrent mode model equations, the derivation is omitted here.

# APPENDIX G

FINAL BACK FLOW CELL MODEL DATA INPUT FILES

**ROSSDALE, COUNTERCURRENT**

5.92E+00,5.00E-02,10.00E+00,
1.42E-01,1.62E-01,1.76E-01,1.90E-01,2.04E-01,
2.17E-01,2.29E-01,2.41E-01,2.51E-01,2.58E-01,
1.51E-01,2.05E-01,1.10E-02,7.48E-01,-1.50E-02,
1.587,1.523,0.948,0.604,
0.240,0.168,
1.00,0.90,0.20,
1.00,0.70,0.20,
1.00,0.60,0.20,
1.00,0.50,0.15,
1.00,0.40,0.10,
1.00,0.35,0.05,
1.00,0.35,0.02,
1.00,0.30,0.02,
1.00,0.20,0.02,
1.00,0.20,0.01

**ROSSDALE, COCURRENT**

5.72E+00,5.00E-02,10.00E+00,
2.12E-01,1.92E-01,1.73E-01,1.58E-01,1.44E-01,
1.33E-01,1.22E-01,1.14E-01,1.06E-01,1.00E-01,
1.56E-01,1.67E-01,1.10E-02,5.73E-01,-1.50E-02,
0.841,1.055,1.046,1.157,
1.198,1.189,
1.00,0.90,0.10,
1.00,0.70,0.10,
1.00,0.60,0.10,
1.00,0.50,0.10,
1.00,0.40,0.12,
1.00,0.35,0.15,
1.00,0.35,0.15,
1.00,0.30,0.12,
1.00,0.20,0.10,
1.00,0.20,0.10

**RED DEER, COUNTERCURRENT**

5.93E+00,5.00E-02,10.00E+00,
1.92E-01,2.12E-01,2.30E-01,2.47E-01,2.64E-01,
2.80E-01,2.96E-01,3.12E-01,3.25E-01,3.37E-01,
1.50E-01,2.01E-01,1.20E-02,6.60E-01,-1.50E-02,
3.592,2.709,1.950,1.253,
0.582,0.329,
1.00,0.90,0.40,
1.00,0.70,0.35,
1.00,0.60,0.30,
1.00,0.50,0.25,
1.00,0.40,0.20,
1.00,0.35,0.15,
1.00,0.35,0.10,
1.00,0.30,0.08,
1.00,0.20,0.06,
1.00,0.20,0.05

**RED DEER, COCURRENT**

9.52E+00,5.00E-02,10.00E+00,
3.60E-01,3.10E-01,2.65E-01,2.31E-01,2.04E-01,
1.81E-01,1.65E-01,1.50E-01,1.37E-01,1.28E-01,
1.50E-01,2.01E-01,1.90E-02,6.60E-01,-1.50E-02,
2.224,2.217,2.358,2.217,
2.857,2.408,
1.00,0.90,0.10,
1.00,0.70,0.10,
1.00,0.60,0.10,
1.00,0.50,0.10,
1.00,0.40,0.12,
1.00,0.35,0.15,
1.00,0.35,0.15,
1.00,0.30,0.12,
1.00,0.20,0.10,
1.00,0.20,0.10

**SLAVE LAKE, COUNTERCURRENT**

6.30E+00,5.00E-02,10.00E+00,
8.02E-01,8.02E-01,8.02E-01,8.02E-01,8.02E-01,
8.02E-01,8.02E-01,8.02E-01,8.02E-01,8.02E-01,
1.53E-01,1.90E-01,1.20E-02,6.60E-01,-1.50E-02,
2.293,1.913,1.328, ,
, ,
1.00,0.90,0.20,
1.00,0.70,0.20,
1.00,0.60,0.20,
1.00,0.50,0.15,
1.00,0.40,0.10,
1.00,0.35,0.05,
1.00,0.35,0.02,
1.00,0.30,0.02,
1.00,0.20,0.02,
1.00,0.20,0.01

**SLAVE LAKE, COCURRENT**

5.45E+00,5.00E-02,10.00E+00,
7.28E-01,5.59E-01,4.38E-01,3.54E-01,2.94E-01,
2.49E-01,2.16E-01,1.89E-01,1.69E-01,1.53E-01,
1.45E-01,2.35E-01,1.10E-02,7.69E-01,-1.50E-02,
1.371,1.525,1.669,1.492,
1.514,1.523,
1.00,0.90,0.10,
1.00,0.70,0.10,
1.00,0.60,0.10,
1.00,0.50,0.10,
1.00,0.40,0.12,
1.00,0.35,0.15,
1.00,0.35,0.15,
1.00,0.30,0.12,
1.00,0.20,0.10,
1.00,0.20,0.10

**HASSE LAKE, COUNTERCURRENT**

5.72E+00,5.00E-02,10.00E+00,
1.24E-01,1.98E-01,2.84E-01,4.03E-01,5.77E-01,
8.48E-01,1.27E+00,1.89E+00,2.78E+00,4.04E+00,
1.50E-01,2.09E-01,1.10E-02,7.15E-01,-1.50E-02,
1.607,1.353,0.673,0.337,
0.127,0.064,
1.00,0.90,0.30,
1.00,0.80,0.23,
1.00,0.76,0.20,
1.00,0.69,0.15,
1.00,0.62,0.10,
1.00,0.55,0.05,
1.00,0.50,0.02,
1.00,0.44,0.02,
1.00,0.39,0.02,
1.00,0.35,0.01

**HASSE LAKE, COCURRENT**

5.49E+00,5.00E-02,10.00E+00,
1.24E+00,7.95E-01,5.46E-01,4.00E-01,3.06E-01,
2.46E-01,2.03E-01,1.71E-01,1.49E-01,1.31E-01,
1.46E-01,2.35E-01,1.10E-02,7.87E-01,-1.50E-02,
0.970,1.030,1.108,1.057,
0.981,1.002,
1.00,0.90,0.10,
1.00,0.70,0.10,
1.00,0.60,0.10,
1.00,0.50,0.10,
1.00,0.40,0.12,
1.00,0.35,0.15,
1.00,0.35,0.15,
1.00,0.30,0.12,
1.00,0.20,0.10,
1.00,0.20,0.10

**WABAMUN LAKE, COUNTERCURRENT**

5.59E+00,5.00E-02,10.00E+00,
1.46E-01,2.40E-01,3.56E-01,5.22E-01,7.80E-01,
1.19E+00,1.83E+00,2.78E+00,4.20E+00,6.13E+00,
1.52E-01,1.98E-01,1.10E-02,6.82E-01,-1.50E-02,
1.674,1.427,0.684,0.511,
0.203,0.124,
1.00,0.90,0.37,
1.00,0.84,0.31,
1.00,0.77,0.24,
1.00,0.70,0.17,
1.00,0.62,0.11,
1.00,0.56,0.06,
1.00,0.50,0.04,
1.00,0.44,0.02,
1.00,0.40,0.01,
1.00,0.35,0.01

**WABAMUN LAKE, COCURRENT**

5.59E+00,5.00E-02,10.00E+00,
2.65E+00,1.30E+00,7.43E-01,4.73E-01,3.28E-01,
2.43E-01,1.90E-01,1.52E-01,1.27E-01,1.07E-01,
1.50E-01,2.09E-01,1.10E-02,7.15E-01,-1.50E-02,
0.921,1.008,1.028,0.991,
1.012,0.947,
1.00,0.90,0.10,
1.00,0.70,0.10,
1.00,0.60,0.10,
1.00,0.50,0.10,
1.00,0.40,0.12,
1.00,0.35,0.15,
1.00,0.35,0.15,
1.00,0.30,0.12,
1.00,0.20,0.10,
1.00,0.20,0.10

**PIGEON LAKE, COUNTERCURRENT**

8.54E+00,5.00E-02,10.00E+01,
5.00E-01,5.00E-01,5.00E-01,5.00E-01,5.00E-01,
5.01E-01,5.01E-01,5.00E-01,5.00E-01,5.00E-01,
1.48E-01,2.31E-01,1.70E-02,7.90E-01,-1.50E-02,
4.600,4.161,3.464,2.218,
1.218,0.857,
1.00,0.90,0.20,
1.00,0.80,0.20,
1.00,0.70,0.20,
1.00,0.60,0.15,
1.00,0.50,0.15,
1.00,0.45,0.10,
1.00,0.40,0.10,
1.00,0.30,0.05,
1.00,0.20,0.05,
1.00,0.20,0.02
****1st observation is an estimate.*

**PIGEON LAKE, COCURRENT**

7.49E+00,5.00E-02,10.00E+00,
5.86E-01,3.93E-01,2.80E-01,2.10E-01,1.64E-01,
1.33E-01,1.11E-01,9.46E-02,8.21E-02,7.25E-02,
1.50E-01,2.04E-01,1.50E-02,6.85E-01,-1.50E-02,
1.784,2.087,1.801,2.048,
2.070,2.242,
1.00,0.90,0.10,
1.00,0.70,0.10,
1.00,0.60,0.10,
1.00,0.50,0.10,
1.00,0.40,0.12,
1.00,0.35,0.15,
1.00,0.35,0.15,
1.00,0.30,0.12,
1.00,0.20,0.10,
1.00,0.20,0.10

**MIQUELON LAKE, COUNTERCURRENT**

8.41E+00,5.00E-02,10.00E+00,
5.16E+12,5.16E+12,5.16E+12,5.16E+12,5.16E+12,
5.16E+12,5.16E+12,5.16E+12,5.16E+12,5.16E+12,
1.52E-01,1.91E-01,1.70E-02,6.47E-01,-1.60E-02,
0.992,0.317,0.167,0.118,
0.096,0.078,
1.00,0.90,0.20,
1.00,0.70,0.20,
1.00,0.60,0.20,
1.00,0.50,0.15,
1.00,0.40,0.10,
1.00,0.35,0.05,
1.00,0.35,0.02,
1.00,0.30,0.02,
1.00,0.20,0.02,
1.00,0.20,0.01

**MIQUELON LAKE, COCURRENT**

8.65E+00,5.00E-02,10.00E+00,
3.32E-04,1.02E-18,2.88E-31,4.06E-42,1.57E-51,
1.23E-59,1.45E-66,1.04E-72,6.14E-78,1.63E-82,
1.53E-01,1.96E-01,1.70E-02,6.92E-01,-1.60E-02,
0.423,0.330,0.352,0.290,
0.220,0.195,
1.00,0.90,0.10,
1.00,0.70,0.12,
1.00,0.60,0.16,
1.00,0.50,0.10,
1.00,0.40,0.18,
1.00,0.35,0.20,
1.00,0.35,0.21,
1.00,0.30,0.22,
1.00,0.20,0.23,
1.00,0.20,0.25

**DRIEDMEAT LAKE, COUNTERCURRENT**

8.30E+00,5.00E-02,1.00E+01,
1.82E+00,1.82E+00,1.82E+00,1.82E+00,1.82E+00,
1.82E+00,1.82E+00,1.82E+00,1.82E+00,1.82E+00,
0.150,0.216,0.017,0.748,-0.016,
1.604,0.823,0.299,0.163,0.069,0.060,
1.00,0.90,0.20,
1.00,0.70,0.20,
1.00,0.60,0.20,
1.00,0.50,0.15,
1.00,0.40,0.10,
1.00,0.35,0.05,
1.00,0.35,0.02,
1.00,0.30,0.02,
1.00,0.20,0.02,
1.00,0.20,0.01

**DRIEDMEAT LAKE, COCURRENT**

8.26E+00,5.00E-02,10.00E+00,
5.43E-01,2.98E-01,1.63E-01,9.24E-02,5.44E-02,
3.35E-02,2.18E-02,1.46E-02,1.03E-02,7.55E-03,
1.50E-01,2.16E-01,1.70E-02,7.48E-01,-1.60E-02,
0.518,0.587,0.645,0.631,
0.595,0.519,
1.00,0.90,0.10,
1.00,0.70,0.10,
1.00,0.60,0.10,
1.00,0.50,0.12,
1.00,0.40,0.15,
1.00,0.35,0.15,
1.00,0.35,0.14,
1.00,0.30,0.13,
1.00,0.20,0.12,
1.00,0.20,0.11